SCOUR OF UNLINED DAM SPILLWAYS

by

Ousmane Sawadogo

Thesis presented in partial fulfilment of the requirements for the degree of Master of Engineering Sciences (Civil) at Stellenbosch University

Study Leader:

Prof. G.R. Basson

December 2010

Declaration

By submitting this dissertation electronically, I declare that the entirety of the work contained therein is my own, original work, that I am the owner of the copyright thereof (unless to the extent explicitly otherwise stated) and that I have not previously in its entirety or in part submitted it for obtaining any qualification.

Signature: . . . . . .

Date : . . . . . .

Abstract

The scour process of unlined spillways is an important research topic of value in engineering practice. In South Africa numerous unlined spillway dams have experienced severe erosion. This led, in some cases, to the costly concrete lining of spillways for erosion protection. On the other hand, the erosion of unlined spillways can lead to damage to, and even failure of dams and consequently can affect public safety, properties, infrastructure and the environment. In this regard, methods to predict erosion of unlined spillways are therefore needed as tools in the risk management and design of existing unlined spillways as well as future spillway structures.

The prediction of the rock scouring process is challenging and empirical formulas have been established to predict incipient conditions for scour. These empirical methods however do not predict the rate of scour or the ultimate equilibrium rock scour.

The key objective in this study was to investigate the applicability of a non-cohesive two-dimensional (2D) sediment transport hydrodynamic mathematical model to simulate unlined spillway scour. A physical model flume test was set up to simulate rock scour represented by uniformly sized polyethylene cubes. The flume slope and discharge were varied in the different test scenarios. The 2D mathematical model correctly predicted the extent and location of scour as observed in the laboratory tests. Temporal changes in the scour formation were also predicted with reliability. This was achieved by only calibrating the hydraulic roughness of the 2D model, and by specifying the "rock" particle settling velocity and material density. The simulation results were satisfactory, providing an accurate and detailed erosion prediction. From this, the mathematical modelling was validated by using a field case study.

The results obtained with the mathematical model were promising for non-cohesive cases and could be applied to field prototype cases if the rock joint structure is known. This would typically apply in fault zones, where the joints would give an idea of the rock size to be used in the mathematical model. In general, where jointed rock is more massive and acts "cohesive", rock parameters describing critical scour conditions for the rock in terms of stream power are required to be built into the mathematical models.

Opsomming

Die uitskuringsproses van onbelynde oorlope is 'n belangrike navorsingsonderwerp in die ingenieurspraktyk. In Suid-Afrika word ernstige erosie in baie onbelynde oorlope van damme ondervind. In sommige gevalle het dit gelei tot die duur belyning van oorlope met beton, om die oorlope te beskerm. Aan die anderkant kan die erosie van onbelynde oorlope lei tot groot skade en selfs tot die faling van 'n dam. Dit kan weer lei tot skade aan eiendom, infrastruktuur en die omgewing, en die publiek in die gevaar stel. Daarom is dit nodig dat daar besin word oor metodes om erosie in onbelynde oorlope te voorspel, sodat die risiko bestuur kan word en om te sorg vir die beter ontwerp van onbelynde oorlope in die toekoms.

Dit is moeilik om die uitskuringsproses te voorspel, maar empiriese formules is bestaan om die aanvang van uitskuring te voorspel. Hierdie empiriese metodes voorspel egter nie die snelheid waarteen die uitskuring sal plaasvind of die uiteindelike mate waartoe dit sal gebeur nie.

Die hoofdoelwit van hierdie studie was om die toepasbaarheid van 'n nie- kohesie, twee-dimensionele (2D) hidrodinamiese wiskundige model te ondersoek, om sodoende die uitskuring van onbelynde oorlope te simuleer. 'n Fisiese model om die uitskuring van rots te simuleer is ook gebou. Die rots is deur polietileen blokkies van dieselfde grootte gemodelleer. Verskillende kanaalhellings en deurstromings is in verskillende toetse gebruik. Die 2D wiskundige model het volgens die waarnemings in laboratorium toetse, die mate en ligging van die uitskuring korrek voorspel. Veranderinge wat met verloop van tyd in die uitskuring formasie plaasgevind het, is ook betroubaar voorspel. Dit is gedoen deur die hidrouliese ruheid van die 2D model te kalibreer en deur te spesifiseer hoe vinnig die "rots" deeljies afsak en wat die digtheid van die materiaal is. Die uitslag van die simulasie was bevredigend en het die erosie akkuraat en in detail voorspel. Die wiskundige modellering is gevalideer deur middel van 'n gevallestudie.

Die uitslae wat met die wiskundige model verkry is, is belowend, en geld vir nie-kohesie gevalle. Dit kan op prototipe gevalle in die veld toegepas word as die rots se naatstruktuur bekend is. Dit kan toegepas word in foutsones waar die nate 'n aanduiding sal gee van die grootte van "rotse" wat in die wiskundige model gebruik moet word. Maar as die rots baie groot is en die kohesie goed is, is dit nodig om meer parameters betreffende uitskuringstoestande gekoppel aan stroomdrywing, in die wiskundige model te gebruik.

Acknowledgements

I would like to take this opportunity to acknowledge my study leader, Professor GR Basson (Director, Institute for Water and Environmental Engineering, Department of Civil Engineering, University of Stellenbosch, South Africa) for his valuable help, assistance and guidance throughout the execution of this thesis.

I would like to thank my former institute, AIMS (African Institute for Mathematical Sciences) for partial funding of my studies. I am grateful to the Department of Civil Engineering for the financial help.

I would like to acknowledge the assistance given by Mr Ning Ma, the Hydraulics Laboratory Manager, for his help and suggestions regarding the physical model tests and his knowledge on the CCHE2D mathematical model software. I am grateful to the Department of Water Affairs (DWA) for survey data and floods hydrology data used in this thesis as part of Mokolo Crocodile Water Augmentation Project (MCWAP). I wish to acknowledge colleagues in the postgraduate student office (S417) and staff of the Institute for Water and Environmental Engineering, Department of Civil Engineering, for their inspiration.

I would like to thank my fellow citizen Dr Laure Gouba for her precious advice and help. I am deeply grateful to my parents for the confidence they put in me and their patience. To my mother for her prayers and benedictions which always guided me. To my father for giving me the opportunity to be educated despite the difficulties and in an environment where schooling was perceived as a matter for rich families. May his soul rests in peace. To all my brothers and sisters with whom I shared a good childhood. To my fiancé and my daughter Majida, I say thank you for their unconditional encouragement and love.

Contents

List of Figures

List of Tables

List of Symbols

A	Area (m^2)
	Cross sectional area of the water profile (m^2)
B	Width of the flume (m)
$\overline{c}_{bk}$	Average concentration of bed load at the bed load zone (kg/m^3)
C_d	Discharge coefficient for the weir
C_D	Drag coefficient
C_f	Friction coefficient
C_k	Concentration of the k^{th} size class of sediment (kg/m^3)
C_{*k}	Depth-averaged concentration (kg/m^3)
d_c, d_f	Diameters of the coarse and fine modes (m)
d_m	Median grain size of foundation material (m)
dt	Duration of the flood event (s)
d_u	Reference diameter used by Proffit and Sutherland (Wu, 2001) (m)
d_k	Diameter of the k^{th} size class of bed material (m)
$d_{\%}$	Sediment diameter where % indicates the percentage of particles finer by mass than the indicated value (mm)
D	Flow depth or hydraulic mean depth (m)
D_{bk}	Deposition (downward) fluxes of the k^{th} size class of sediment at the interface between suspended-load zone and bed-load zone $(kg/s.m^2)$
D_S	Sedimentation diameter (m)
e	Void ratio
E_{bk}	Entrainment (upward) fluxes of the k^{th} size class of sediment at the interface between suspended-load zone and bed-load zone $(kg/s.m^2)$
f_{Cor}	Coriolis parameter
f'	Friction factor
g	Gravitational acceleration (m/s^2)
G_S	Specific gravity of the sediment
h	Tailwater depth above original ground surface (m)
	Water depth (m)
h_1	Head of water above the weir crest (m)

H	Total energy head (m)
J_a	Joint alteration number
J_n	Joint set number
J_r	Joint roughness number
J_s	Relative ground structure number
k	Turbulence kinetic constant
k_s	Roughness height of the bed surface (m)
K	Erodibility Index
K_b	Particle/block size parameter
K_d	Discontinuity/inter-particle bond shear strength number
m	Power index (default value in CCHE2D Model $= 0.45$)
M_s	Mass strength number
n	Sediment porosity
	Manning's roughness value
p_{bk}	Bed material gradation
p_{hk}, p_{ek}	Hiding and exposure possibilities for the k^{th} size class of bed material
p_k	Percentage of k^{th} size class of sediment
p_m	Portion of the sediment mixture contained in the coarse and fine modes
P	Unit stream power (kW/m^2)
	Wetted perimeter (m)
PVC	Polyvinyl chloride
P'	Porosity of bed material
q	Unit discharge $(m^3/s.m)$
q_{bkx}, q_{bky}	Components of bed load transport rate in x and y directions (m^2/s)
q_{b*k}	Equilibrium transport rate of the k^{th} size class of bed load per unit width (m^2/s)
q_{t*k}	Bed-material load transport rate (m^2/s)
Q	Discharge (m^3/s)
R	Hydraulic radius (m)
Re_*	Particle Reynolds number
RQD	Rock quality designation number
S	Slope of the hydraulic gradient (m/m)
S_s	Relative density of sediment

S_0	Gradient of the bed channel (m/m)
T	Total power (W)
u	Depth-integrated velocity components in the x direction (m/s)
u^*	Shear velocity components in the x direction (m/s)
v	Depth-integrated velocity components in the y direction (m/s)
v_t	Eddy viscosity coefficient
V	Flow velocity (m/s)
V_{cr}	Critical average flow velocity (m/s)
w	Water surface width (m)
Y_S	Depth of erosion below tailwater (m)
z_{bk}	Elevation of the k^{th} size class of sediment in z direction (m)
Z	Difference between the free surface in the reservoir and the lip of the flip bucket (m)
α	Ratio between the near-bed concentration and the depth-averaged concentration
γ	Unit weight of water (N/m^3)
γ_s	Unit weight of sediment (N/m^3)
δ	Thickness of the bed-load zone (m)
ΔE	Energy loss in terms of head per unit length of flow (m/m)
ε	Rate of dissipation of turbulence energy
ε_k	Correction factor accounting for the hiding and exposure effect of nonuniform sediment transport
ε_s	Eddy diffusivity of sediment (m^2/s)
ν	Kinematic viscosity (m^2/s)
θ	Angle of the notch of the weir
	Shield's parameter
λ	Unit weight of water (N/m^3)
ρ	Density of water (Kg/m^3)
ρ_d	Dry bulk density (kg/m^3)
ρ_w	Density of water (Kg/m^3)
τ_{by}, τ_0	shear stresses on the bed surface (N/m^2)
τ_{ck}	Critical shear stress (N/m^2)
τ_{ij}	Depth integrated Reynolds stresses (N/m^2)
τ_{*k}	Dimensionless bed shear stress

ϕ_{bk}	Dimensionless bed load transport capacity
ϕ_k	Dimensionless sediment transport rate
ω	Settling velocity (m/s)
Ω	Average energy per unit area during a flood $(N.m/m^2)$
$2D$	Two-dimensional

List of Abbreviations

DWA	Department of Water Affairs
GSI	Geological Strength Index
$masl$	Metre above the sea level
$NCCHE$	National Centre of Computational Hydroscience and Engineering
RCC	Roller Compacted Concrete
RDD	Recommended Design Discharge
RMF	Regional Maximum Flood
SED	Safety Evaluation Discharge
$SEDTRA$	Sediment Transport Module in the CCHE2D Model
UCS	Uniaxial Compressive Strength

1. Introduction

1.1 Background and Motivation

The scouring process of unlined spillways is an important research topic in engineering practice. Although several studies have been conducted on erosion of rock formations in unlined spillway channels, no satisfactory methods combining both hydraulic and rock mass parameters, have been developed for the prediction of scour depth and rate of scour of rock formations. This lack of knowledge has resulted in severe damage that has resulted in major repairs at several unlined spillways where rock formations were not adequately resistant to erosion. In other cases where erosion resistant rock formations exist, spillways have been unnecessarily lined at high cost. In the case of many dams, the cost of lining a spillway channel may seriously jeopardise the feasibility of the project. On the other hand, erosion of an unlined spillway channel may result in the loss of the water, failure of the dam, loss of life and serious damage to property and negative environmental impacts.

Rock of unlined spillways is frequently subjected to intensive hydrodynamic processes, which could result in dam foundation instability. The rock resistance and the extent of failure depend on its properties and the hydraulic parameters.

In South Africa numerous unlined spillway channels have experienced severe erosion. The Marico Bosveld Dam has undergone erosion along the spillway channel which reached a depth of over $10\,m$ and led to undercutting and failure of the control weir, as reported by Van Schalkwyk (1994). The unlined spillway of Mokolo Dam scoured about $25\,m$ deep after a large flood in 1996 $(914\,m^3/s)$. Some small dams such as Osplaas Dam and Rocklands Berg Dam also experienced severe erosion that necessitated major remedial measures. These are some of a number of serious erosion cases in spillway channels observed in South Africa. This highlights the need for an in depth study of the erodibility of unlined spillway rock.

1.2 Objectives

Combining geotechnical and hydraulic concepts, rock scour of unlined spillways remains a complicated phenomenon. The prediction of the scouring process is challenging and empirical formulas have been

established to predict scour depth. Many studies have been undertaken with the aim of investigating scour depth development below plunging spillway jets, while much attention has also been given to the erosion potential of the soil along slopes or in unlined spillway channels.

Several researchers including Annandale (1995) and Van Schalkwyk (1994) have developed analytical methods that can be used to predict the occurrence and the extent of rock scour. These analytical approaches are derived from numerous laboratory tests and field observations. The key element of these methods is the existence of a significant correlation between the hydraulic and geo-mechanical properties of unlined spillways that can be used to predict scouring process of rock.

The accuracy of prediction of the occurrence and the extent of erosion is enhanced by the rapid progress of the computer software capabilities. Software development enables unique programs which create complex numerical models capable of simulating the flow and sediment transport, in order to predict erosion. Furthermore numerical methods take into account the physical, hydraulic and geo-mechanical properties of unlined spillways.

The objective of the present study is to make use of the mathematical modelling approach to examine the scouring process of unlined spillways. Therefore, in this study the results of the numerical modelling methods will be compared with actual results of erosion from laboratory tests and field observations based on a case study. Results of the comparison between physical and numerical methods will be evaluated in order to determine advantages and limits of mathematical modelling tools in the rock scour assessment of unlined spillways.

1.3 Methodology

The investigation into unlined spillway scour prediction methods was begun with an extensive review of the technical literature to establish the current state of knowledge regarding the erodibility of rock and the potential for scour under different hydraulic conditions. In this regard, various books, scientific journals, reports and guidelines were reviewed. In literature review, different conventional empirical methods used to estimate the scour depth were firstly described. Secondly, analytical approaches developed by Annandale (1995) and Van Schalkwyk (1994) providing a basic understanding of the erosion process were explained. These analytical methods establish the key parameters and relationships that can be used to predict erosion analytically. Finally, some possible mitigation measures to limit unlined spillway scour are evaluated in literature review.

A physical model of an unlined spillway was set up and tested in a laboratory flume to yield measurable data in order to be able to analyse the erosion process in a controlled environment.

Subsequently, scour of unlined spillways in physical conditions was simulated by means of a mathematical model using specialised computer programs to predict erosion. Data from field observations were also utilised as a case study for the investigation of unlined spillway scour.

Numerical modelling erosion prediction methods were applied to erosion data from laboratory tests and field observations in order to estimate and evaluate the erosion process. The results of the mathematical modelling method were then validated by a comparison of the actual erosion obtained in the physical model which includes laboratory tests and a case study.

Due to the importance of incipient motion in the study of sediment transport, various simplified incipient motion models were presented in this thesis and subsequently a simple methodology for incipient motion or scour threshold is proposed.

In this thesis, the terms *erosion* and *scour* are used interchangeably.

2. Literature Review

2.1 Background

According to Breusers and Raudkivi (1991) scouring is a natural phenomenon caused by the flow of water in rivers and streams. It occurs as part of the morphologic changes of rivers and as result of man-made structures. The scour process involves both turbulence with its great complexity and variability and sediment transport with its strong dependence on the complex interactions with turbulence flows. According to Annandale (2006), scour, another name for extreme erosion, is a term generally used to describe severe localised erosion of earth material that occurs when the erosive power of water exceeds the ability of earth material to withstand it. The extent of the resulting scour depends upon whether the bed consists of cohesive, non-cohesive or rock material. If the bed material consists of rock material, scour will depend on rock type, weathering, the presence of fissures etc. Scouring can have three major effects:

- undermining the stability of the structure itself by structural failure or increased seepage
- undermining the stability of downstream riverbed or side slopes
- the formation of the deposition of eroded material which can raise the tailwater level at the dam.

2.2 Definitions

The scour which may occur at a structure can be divided into two different categories namely; type of scour and scour in different conditions of transport. The latter is subsequently subdivided into separate groups as described by Breusers and Raudkivi (1991).

2.2.1 Types of Scour

2.2.1.1 General Scour

General scour occurs in a river or stream as the result of natural processes, irrespective of whether a structure is there or not. Armitage (2002) states that general scour can be broken down into four

sub-categories:

1. Overall degradation

   This occurs as a river adjusts to changes in the water or sediment flow. The changes may be natural or as a result of human interference. Changes could be: flow-rate variation, construction of weirs or dams, inter-basin water transfers, etc.

2. Constriction scour

   This is a special, localised case of overall degradation and occurs if a structure causes the narrowing of a water course or the rechanneling of berm or flood plain flow. As a result, the lowering of the bed level and the increased flow velocity are noticed in the constricted section.

3. Bend scour

   This is induced by the large coherent flow structure/secondary currents that are set up whenever the flow is forced to follow a curved path. These secondary currents result in increased local velocities in the vicinity of the bed on the outside of the bend and can cause scour with local depths up to twice the average flow depth (Armitage, 2002).

4. Confluence scour

   This occurs when two branches of a river meet. Differences between the two branches in terms of the flow rates, slopes, sediment transport and angle of approach relative to the downstream channel result in complicated secondary flow patterns with associated scour and deposition downstream of the confluence.

2.2.1.2 Local Scour

Local Scour is directly caused by the impact of a structure on the flow. This scour, which is a function of the type of structure, is superimposed on the general scour.

2.2.2 Scour in Different Conditions of Sediment Transport

Breusers and Raudkivi (1991) also state that scour can be classified according to the way bed material is transported by the flow and therefore they described two different categories of scour which are explained in the following subsections.

2.2.2.1 Clear-water Scour

Clear-water scour occurs if the bed material in the natural flow upstream of the scour area is at rest. The shear stresses on the bed some distance away from the structure are thus not greater than the critical or threshold shear stress for the initiation of particle movement.

2.2.2.2 Live-bed Scour

Live-bed scour also known as scour with bed material sediment transport, occurs when the flow induces a general movement of the bed material. The shear stresses on the bed, therefore, are generally greater than the critical one. Equilibrium scour depths are reached when the amount of material removed from the scour hole by the flow equals the amount of material supplied to the scour hole from upstream.

Clear-water scour can theoretically reach static equilibrium, whilst live-water scour can only reach dynamic equilibrium. This is illustrated in Figure 2.1 showing the scour depth versus time for the two types of scour and it will be noted that the scour hole develops much more rapidly in the case of live-bed scour.

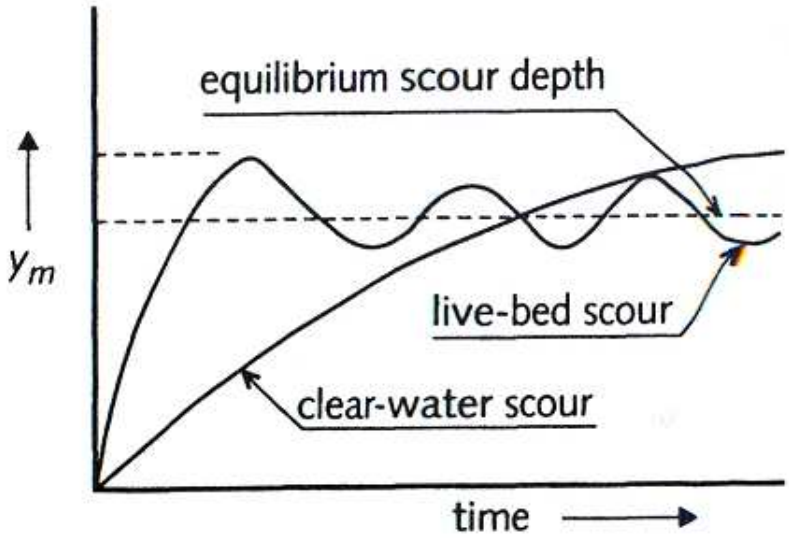

Figure 2.1: Scour depth as a function of time (Hoffmans and Verheij, 1997)

2.2.3 Phases of Scour Development

The evolution of a scour hole can be divided into four different phases namely; the initiation phase, the development phase, the stabilization phase and equilibrium phase. Different phases of scour process are illustrated in Figure 2.2.

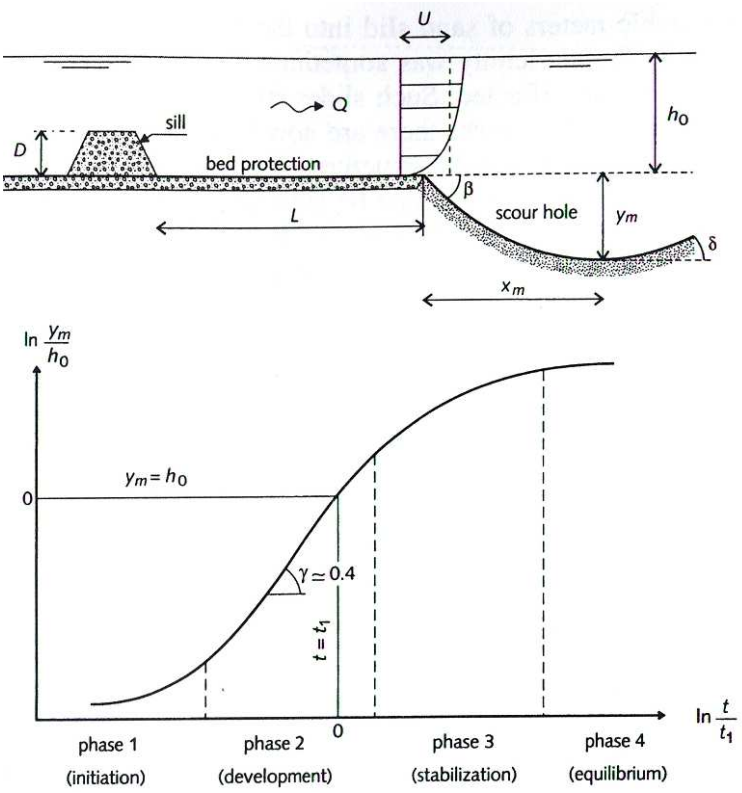

Figure 2.2: Development of scour process (CUR, 1995)

2.2.3.1 The Initiation Phase

In the initiation phase, the transport capacity of the flow leading to sediment transport along the original bed entails gradual erosion downstream of the bed protection. The duration of this phase is generally short.

2.2.3.2 The Development Phase

Due to the enlargement of the scour hole, flow separation starts in this phase. As a result, a circulation flow takes place and near-bed velocities inside the eddy are directed towards the structure, whereas they are in the direction of the main flow outside the eddy. Thus, the stabilisation of the upper slope of the scour hole is reached. This development phase generally lasts much longer than the initiation phase.

2.2.3.3 The Stabilisation Phase

The depth of the scour hole in this phase becomes so large that the decreasing near-bed velocities almost reach either the critical value of initial motion and transport of sediment or a value corresponding to the upstream sediment transport. Therefore, the scour development in the stabilisation phase stops or proceeds very slowly.

2.2.3.4 Equilibrium Phase

The near-bed velocity or shear stress is equal to the critical value in the case of clear-water scour and equal to the upstream value of the undisturbed under live-bed condition. At this stage, the local flow is not able to carry sediment out of the scour hole, against its downstream slope. As a result, the maximum depth of the scour hole is reached and defined as equilibrium depth.

2.2.4 Types of Rock

Geologists divide all rock into three primary groups depending on their mode of formation (CUR, 1995):

1. Igneous rock

   This is formed by the crystallisation and solidification of a molten silicate magma.

2. Sedimentary rock

   This is formed by the sedimentary and subsequent lithification of mineral grains, either under water or more rarely on an ancient land surface.

3. Metamorphic rock

   This is formed by the effect of heat and pressure on igneous or sedimentary rocks for geological

periods of time with the consequent development of new minerals and textures within the pre-existing rock.

In addition, the three primary groups are also subdivided into some eighteen families of rock as indicated in Table 2.1.

Table 2.1: Families of rocks (CUR, 1995)

IGNEOUS	SEDIMENTARY	METAMORPHIC
Granite	Quartzite	Slate
Diorite	Sandstone	Phyllite
Gabbro	Siltstone	Schist
Rhyolite	Shale	Gneiss
Andesite	Limestone	Marble
Basalt	Chalks	
Serpentine		

It is to be noted that characteristics of each family of rock are similar in terms of engineering properties and applicability.

2.3 Unlined Rock Scour

Although the scouring is most pronounced in alluvial materials, deeply weathered rock can also be vulnerable in certain circumstances. Unlined rock can provide an economical discharge channel where the excavated material is to be used elsewhere in the dam construction. Field observations have shown that scouring can progressively undermine the foundation of a structure. Due to high costs involved in the complete protection of a structure against scouring, guidance and control of scouring remain the reasonable way to minimise the risk of failure. Unfortunately information on resistance of rock to erosion is limited, and assessments are largely based on judgement and the behaviour of other similar spillways. Rock scour is essentially caused by the erosive action of flowing water, excavating and carrying away loose material from the bedrock. Previous studies on the erosion process have identified short-term changes in streambed morphology as scour and fill phenomena, whereas long-term changes are referred to as degradation and aggradation processes (Stephen and Michael, 1999). It is worth noting, however,

that erosive processes in rock can be significant over both time intervals that is, during one extreme flood event or during decades of average flow conditions. Accordingly, scour can occur in any rock mass given sufficient time.

The potential for scour of a rock mass is a complex function of the geologic and geotechnical characteristics of the rock namely; lithology, the characteristics of discontinuities and rock mass quality, strength and abrasion resistance as well as the hydraulic parameters such as boundary shear stresses, the frequency and duration of flood events and bedload composition.

2.4 Conceptual Models of Rock Scour

A conceptual model of jointed rock scour including both hydraulic and geological factors has been developed by Akhmedov (1988). This model consists of three modes or stages of scour and the key parameters of these stages are the velocity and turbulence of water adjacent to the rock. These modes of scour are described in the following paragraph.

1. The first stage is characterised by the removal of rock fragments due to hydraulic pressure gradients which are essentially induced by the turbulence of the flow. At this stage, the removal process is mainly influenced by rock jointing and the strength properties of the rock are less significant in this mode of scour. To remove a fragment, the flow must overcome that fragment's weight and its cohesive resistance in order to pull it out of the rock mass. Although the energy decreases as the scour depth increases, the energy of the flow is still large enough to cause hydrodynamic pressure fluctuations.

2. At the second stage of scour, the flow velocity and the bed-flow energy decrease as a result of the increase in the flow area, but the turbulence and flow energy are still great enough to remove fragments. In this mode of scour, the strength properties of the rock and the abrasive forces are more important. The latter contribute to the reduction of the weight of the fragment which is easily dislodged and removed by the flow.

3. The last mode of scour is simply described as the abrasive stage of scour. The flow energy is not sufficient and reaches the point where the flow cannot disturb the rock fragments from their equilibrium condition. It should be noted that the strength properties of the rock are very important in this mode of scour.

A similar conceptual model of rock scour is also illustrated in a paper published by Annandale (1995). According to the author, a conceptual model of scour is viewed as a process of progressive dislodgement characterised by three stages:

- Jacking
- Dislodgement
- Displacement

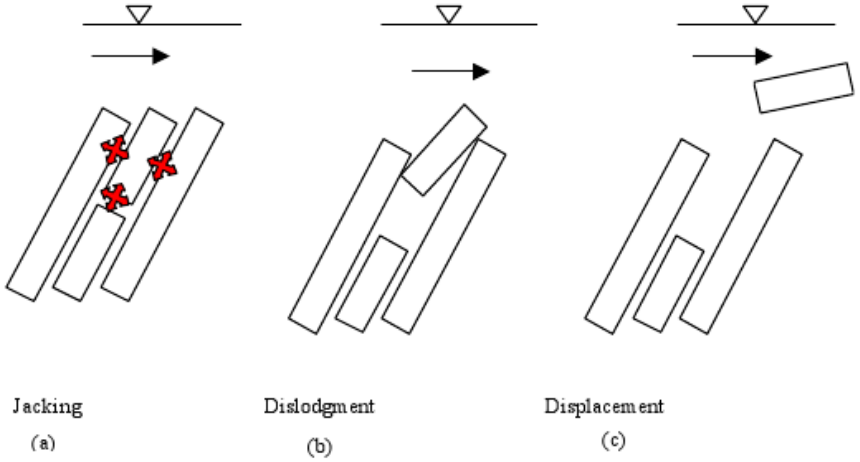

Figure 2.3: Conceptual model explaining erosion process in rock (Annandale, 1995)

Figure 2.3 is a simplified illustration of this conceptual model of rock scour with three stages of scour in a stratum (layer of a particular type of rock) of jointed rock with a dip against the direction of flow. A dip is defined as the angle between the horizontal plane and the plane of the discontinuities within the rock. The flow of water at the surface of the rock material will penetrate the discontinuities existing within the rock and, consequently, the water pressure in the discontinuities will equal the hydrostatic head above it. In most problems pertaining to scour process, the turbulence of water is more pronounced at the bed. As a result of this, pressure fluctuations are created at the bed and subsequently, the net forces acting on the blocks of rock can be determined. According to Annandale et al. (2000), the net pressures acting on blocks of rock are defined as the algebraic sum of the hydrostatic pressure within the rock material and the fluctuating pressures at the surface of the bed.

The first stage of scour in this conceptual model of rock scour is characterised by the occurrence of pressure fluctuations capable of progressively jacking material units out of their positions of rest (Figure

2.3.(a)).

At the second stage of scour, material units are dislodged due to the power of the flowing water (Figure 2.3.(b)). They are finally displaced as shown in Figure 2.3.(c).

Generally, rock scour occurs when the erosion resistance of rock material is exceeded by the forces induced by pressure fluctuations. Therefore, methods to predict the occurrence of rock scour require the quantification of the relative magnitude of fluctuating pressures in flowing water and the relative ability of rock material to resist erosion, as pointed out by Annandale (1995).

2.5 Overview of Different Methods to Predict Scour of Rock

Numerous methods exist to predict the erosion of rock formations and these methods can be subdivided into physical hydraulic model studies, rigorous constitutive model and empirical methods. Physical hydraulic model studies are conducted through conventional procedures and provide qualitative information regarding the scour process. The rigorous constitutive model based on Keyblock Theory (Annandale et al., 2000) is directed at solving scour problems in hard rock blocks. Conventional empirical methods primarily deal with predicting scour in cohesionless granular material. The analytical approach to predict scour of rock is proposed by Annandale (1995) and Van Schalkwyk (1994). This approach is a semi-empirical method based on field observations and laboratory tests and provides a unique relationship between the hydraulic and geo-mechanical properties.

The different methods to predict scour of rock are outlined in the next subsections.

2.5.1 Keyblock Theory

Keyblock Theory basically consists in providing a rigorous solution for the removability of block from a rock mass. This theory describes the joint sets and free faces as three-dimensional planes by their dip (angle from horizontal) and dip direction (angle from north) and identifies the combination of joints that form blocks which may be removed from the rock mass. Furthermore, the stability of such blocks can be calculated using three-dimensional limit equilibrium techniques knowing the strength of the joint planes and the forces acting on these particular blocks (Annandale et al., 2000).

The procedure of the Keyblock Theory for the examination of the removability of blocks from a rock

mass was developed by Goodman and Hatzor (Annandale et al., 2000) and described by the following steps:

1. Joints are mapped, plotted on stereographic projection, and divided into joint sets. Each joint set is linked to a representative attitude, spacing and friction angle.

2. Block Theory is used to analyse each sub-combination of three joint sets in order to determine removable combinations.

3. The relative failure likelihood for each removable sub-combination is assessed by examining the angles between the joints, the friction angles of the potential sliding faces and the frequencies of the bounding joints. Blocks of the most likely combinations with a high probability to be removed from rock mass are described as "critical keyblocks.

4. The traces of the bounding joints of the critical keyblocks are marked and drawn in the same way they would appear on the area of interest. These traces are then compared to trace maps or photo overlays of joints on the actual surface in order to identify actual critical keyblock faces.

5. After identifying critical keyblocks under their own weight, a limit equilibrium analysis is perfomed to find the faces that would tend to open upon movement of the block in its probable mode of sliding.

6. A water pressure is assigned to the potential open faces of the critical keyblocks and the limit equilibrium analysis is repeated. In this theory, a factor of safety which is less than one means that the block is unstable and, therefore, would be subject to a removal by the flowing water.

The concept of Keyblock theory is well illustrated in Figure 2.4. If the keyblock is removed, as shown in (b), it causes the removal of the next keyblock (c), and the next (d), and so on. This sequential of removal of rock is known as the keyblock effect (Annandale, 2006).

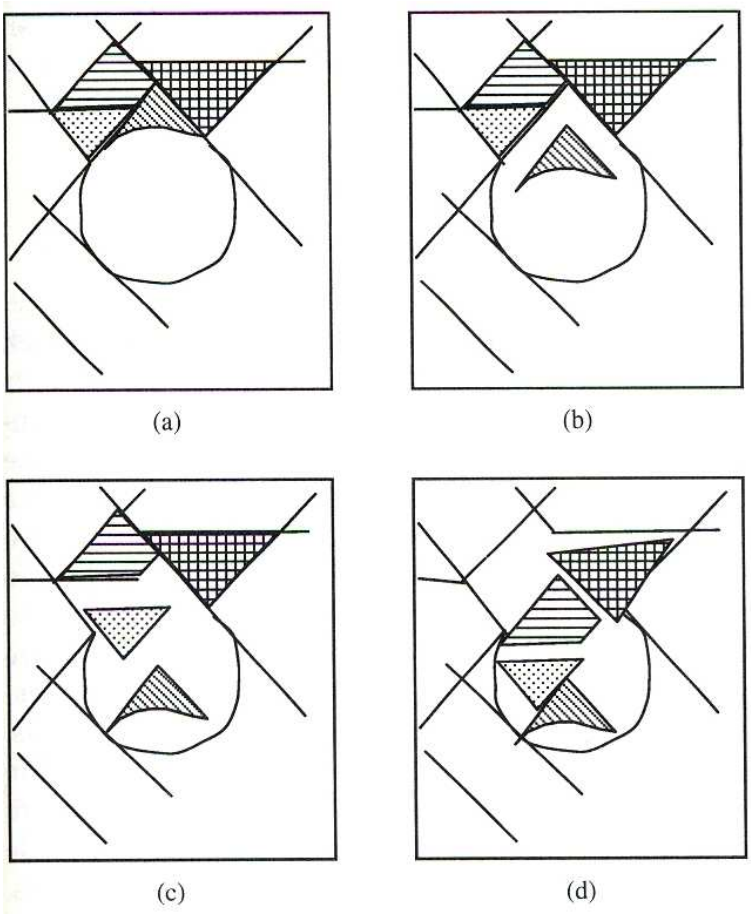

Figure 2.4: Illustration of keyblock effect (Annandale, 2006)

2.5.2 Existing Methods for the Evaluation of Ultimate Scour Depth

Most of the conventional empirical equations that are used to calculate scour depth were derived from data on scour obtained from small scale tests with non-cohesive material or from field observations (Breusers and Raudkivi, 1991).

Details on conventional empirical equations are given in the next subsections.

2.5.2.1 Veronese Equation

Veronese Equation (2.1) (Breusers and Raudkivi, 1991) is used to predict the scour depth in a plunge pool.

$$Y_S = 1.90 H^{0.225} q^{0.54} \tag{2.1}$$

where,

Y_S = depth of erosion below tailwater (m)

H = elevation difference between reservoir and tailwater (m)

q = unit discharge $(m^3/s.m)$

Equation 2.1 is recommended by USBR (United States Bureau of Reclamation) to be used as a limiting scour depth (Breusers and Raudkivi, 1991).

2.5.2.2 Yildiz and Uzucek Equation

This equation presents the modified version of the Veronese Equation (2.1) by including the angle α (incidence from the vertical of the jet) (Annandale et al., 2000).

$$Y_S = 1.90H^{0.225}q^{0.54}cos\alpha \tag{2.2}$$

2.5.2.3 Eggenberger Equation

The Eggenberger Equation (2.3) (Breusers and Raudkivi, 1991) is derived for an overflow weir.

$$Y_S = 22.88H^{0.5}q^{0.6}d_{90}^{0.40} \tag{2.3}$$

where,

Y_S = depth of erosion below tailwater (m)

H = elevation difference between reservoir and tailwater (m)

q = unit discharge $(m^3/s.m)$

d_{90} = grain size of foundation material for which 90% is smaller (mm)

Breusers and Raudkivi (1991) found that Equation 2.3 tends to overestimate the prediction of the value of scour depth.

2.5.2.4 Damle et al. Equation

Equation 2.4 was initially developed from model data and some field data of Indian dams with ski jumps (Raudkivi, 1998).

$$Y_S = 0.55(qH)^{0.5} \tag{2.4}$$

where,

Y_S = depth of erosion below tailwater (m)

q = unit discharge $(m^3/s.m)$

H = elevation difference between reservoir and tailwater (m).

2.5.2.5 Chian Min Wu Equation

The Chian Min Wu Equation (2.5) (Raudkivi, 1998) was derived from model and prototype data from dams in Taiwan.

$$Y_S = 1.18q^{0.51}H^{0.235} \tag{2.5}$$

where,

Y_S = depth of erosion below tailwater (m)

q = unit discharge $(m^3/s.m)$

H = elevation difference between reservoir and tailwater (m).

2.5.2.6 Martins Equation

The Martins Equation (2.6) (Raudkivi, 1998) was derived from prototype observations and given by:

$$Y_S = 1.5q^{0.6}Z^{0.1} \tag{2.6}$$

where,

Y_S = depth of erosion below tailwater (m)

q = unit discharge $(m^3/s.m)$

Z = height difference between the free surface in the reservoir and the lip of the flip bucket (m).

2.5.2.7 Mason and Arumugam Equation

Mason and Arumugam (Breusers and Raudkivi, 1991) analysed model and prototype data from outlet types including low level outlets, tunnel outlets, free overfalls and spillway chute flip buckets . This led to the following relationship.

$$Y_S = Kq^x H^y h^{0.15} g^{-0.3} d_m^{-0.1} \tag{2.7}$$

where,

K = $6.42 - 3.1H^{0.10}$

x = $0.6 - 0.0033H$

y = $0.05 + 0.005H$

Y_S = depth of erosion below tailwater (m)

q = unit discharge $(m^3/s.m)$

H = elevation difference between reservoir and tailwater (m)

h = tailwater depth above original ground surface (m)

d_m = median grain size of foundation material(m) (assumed to be $0.25\,m$ for prototype data)

g = gravitational acceleration (m/s^2)

2.5.2.8 Hartung Equation

Hartung (Raudkivi, 1998) proposed the following equation after repeating the tests done by Veronese (see subsection 2.5.2.1):

$$Y_S = 12.40H^{0.36}q^{0.64}d_{85}^{-0.32} \tag{2.8}$$

where,

Y_S = depth of erosion below tailwater (m)

H = elevation difference between reservoir and tailwater (m)

q = unit discharge $(m^3/s.m)$

d_{85} = grain size of foundation material for which 85% is smaller(m)

Although the Eggenberger Equation (2.3), the Mason & Arumugam Equation (2.7) and the Hartung Equation (2.8) contain an allowance for particle diameter, the material properties are generally not specified in the above-mentioned empirical formulas for predicting scour depth.

2.6 The Annandale and Van Schalkwyk Procedures for Evaluating Rock Scour

2.6.1 Annandale's Method

Annandale (1995) developed an analytical method for evaluating scour of rock masses. This method also known as the Erodibility Index Method utilises information obtained from the analysis of scour

events from approximately 150 field observations of spillway performances and published laboratory data regarding the erosion process. This approach is basically based on the rational correlation between an earth material's resistance to erosion and the erosive power of water. As a result, an erosion threshold is established by plotting the Erodibility Index for different rock types and cohesive and non-cohesive granular soils against stream power, and noting whether scour occurred or not for each event under consideration.

2.6.1.1 Erodibility Index

The Erodibility Index that was used to quantify the relative ability of the earth material to resist erosion is identical to Kirstens Excavatability Index (Kirsten, 1982). Kirstens Excavatability Index is used to characterise rock in order to determine the power requirements of earth moving equipment that can rip the subject material. It makes use of primary geo-mechanical properties such as earth mass strength, particle size, discontinuity/inter-particle bond shear strength, and the shape and orientation to flow of the material particles, to calculate the earth material's unique erodibility index value. These geo-mechanical properties are easily determined by making use of borehole data as well as using simple field tests and measurements. The Erodibility Index , as formulated in the Erodibility Index Method, is expressed as the product of four parameters and calculated using the following equation:

$$K = M_s K_b K_d J_s \tag{2.9}$$

where,

- K is the Erodibility Index which is a dimensionless value.
- M_s represents the mass strength number. It is the product of material's uniaxial compressive strength and its coefficient of relative density (Refer to Table A.1 in Appendix A for values).
- K_b is a particule/block size parameter. This number is a measure of the mean block size for rocks. For rock material, particle/block size number is calculated by Equation 2.10

  $$K_b = \frac{RQD}{J_n} \tag{2.10}$$

  where RQD is the rock quality designation number, which is a standard drill core logging parameter and J_n is the joint set number which is a function of the number of joints in a certain rock mass (Refer to Tables A.2 and A.3 in Appendix A for these values).

- K_d represents the discontinuity/inter-particle bond shear strength number. This number indicates the shear strength of inter-particle bonds in soils and the strength of joint interfaces in rocks. It is determined by the ratio J_r/J_a where J_r is the joint roughness number and J_a represents the joint alteration number (Refer to Table A.4 in Appendix A for these values).

- J_s represents the relative ground structure number. This number accounts for the complexity of the ground structure and is a function of the joint set spacing, dip angles and dip directions. It is also a measure of the shape of the material unit and the ability with which water can penetrate the ground and dislodge an individual unit (Refer to Table A.5 in Appendix A).

The erodibility index can be calculated using Equation 2.11 and the values of the parameters are determined by making use of tables and equations that are published in Annandale (1995) and Kirsten (1982)

$$K = M_s[RQD/J_n]J_s[J_r/J_a] \tag{2.11}$$

2.6.1.2 Stream Power

The relative magnitude of the erosive power of water is quantified by the stream power, also known as rate of energy dissipation. This parameter is used because of the following reasons:

i) Turbulence causes both pressure fluctuations and energy loss.

ii) Increases in turbulence intensity will result in increased rates of energy dissipation and increases in the magnitude of fluctuating pressures.

Therefore estimates of the rate of energy dissipation should represent the relative magnitude of fluctuating pressure, and thus the erosive power of the water (Annandale 1995). Equation 2.12 represents the rate of energy dissipation per unit area (kW/m^2) in an open channel flow,

$$P = \gamma q \Delta E \tag{2.12}$$

where,

P = stream power (kW/m^2)

γ = unit weight of water $(9.81\,kN/m^3)$

q = unit discharge $(m^3/s.m)$

ΔE = energy loss in terms of head per unit length of flow (m/m)

2.6.1.3 Erodibility Threshold

After compiling case study data for numerous unlined spillways, Annandale (1995) plotted the Erodibility Index versus the Rate of Energy Dissipation and noted cases where scour was observed in the rock at the base of the channels. This data plotted in Figure 2.5 shows clearly that there exists a threshold for scour.

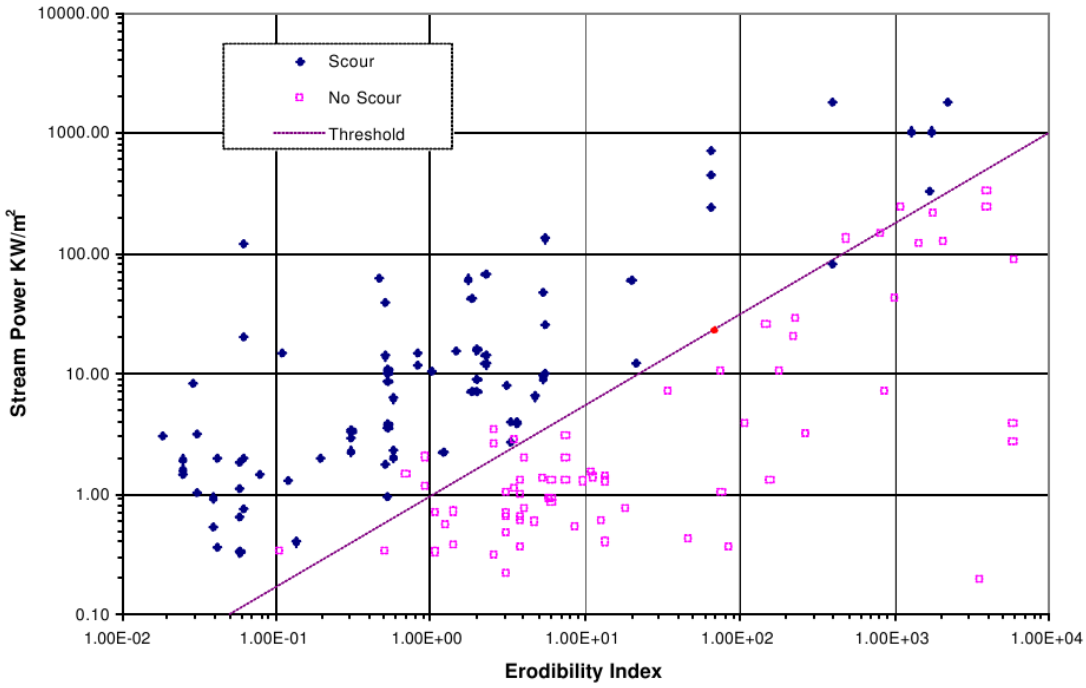

Figure 2.5: Erosion threshold as defined by the Erodibility Index Method (Annandale et al., 2000)

Given the erosion threshold, only the Erodibility Index of the rock is required to establish the flow conditions necessary for the initiation of scour. Annandale (1995) shows that the correlation between

rate of energy dissipation (P) and a material's resistance (K) to erosion can be expressed as the function:

$$P = f(K) \tag{2.13}$$

at the erodibility threshold. If $P > f(K)$, the erodibility threshold is exceeded, and the material can be expected to erode. Conversely, if $P < f(K)$, the erodibility threshold is not exceeded, and erosion is not predicted. The identification of threshold conditions at which scour will occur in rock is extremely useful as this method can be used as a screening tool for spillways excavated into rock.

2.6.2 Van Schalkwyk's Method

Van Schalkwyk's (1994) work is essentially based on the field observations of eighteen unlined spillways that represent nine major rock types as well as some modelled laboratory tests. Similar to the Erodibility Index Method discussed in the previous subsections, Van Schalkwyk's approach attempted to establish a correlation between the observed erosion, the hydraulic properties of the peak flow responsible for the erosion and the rock mass condition. Van Schalkwyk (1994) classified the potential extent of erosion in three categories, namely: no erosion, little to moderate erosion and excessive erosion.

2.6.2.1 Rock Characterisation

Van Schalkwyk (1994) makes use of the Kirsten excavation index (K) as defined by Equation 2.9 to evaluate the geo-mechanical properties of rock mass.

2.6.2.2 Unit Stream Power

Based on the previous work done by researchers including Rooseboom and Kirsten, Van Schalkwyk (1994) decided to use the unit stream power as hydraulic parameter to predict the erosion process of rock. Therefore the main channel within each spillway is identified in order to determine longitudinal profiles. Total stream power (T) is calculated as follows :

$$T = \rho g Q H \tag{2.14}$$

where,

T = total stream power (W)

ρ = density of water $(1000\,kg/m^3)$

g = gravitational acceleration $(9.81\,m/s^2)$

Q = stream flow (m^3/s)

H = total energy head (m)

According to Van Schalkwyk (1994), Unit stream power (P) is the total power (T) divided by the area (A) on which it is dissipated: $(P = T/A)$.

For flow in channels, the unit power (P) is expressed as follows:

$$P = \rho g q S \tag{2.15}$$

where,

P = unit power (W/m^2)

q = discharge per unit width $(m^3/s.m)$

S = dH/dx, the slope of the hydraulic gradient which is equal to the water surface and bed slope in uniform flow (m/m).

It is interesting to note that the calculation of stream power when using the methods of both Annandale (1995) and Van Schalkwyk (1994) results in the same answer. The difference between the methods lies in the justification of what parameters are of importance when calculating the power of water in an open channel flow.

2.6.2.3 Classification System for the Extent of Erosion

Van Schalkwyk (1994) classified the extent or class of erosion in terms of the depth below the previous or original ground (Table 2.2). The data obtained from both model and field studies indicates a good correlation between the Kirsten value and the unit stream power. In addition, the data also shows a definite grouping of different classes of erosion along three bands at positive slope on the logarithmic plots (Figure 2.6).

Table 2.2: Classification system for the extent of erosion

Depth of erosion (m)	Extent (class) of erosion
0	None (O)
$0-1$	Little (L)
$1-5$	Moderate (M)
>5	Excessive (E)

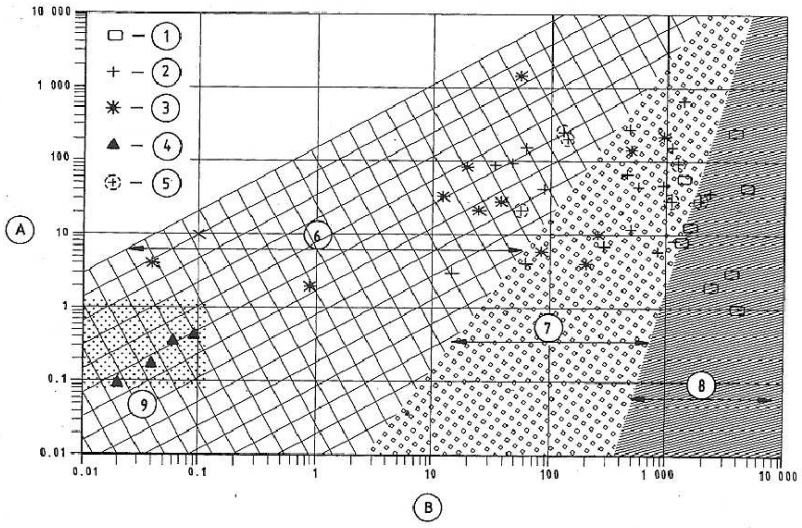

Power per unit area vs. Kirsten K_n

(A) P, power per unit area (kW/m²)

(B) K_n, Kirsten value
(1) No erosion
(2) Little - moderate erosion
(3) Excessive erosion
(4) Laboratory sample tests
(5) Direct drop cases
(6) Mainly excessive erosion
(7) Mainly moderate to little erosion

(8) Mainly no erosion
(9) Laboratory test samples (joint fill material)

Figure 2.6: Different classes of erosion (Van Schalkwyk, 1994)

2.7 Flood Characteristics and the Extent of Rock Scour

Studies conducted by Costa and O'Conner (Stephen and Michael, 1999), show that there is a close relationship between the flow duration and the extent of scour. They, therefore, describe the term "geomorphically effective floods" as flood events able to alter the stream channel and overbank area. The Erodibility Index Method developed by Annandale (1995) (see subsection 2.6.1) to assess the scour of rock utilises the maximum flow, and therefore the maximum rate of energy dissipation, as the main hydraulic variable in evaluating a threshold for scour, whereas according to Costa and O'Conner (Stephen and Michael, 1999), the duration and the intensity of the flood are the most important hydraulic variables related to the extent of scour. Their conceptual model is depicted in Figure 2.7.

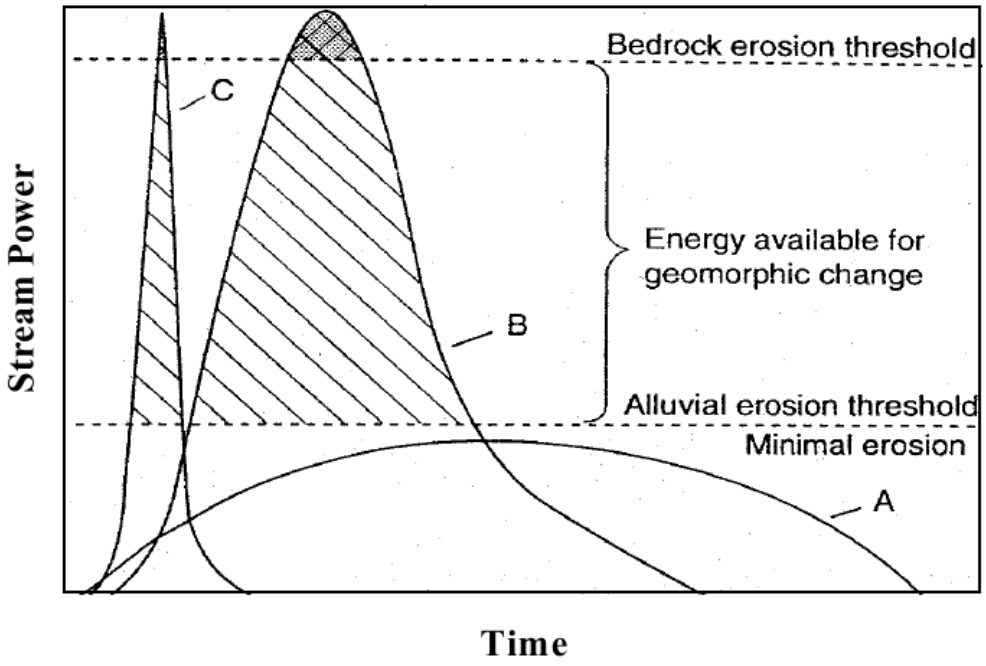

Figure 2.7: Conceptual stream power graphs for different floods (Stephen and Michael, 1999)

This model expresses the intensity of a flood as a stream power which is similar to the rate of energy dissipation developed by Annandale (1995). Flood (A) is a long duration flood that would cause insignificant scour due to low power flood. Flood (B) with a high intensity and long duration could cause significant rock scour, whereas Flood (C) is a short duration, high power flood with potentially small scour. Further studies done by Costa and O'Conner (Stephen and Michael, 1999) establish a relationship between the geomorphic effectiveness of a flood and the cumulative stream power during

a flood which is the stream power integrated with respect to time. From this study, an average energy per unit area during a flood (Ω) is given as:

$$\Omega = \int \frac{\lambda Q S}{w} dt \tag{2.16}$$

where,

Ω = average energy per unit area during a flood ($N.m/m^2$)

λ = unit weight of water (N/m^3)

Q = discharge (m^3/s)

S = energy grade (m/m)

w = water surface width (m)

dt = duration of the flood event (s)

2.8 Incipient Motion Theory

2.8.1 Background

Due to the importance of incipient motion in the study of sediment transport, various simplified incipient motion models were presented in this thesis. Incipient motion is defined as the conditions under which the movement of sediment, and hence scour, will begin. Due to the stochastic nature of sediment movement along the bed, it is difficult to determine precisely at what flow condition a sediment particle will begin to move (Yang, 2003). However, significant progress has been made on the study of incipient motion, both theoretically and experimentally.

Incipient motion can be described in terms of flow velocity, bed shear stress and unit stream power. The main focus of the following incipient motion theory review will be placed on incipient motion in terms of shear stress and in terms of velocity.

Different approaches to characterise the incipient motion are described in subsequent sections.

2.8.2 Shear Stress Approach

The incipient motion theory in terms of shear stress was developed by Shield known as one of the most cited references in field of sediment transport and river hydraulics (Armitage and McGahey, C. (2003)).

Based on experiments covering developed sediment motion and using dimensional analysis, Shield shows

that drag force is a function of the particle diameter, the particle density, the fluid viscosity, the bed form, the particle Reynolds Number and the bed shear stress. By assuming that resistance to motion depends only on the form of the bed and the immersed weight of the particles, Shield deduces the "Shield's parameter" θ as a dimensionless shear stress. The Shield's parameter is a function of the particle Reynolds Number Re_*, and is defined as follows:

$$\theta = \frac{\tau}{(\gamma_s - \gamma)d} = \frac{u_*^2}{(S_s - 1)gd} \tag{2.17}$$

where,

θ = shield's parameter

τ = bed shear stress (N/m^2)

d = particle diameter (m)

S_s = γ_s/γ

γ_s = unit weight of sediment (N/m^3)

γ = unit weight of water (N/m^3)

u_* = shear velocity $(\sqrt{\tau/\rho})(m/s)$

g = gravitational acceleration (m/s^2)

The erosion threshold relationship between the dimensionless shear stress and the particle Reynolds number is given by Shield's diagram depicted in Figure 2.8

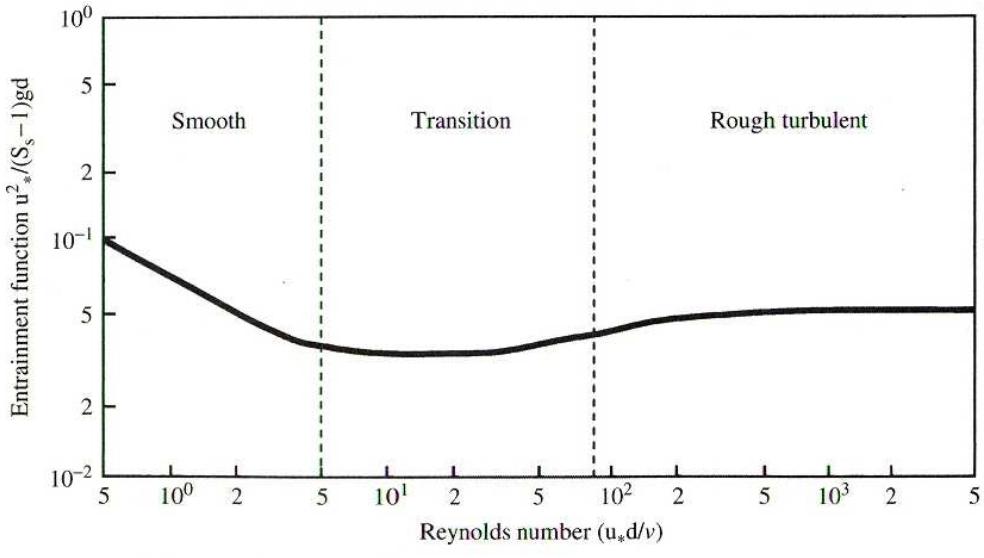

Figure 2.8: Shields diagram to determine conditions of incipient motion for non-cohesive granular material (Annandale, 2006)

According to Shield's diagram, Shield's parameter varies inversely to the particle Reynolds number in a laminar boundary flow region whereas in a region of fully developed turbulence the Shields parameter increases slightly and then stabilises reasonably at a value of approximately 0.05 to 0.06 (Annandale, 2006). A value of 0.056 as Shield's parameter value for the same region of turbulence is given by Henderson (1966).

2.8.3 Velocity Approach

Based on the unit stream power, Yang (2003) developed a graph to determine conditions of incipient motion that relates the particle Reynolds number (Re_*) to dimensionless critical velocity (V_{cr}/ω). The threshold relationship is expressed as follows:

$$\frac{V_{cr}}{\omega} = \frac{2.5}{\log(Re_*) - 0.006} \quad \text{for} \quad 1.2 < Re_* < 70 \tag{2.18}$$

and

$$\frac{V_{cr}}{\omega} = 2.05 \quad \text{for} \quad Re_* \geq 70 \tag{2.19}$$

where V_{cr} is the critical average flow velocity that initiates the particle movement and ω is the settling velocity of the sediment particle. The incipient motion relationship as described by Yang (2003) is shown in Figure 2.9.

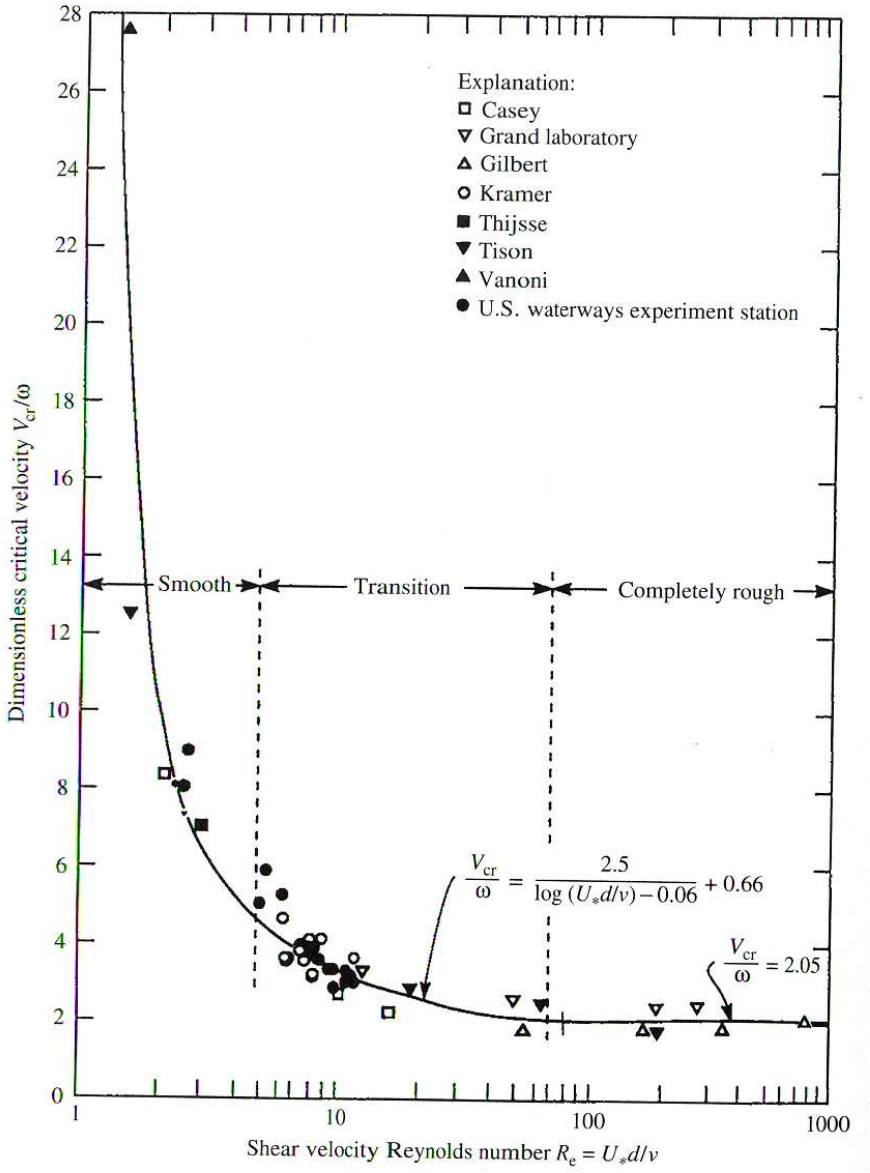

Figure 2.9: Relationship between dimensionless critical average velocity and particle Reynolds number (Yang, 2003)

In this relationship three different flow conditions leading up to incipient motion were defined namely; smooth, transition and completely rough conditions.

A simple methodology for incipient motion or scour threshold based on stream power is proposed in chapter 6.

2.9 Mitigation Measures to Limit Unlined Spillway Scour

2.9.1 Background on Mitigation Measures

The main objective of mitigations is to minimise or reduce unlined spillway scour under conditions of the necessary primary hydraulic design criteria for flood. Therefore the spillway surface need to be evaluated in order to choose the mitigation methods required to maintain the spillway under Recommended Design Discharge (RDD) or Safety Evaluation Discharge (SED). However RDD or SED have insignificant relation to the ability of unlined spillway rocks to resist the erosion process. Although the above mentioned hydraulic parameters are used in the hydraulic design phase of spillway structure, they do not take into account the geotechnical aspects of unlined spillways. As a result of this, numerous unlined spillways experience severe channel erosion during overflow representing only a small fraction of the design discharge (Cameron et al., 1988).

Basically mitigation techniques for unlined spillways are based on the ability of the spillway channel earth materials to withstand erosion and, therefore, site-specific identification of material properties leading to erosion must be established.

2.9.2 Mitigation Measures for Unlined Spillway Scour

Most of mitigation techniques for unlined spillways that have been discussed in this study are well proven in a variety of engineering applications. Although these techniques are not well documented for use on unlined spillways, they can, nevertheless, provide viable and cost-effective alternatives to scour problems at many unlined spillways.

According to Cameron et al. (1988), potential remedial engineering techniques for unlined spillway scour include cement-based methods such as grouting, shotcrete, soil cement/rollcrete, and high-strength unreinforced and reinforced concrete and also rock bolts, wire mesh, gabions and riprap. Potential erosion preventive measures comprise of the construction of energy dissipators, cutoff walls, and the removal of vegetation and other obstacles to flow. In addition, reservoir drawdown or pre-release before floods, flow routing, the relief of uplift pressures, and the placement of geotechnical and natural grasses could also be used as useful alternatives. More details on different mitigation techniques for unlined spillways scour are given in the following sections.

2.9.3 Reservoir Drawdown or Pre-release before Floods

According to Cameron et al. (1988), the technique of reservoir drawdown consists of lowering the reservoir water level before the flood season in order to allow the unlined spillway to experience flow with velocities and heads less than those estimated to initiate erosion. This approach is considered as a temporary solution, reducing the potential for erosion of unlined spillways and it is not applicable to dams without mechanical regulatory structures. This method can provide additional reservoir storage capability where the reservoir is used as flood regulation facility and subsequently, reduces potential for negative downstream impacts. On the other hand, this technique cannot be applied where the dam is primarily for hydropower, navigation or irrigation because this could lead to water supply loss. Flood warning is required and pre-releases could lead to larger floods downstream compared to what is coming into the dam.

2.9.4 Cement-Based Method

Concrete and cement-based pavings are traditional linings materials for a wide range of spillway channel construction and repair applications. Most of the cement-based mitigation techniques tend to eliminate or decrease the possibility of rock plucking occurring within unlined spillway channel. In many cases, the cement-based approach could be the best choice to mitigate erosion impacts on unlined spillways (Cameron et al., 1988). On the other hand, in some cases the application of these mitigation techniques is cost-prohibitive or inappropriate. Commonly used as a reinforced lining blanket, cement-based technique comprises of grouting, lean concrete, high-strength concrete, rollcrete, reinforced concrete and dental concrete.

More details on cement-based techniques for scour mitigation of unlined spillways are given in the following paragraphs.

2.9.4.1 Grouting

Unlike most of cement-based mitigation techniques that are applied by workers and/or machines to the area of interest, grout is a cement or chemical-based mixture generally placed by borehole injection in voids and open rock discontinuities that are not accessible by workers or equipment. There are two types of grout namely; chemical grout which is used for soil consolidation and Portland cement which

is generally used to consolidate a mass of rock. Grouting techniques have many advantages which are:

- to consolidate or strengthen the whole rock mass by grout filling the open discontinuities
- to strengthen the entire treated rock mass in order to increase the overall strength of the rock mass
- after consolidation the grouted rock mass could likely resist uplift forces even during the maximum flood discharge event.

2.9.4.2 Lean Concrete

Lean concrete is defined as a low cement content mixture comprising of fine sand, aggregate and cement. Its main purpose is to fill voids and open discontinuities in order to prevent plucking and increase erosion resistance. According to Cameron et al. (1988) lean concrete is assumed to be a low-cost material and is typically used where high structural loads are absent, for instance it can be used to fill discontinuities located in the channel bottom .

2.9.4.3 Shotcrete

Shotcrete is a specific mixing and placement method. The shotcrete mitigation technique consists of spraying concrete on the area of attention through a nozzle equipped with a perforated manifold. Due to its low water-cement ratio, shotcrete can reach a high compressive strength, as pointed out by Merritt (Cameron et al., 1988) and therefore can play an erosion resisting and rock mass reinforcing role in unlined spillways. This mitigation method is recommended for exposed inclined surfaces.

2.9.4.4 High-strength Concrete

High-strength reinforced or unreinforced concrete consists of varying mixtures of concrete so that abrasive resistance and compressive strength are provided. These mixtures comprise of a basic concrete mixture, silica fume and a high-range water reducer providing a low water-cement ratio and a hard aggregate. Although high-strength concrete is especially effective in resisting abrasive-erosion at unlined spillways, it remains the most expensive of concrete-based treatments when applied over large areas (Cameron et al., 1988). In addition, its application requires drainage facilities to withstand uplift pressures.

2.9.4.5 Soil Cement and Rollcrete

Rollcrete is a combination of a small fraction of cement mixed with soil before compaction and it is used to fill in relatively large voids. This technology is widely and successfully used as a remedial measure to erosion on some unlined spillways (Cameron et al., 1988). Nevertheless, it is generally not recommended for primary resistance to erosion and has relatively high shear strength and very low compressibility when placed in thick bodies (Cameron et al., 1988).

2.9.4.6 Reinforced Concrete

Reinforced concrete is the cement-based mitigation technique that has commonly been used for a long time in hydraulic structure. Its particularity lies in the use of large amounts of reinforced steel which must be installed before placement of the concrete. This makes reinforced concrete cost-prohibitive when it has to be applied over a large area of unlined spillways. Therefore this remedial technique is recommended only for use in a small portions of the spillway channel. Special care should be taken not to allow flood waters to flow beneath a reinforced concrete section in order to avoid the removal of the subgrade material that can be caused by turbulence which could possibly lead to the failure of the remedial measures. Although reinforced concrete often proves to be very expensive and susceptible to undercutting erosion, it is believed that it offers highest assurance of erosion resistance for unlined spillways, under conditions of proper placement.

2.9.4.7 Dental Concrete

Dental concrete mitigation technique is based on the use of high-strength concrete to fill in irregularities on excavated bedrock. This technique is generally applied directly to joint-bounded surfaces in order to yield a high-integrity bond between rock and concrete. As a result, the dental concrete technique is basically suitable to remediation at unlined spillways in which the high-strength concrete is used to fill in joint-bounded surfaces on dipping and jointed bedrock. One great advantage of dental concrete is that it does not only reduce the entrance of water into the joints but also smooths the channel surface which contributes to a decrease in the flow turbulence and, therefore, keeps overall erosive forces to a minimun. To be more effective, dental concrete can be used in conjunction with rock bolts.

Rock bolting is a technique that essentially consists of distributing compressive forces across discontinuity

surfaces. This helps to withstand sliding or to bring individual discontinuity-bounded rock-mass blocks closer together in order to resist the erosive capacity of the water (Annandale, 2006).

Dental concrete combined with rock bolts is illustrated in Figure 2.10.

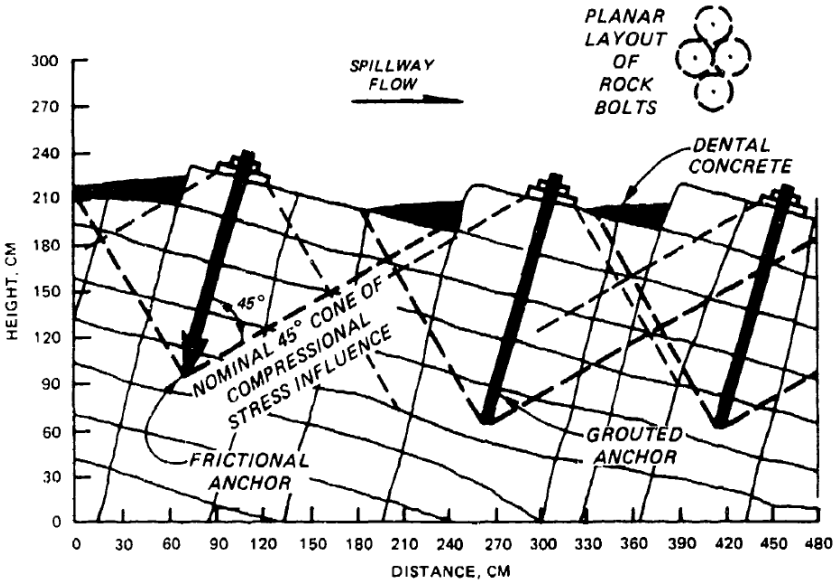

Figure 2.10: Representation of rock bolting at spillway (Cameron et al., 1988)

2.9.5 Wire Mesh

The wire mesh technique is generally used over the channel way where weathered rock is not extensive . A proper application of wire mesh provides an effective resistance to the scouring of rock blocks larger than the mesh openings, essentially retaining the competence of the unlined spillway channel surface. Design requirements for mesh retention are:

- an appropriate mesh-opening size which is smaller than the smallest blocks in the channel
- a proper anchorage in competent rock.
- the use of an upstream debris barrier to eliminate ripping of the mesh by floating and suspended trees and other debris.

The effectiveness of the wire mesh technique in withstanding erosion is totally dependent on mesh continuity and anchorage. Therefore, debris which are potential causes of damage to both mesh and

anchorage should be cleared from unlined spillway channels.

2.9.6 Hydraulic Energy Dissipators

An energy dissipator is a concrete, gabion, riprap (rock) or any other durable material structure built to dissipate flow energy in order to reduce the erosive force of any given flow event. Design of energy dissipators is based on hydraulic parameters such as channel shape, discharge, tailwater elevation, and maximum expected flow velocity. An energy dissipator is particularly advisable for steep unlined spillway channel gradients where turbulent flow is observed. A suitable subgrade or anchor for dissipation structures to ensure their competence needs to be provided. To resist erosion, hydraulic energy dissipators may be used in conjunction with other mitigation or protection measures.

2.9.6.1 Stairstep Energy Dissipators

Stairstep energy dissipators are composed of slope backward, into the upstream section of a spillway, forming several inclined surfaces able to dissipate flow energy as the water travels up each surface. This method is suitable in cases where the unlined spillway is excavated into tightly jointed, competent bedrock, with weak or weathered rock in the channel. In this case , the downstream portion of the unlined spillway channel is built as a tilted, stairstep structure. This would contribute to a decrease in the energy of the water at the toe of the spillway and subsequently, reduce the erosion effect of the flow downstream. This approach is also applicable to cases where the unlined spillway channel has a relatively steep outlet slope.

2.9.6.2 Gabions/Reno Mattress

Gabions are basically used as liners for channels exposed to erosion. They may be used in conjunction with a proper filter bed to prevent channel-type undercutting and the removal of the subgrade material in the case of high velocity flow beneath gabions. For designs against high-velocity flow, it is recommended that a sufficient thickness of filter bedding should be placed between the surface of the channel and the gabions to provide relief of uplift pressures without the removal of the natural ground (Cameron et al., 1988). During a study conducted at Colorado State University it was found that gabion or Reno Mattress (essentially, a gabion that is mattress-shaped) of specific diameter can resist higher flow velocities than

riprap of the same diameter (Cameron et al., 1988). Due to its prohibitive cost, gabion/Reno Mattress should only be used for portions of the unlined spillway channel and not as a whole lining.

2.9.6.3 Cutoff Wall

The cutoff wall technique consists of placing a vertical wall-barrier to an appropriate depth at the top of the spillway and/or at other locations along the channel. There are numerous types of cutoff walls and they can be made of a number of materials including concrete, sheet piles, logs, gabions, etc. This technique is appropriate for mitigation situations where headward cutting is likely to occur during a flow event and also suitable in weak rock with closely spaced discontinuities.

2.9.6.4 Removal of Woody Vegetation

Turbulent flow concentration which locally increases the velocity and flow rate, can be caused by the presence of woody vegetation and fallen trees in the waterway. This results in increased erosive forces or causes a logjam which can obstruct the unlined spillway channel. Removal of woody vegetation could be an appropriate mitigation technique for erosion in some cases because it is cost-effective compared to the possible damage that such vegetation could cause during a flood event.

2.9.6.5 Removal/Modification of Erosional Outliers

Erosional outliers are defined as any structure or natural feature that causes the concentration of flow and consequently, increases the erosive power in a specific section of the unlined spillway channel (Cameron et al., 1988). These types of features including boulders, fences, access roads, or a stand of trees can severely undermine the spillway channel by creating a breach through the spillway during a flood event. Removal of such features regarded as erosional outliers may be relatively inexpensive, whereas modifications of structure may in some cases be cost-prohibitive. In order to ensure adequate channel protection against erosion, it is recommended to use removal or modification of erosional outliers in conjunction with another technique.

2.9.6.6 Riprap

This technique consists of placing rock layers with specific dimensions on top of a filter over the underlying soil in order to prevent the surface of the spillway channel from eroding. The design of riprap protection requires the determination of the equivalent thickness of large rock to withstand removal by the erosive capacity of the design discharge flow. The success of riprap protection against the effect of scour could depend on the interlocking effect of the rock particles and also the use of an appropriate filter (Annandale, 2006). The interlocking effect between particle rocks provides additional resistance to the erosive capacity of the water while the function of the filter is to prevent removal of the fine material underneath the protection subjected to the fluctuating pressure of water. Riprap protection can be considered as a remedial measure in the case of unlined spillways where appropriate near-horizontal channel slopes exist.

2.9.6.7 Grass Lining

Although there would be little applicability for the use of grass lining in excavated unlined spillways in hard rocks, grass lining may be helpful as a protection measure against erosion in unlined spillway cut in softer rocks and in the outlet channel. Grass lining is efficiently used under conditions of sufficient annual precipitation and appropriate temperatures, and also expected velocities should be low enough to allow grass to offer the desired protection against erosion.

2.9.7 Modified Ogee Weir (Ski-Jump Structure)

The modified ogee weir technique can be utilised in situations where the outlet slope on the unlined spillway channel is relatively steep and approaching a small cliff. In these situations, the channel needs to be lined with a competent erosion-resistant geologic unit that extends to the point of cliff-like outlet slope (see figure 2.11). This remedial structure reduces the possibility of undercutting by causing the water to plunge away from the base of the cliff. The modified ogee weir can be applied either in situations with a high potential undercutting or at steep discharge slopes with very erodible material.

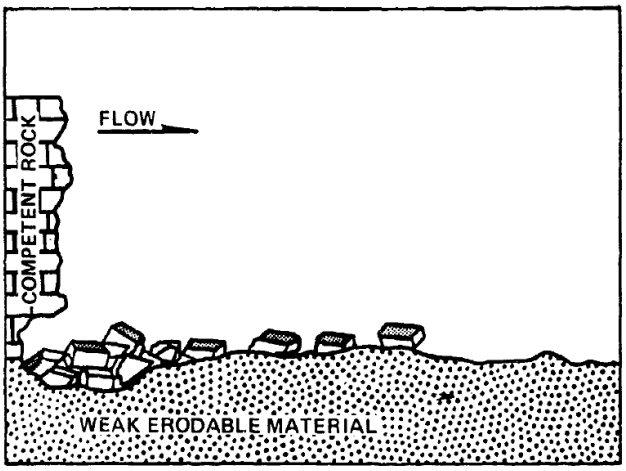

(a) Spillway channel before remediation

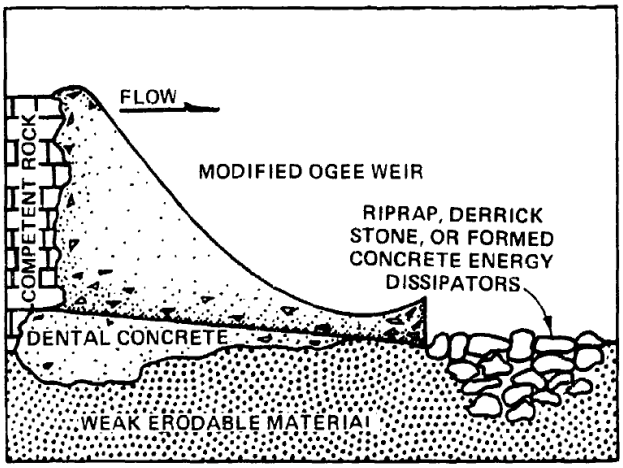

(b) Spillway channel after remediation

Figure 2.11: Use of a modified ogee weir as a mitigation or preventive measure (Cameron et al., 1988)

3. Laboratory Investigation of Rock Scour

3.1 Determination of Sediment Characteristics

The determination of the geo-mechanical characteristics of sediment is an important aspect in erosion prediction methods. Cubes of PVC material were used as sediment in the physical model. This material was chosen because it is relatively light and can easily be removed by the flow of water. A total of approximately ten thousand cubes were needed to set up the physical model. Therefore strips of cable PVC with a square cross section of $10\,mm$ by $10\,mm$ were cut manually, at $10\,mm$ intervals using a band saw, which led to the production of cubes. Typical cubes used in the physical model are shown in Figure 3.1

Figure 3.1: Typical cubes used in the laboratory flume test

After manufacturing, it was noticed that the PVC cubes had swollen leading to a slightly large cross-section. As a consequence of this, and considering inaccuracies that occurred during the cutting process, an average dimension (width, breadth and height) of $11\,mm$ was found. The properties of a randomly selected sample size of 35 cubes were analysed and are described in Table B.1 in Appendix B.

The sediment's various geo-mechanical properties are described in the subsequent subsections.

3.1.1 Relative Density

The relative density is defined as the ratio of the density of a sediment relative to the density of a reference substance and can be determined using Equation 3.1,

$$Relative\ density = \frac{\rho_{Sediment}}{\rho_{Reference}} \tag{3.1}$$

Water was chosen as a reference substance in this case. A sample of 35 randomly selected cubes were weighed and their volumes calculated in order to determine an average density. It was found that the PVC material had an average density of $1424.55\,kg/m^3$. Water has an approximate density of $1000\,kg/m^3$. The relative density was thus calculated to be 1.424. Details of the calculations can be seen in Table B.2 in Appendix B.

3.1.2 Settling Velocity

A sample of 35 randomly selected cubes was used in order to calculate the average settling velocity of a typical cube. Cubes were individually dropped into a Perspex cylinder filled with water. A stop watch was used to record the time taken for each cube to cover a known distance. Measurements were only taken after paying careful attention and to allow the cubes to reach their terminal velocity first. The water used was at room temperature, approximately 20° C . The average settling velocity of the cubes was calculated as being $0.261\,m/s$. Detailed results can be seen in Table B.3 in Appendix B.

3.1.3 Effective Diameter

The sedimentation diameter is defined as the effective diameter of a sphere that has the same fall velocity and the same relative density as an average cube would have. The calculation of the settling velocity requires the sedimentation diameter. Since the settling velocity was determined practically in the case of the cable PVC cubes, the effective diameter can be calculated by performing the back-calculation. Equation 3.2 describes the settling velocity (also named falling velocity) of a single particle in an infinite body of still water (Simons and Sentũrk, 1992).

$$\omega^2 = \frac{4g\gamma' D_S}{3C_D\gamma} \tag{3.2}$$

where,

ω = settling velocity (m/s)

g = gravitational constant (m/s^2)

γ' = specific weight of a submerged particle (N/m^3)

D_S = sedimentation diameter (m)

C_D = drag coefficient

γ = specific weight of water (N/m^3).

By assuming the drag coefficient to be 0.40, the only unknown is the effective diameter and through back-calculation, the average effective diameter of cubes was found to be $4.9235\,mm$. Details of calculations can be seen in Tables B.4 and B.5 in Appendix B.

3.1.4 Effective Diameter Distribution

Although the properties and behaviour of individual sediment particles are of fundamental concern, the greatest interest is paid to groups of sediment particles. Knowing the settling velocity for each PVC cube (see subsection 3.1.2), the corresponding effective diameter is calculated using Equation 3.2. A sample of 35 randomly selected cubes and their cumulative size-frequency distribution curve is depicted in Figure 3.2. Detailed results can be seen in Tables B.5 and B.6 in Appendix B.

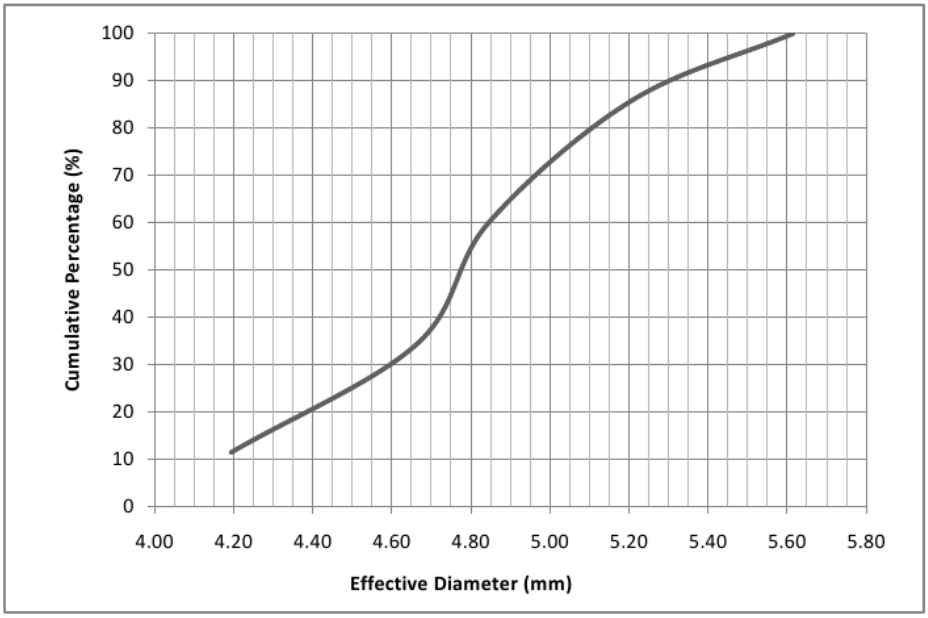

Figure 3.2: Particle size distribution used in the laboratory test

3.1.5 Porosity

The porosity of a sediment is described as the ratio of the volume of voids to the total volume of the sediment. Care was given to calculate the porosity of the cubes based on how they would be packed in the physical model test. Two methods were used and the results were compared. The first method was a practical method that consisted of packing cubes in a metal box of known dimensions. A known volume of water was then poured into the box until the water level reached the top of the cubes. The volume of water poured into the box thus represents the total volume of voids. The total volume of the cubes is easily measured by seeing how much water they displace in a measuring cylinder. The second method is more mathematical in nature and involved the calculation of porosity through the back calculation of bulk density for dry sediments. The bulk density for dry sediments is given by Equation 3.3 (Craig, 2004).

$$\rho_d = \frac{G_S \rho_w}{1+e} \tag{3.3}$$

where,

ρ_d = dry bulk density (kg/m^3)

G_S = specific gravity of the sediment

ρ_w = density of water (Kg/m^3)

e = void ratio.

The void ratio e is the only unknown. Once it has been calculated it is used in Equation 3.4 (Craig, 2004) to calculate the porosity of the sediment.

$$n = \frac{e}{1+e} \tag{3.4}$$

where,

n = sediment porosity

e = void ratio.

The two methods used produced the following results:

- Method 1 (practical method) Porosity = 0.1302 (13.02%)
- Method 2 (mathematical method) Porosity = 0.1068 (10.68%)

The computed porosity values are reasonably close and provide a good estimation of the porosity of the sediment. Details of calculations are provided in Table B.7 in Appendix B.

3.1.6 Bed Roughness

The bed roughness that is associated with the cable PVC can be derived from the back calculation of Equation 3.5 known as Manning's equation (Chadwick et al., 2004). It is applicable to open channel uniform flow. The bed roughness calculation was made possible as the flow rate and water surface level were recorded during the physical model test.

$$Q = \frac{1}{n}\frac{A^{5/3}}{P^{2/3}}S_0^{1/2} \tag{3.5}$$

Q = discharge (m^3/s)

A = cross sectional area of the water profile (m^2)

n = Mannings roughness value

P = wetted perimeter (m)

S_0 = gradient of the channel.

A Manning n value of 0.016 was calculated. Calculation details can be found in Table B.8 in Appendix B.

3.2 Physical Model Test

3.2.1 Background

The prediction of the erosion process is challenging and one of the methods to assess the extent and depth of erosion is to perform a laboratory test and survey the results. A physical model study, therefore, was conducted which involved a laboratory flume test setup in order to model the erosion of a typical unlined dam spillway. Unique sediment, chosen to represent a bed rock structure, was packed in layers on the flume bed. Water was then made to flow over these sediment layers. The flow rate was increased in incremental steps until erosion became apparent. The same procedure was adopted for four different bed slopes. Time was allowed before each flow rate increment for the model setup to stabilise. Erosion was then surveyed using a needle gauge. Water levels and flow rates were carefully measured during the laboratory flume test. The extent and depth of erosion was surveyed once each individual test was completed. Free flow and "clear water" conditions were maintained during the laboratory flume test to reflect, as far as possible, the conditions experienced in a typical unlined dam spillway.

3.2.2 Laboratory Flume Setup

A $0.15\,m$ wide and $5.20\,m$ long flume was made available by the Civil Engineering Department at the University of Stellenbosch. The flume, in conjunction with a downstream V-notch weir, provided the ideal setup for the analysis of the extent and depth of erosion. The flow in the flume was controlled by an adjustable valve located at the inlet of the flume. A special feature of the laboratory test flume is its ability to create different slopes with minimal effort. Due to the predefined lifting facilities of the laboratory flume, only four slopes ranging from 0.72% to 3.52% were tested. This was made possible due to the use of a jack tool to lift the flume to desirable slopes. A $3\,mm$ opening sieve was fixed downstream of the flume in order to retain eroded cubes from the flow during the test. Figure 3.3 through to Figure 3.7 show the laboratory flume with its different features.

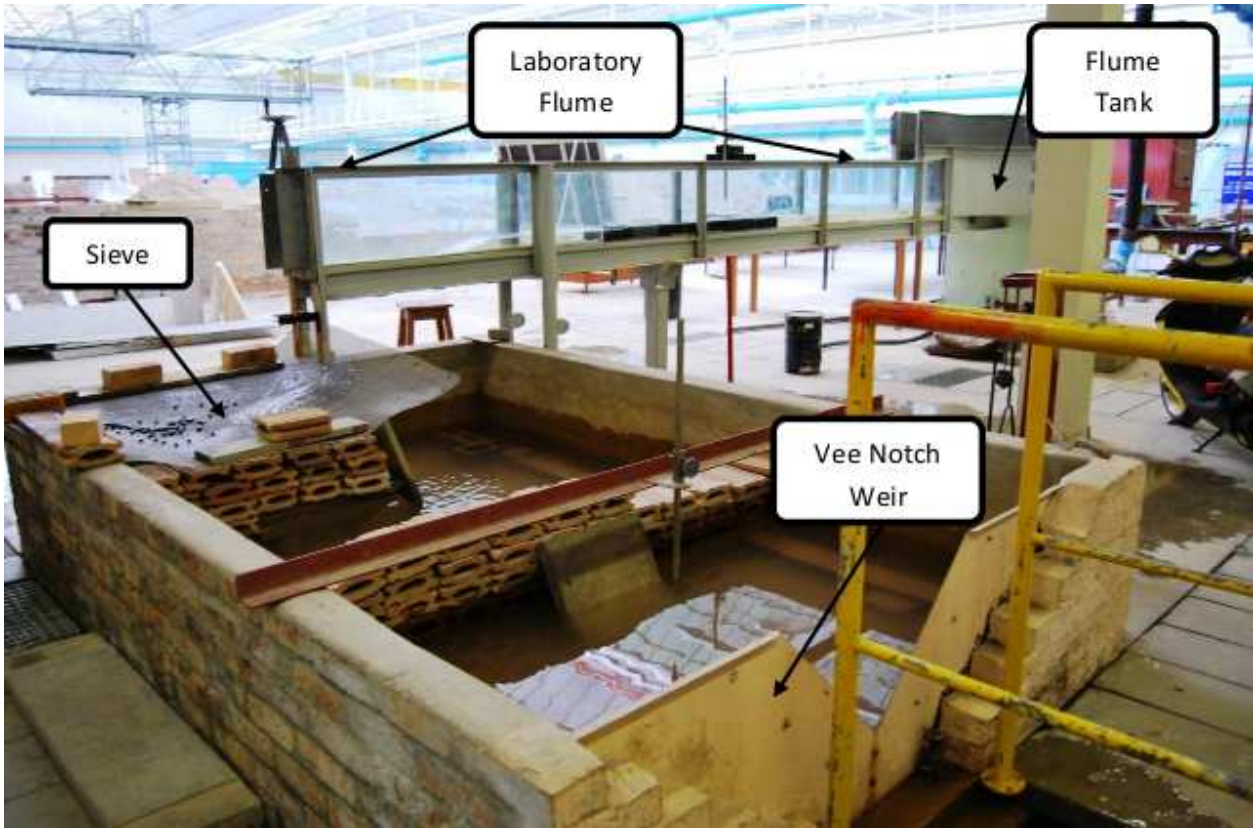

Figure 3.3: The laboratory test setup

Figure 3.4: Jack for slope adjustment

Figure 3.5: Valve and tank

3.2.3 Unlined Spillway Model Design

The typical channel of an unlined spillway was modelled in the laboratory flume. A total length of $3.428\,m$ was allocated with the same channel width ($0.15\,m$) as the laboratory flume. The model area comprised of $1.5\,m$ long erodible section (cube layers) and a $0.964\,m$ for each of two Perspex ramps utilised in the model. Approximately ten thousand cubes were manufactured for use in the model. The cubes were packed in a uniform manner along the flume so as to create a six layer bed of sediment. A ramp made of Perspex, with a 1 in 4 slope, was mounted in front of and at the downstream end of the sediment layers in order to provide a smooth uniform transition for the flow causing minimal disturbance to the flow. Figures 3.6 to 3.8 show the physical layout and dimensions of the model.

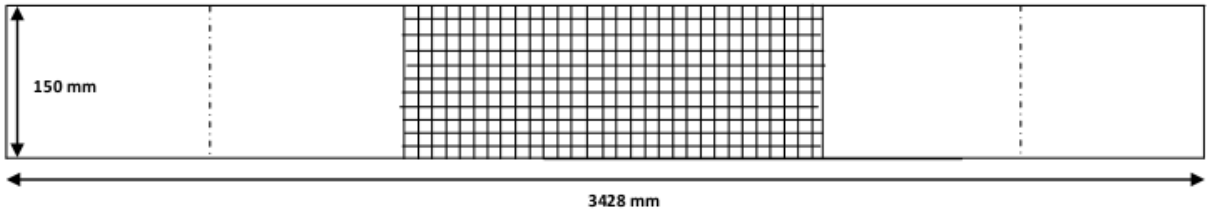

Figure 3.6: Plan view of the laboratory flume setup

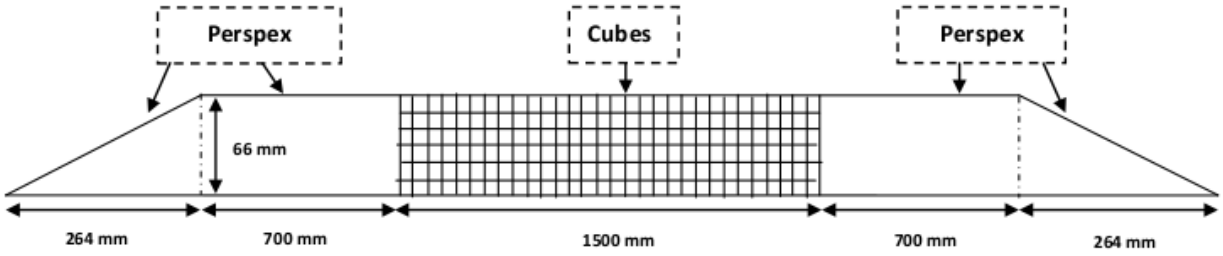

Figure 3.7: Elevation of the laboratory flume setup

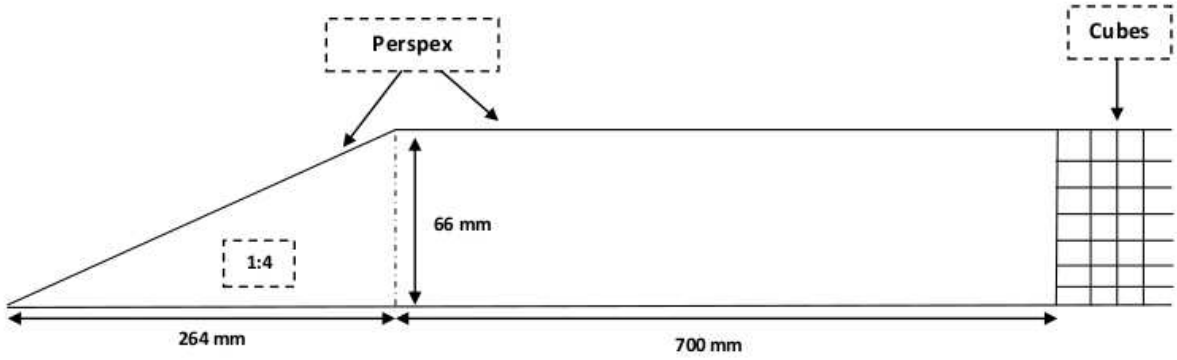

Figure 3.8: Perspex ramp layout

The unlined spillway model was built inside the laboratory flume. For this physical model, four different slopes varying from relatively gentle slope (0.72%) to steeper slope (3.52%) were chosen and tested.

The Perspex ramp used during the previous study conducted by Baret (2009) was altered by adding a horizontal part that connected the erodible region with the slope, which allowed less turbulence and smooth flow through the sediment layers. The adopted perspex ramp used in this model is portrayed in Figures 3.8 and 3.9.

Figure 3.9: Close up view of the Perspex ramp used in the physical model

Sediment layers and final configuration of the unlined spillway model are shown in Figures 3.10 and 3.11

Figure 3.10: Different layers of cubes at mid-construction of the physical model

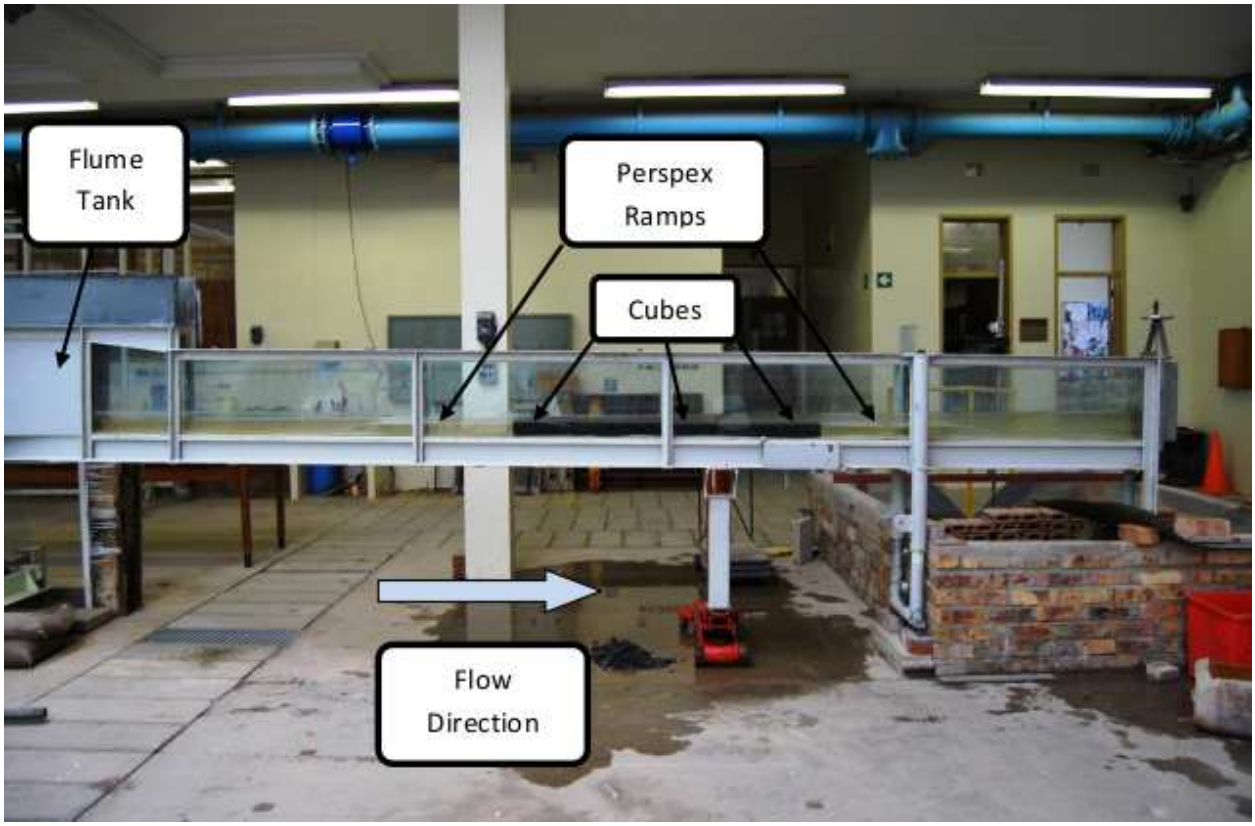

Figure 3.11: The completed unlined spillway model

3.2.4 Measurement Procedures

A short description of the various methods that were used to measure the necessary data during each test is given in the subsequent subsections.

3.2.4.1 Water Depth

The water depth was measured using a needle gauge at three locations along the spillway model region in order to obtain an average water depth. Additional water depth measurements were also made at the upstream and downstream points. These measurement points are indicated in Figure 3.12. Figure 3.13 illustrates the measurement technique of the water depth.

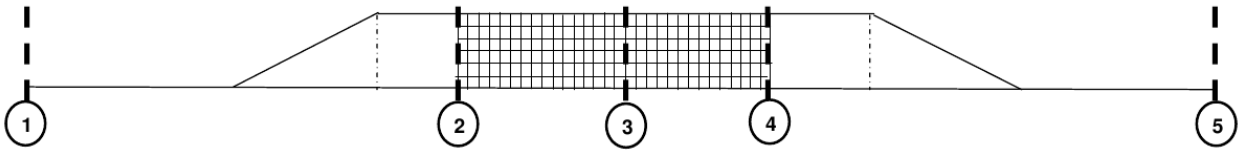

Figure 3.12: Water depth measurement points along the unlined spillway model

Figure 3.13: Water depth measurement technique

3.2.4.2 Discharge

Water was collected and stilled in a basin at the exit of the flume. The basin is equipped with a V-notch weir, which is suitable for the accurate determination of discharge at relatively low flows (see Figure 3.3). Equation 3.6 describes how the discharge through a V-notch weir is calculated (Chadwick et al., 2004).

$$Q = \frac{8C_d\sqrt{2g}(\tan\theta/2)h_1^{5/2}}{15} \tag{3.6}$$

where,

Q = flow discharge (m^3/s)

C_d = discharge coefficient for the weir (approximately 0.59 in this case)

g = gravitational constant (m/s^2)

θ = angle of the notch of the weir (90° in this case)

h_1 = head of water above the weir crest (m)

3.2.4.3 Erosion Survey

The measurement of erosion was done by surveying the extent and depth of the scour in a grid fashion. Depth measurements were made with a needle gauge every $10\,mm$ across the width of the flume and at $100\,mm$ intervals along the erodible region of the model.

3.2.5 Test Procedure

An adjustable valve that allowed water into the laboratory test flume was used to control the flow of water into the flume. The tests began with low flow rates in order to fill up the basin of the V-notch weir up to its crest height. The next step consisted of closing the outlet gate of the flume and allowing the water to stay inside the flume. After stabilising the flow, the valve was shut down and the slope measurement was conducted by recording the upstream and downstream water level at a given distance. After the above-mentioned steps, the flow rate was adjusted in small increments until the point at which erosion occurs. Flow and water depth measurements were made once the equilibrium conditions had been reached before any adjustment in flow was made. The times from the beginning and the end of the erosion process at specific flow rates were also recorded. Once erosion reached its equilibrium point, the flow was stopped and the extent and depth of the erosion was surveyed. The same procedure was repeated for all the different slopes that were used in the model tests.

3.3 Results of the Physical Model Test

Previous tests done by Baret (2009) on the unlined spillway model revealed that a narrowing inside the laboratory flume approximately at the mid-point of the length of the model was influencing the erosion results. This increased water velocity and greater turbulence resulting in the local erosion of sediment in this region. To avoid this external influence, the inside of the laboratory flume was straightened by adjusting the glass walls so that the passage of water along the flume was smoother with uniform velocity. The Perspex ramp initially used was also altered by adding a horizontal part that connects the erodible region, which allows less turbulence and smooth flow through the sediment layers.

Testing was then conducted and the erosion was surveyed. It is worth noting that clear-water conditions were maintained throughout the whole model testing. The results are presented and discussed in the following sections.

3.3.1 Test Results for Gentle Slopes (0.72% and 1.55%)

3.3.1.1 Flow Results

The water depth was recorded at three different points located along the spillway model and also both upstream and downstream of the laboratory flume (see Figure 3.12). Measurements were taken at the V-notch weir and Equation 3.6 was applied to calculate the corresponding flow rate. Flow velocity was computed using the following equation

$$V = \frac{Q}{Bh} \tag{3.7}$$

where,

V = the flow velocity (m/s)

Q = the flow discharge (m^3/s)

B = the flume width (m)

h = water depth (m)

Table 3.1 summarises the recorded water depth during the test for the 0.72%-slope and the 1.55%-slope.

Table 3.1: Flow results of the physical model test for 0.72% and 1.55% slopes

Slope = 0.72%				Slope = 1.55%			
Position	**Water depth (m)**	**Discharge (m^3/s)**	**Velocity (m/s)**	**Position**	**Water depth (m)**	**Discharge (m^3/s)**	**Velocity (m/s)**
1	0.134	0.0058	0.29	1	0.101	0.0032	0.21
2	0.049	0.0058	0.79	2	0.027	0.0032	0.79
3	0.070	0.0058	0.56	3	0.033	0.0032	0.65
4	0.052	0.0058	0.75	4	0.028	0.0032	0.76
5	0.026	0.0058	1.50	5	0.021	0.0032	1.01
V-notch	0.112	0.0058		V-notch	0.088	0.0032	

The average velocities at the spillway model (positions 2,3 and 4) are $0.70\,m/s$ and $0.73\,m/s$ for the 0.72%-slope and the 1.55%-slope respectively. The corresponding average water depths for the same control points are $0.057\,m$ and $0.029\,m$ for the 0.72%-slope and the 1.55%-slope respectively.

3.3.1.2 Erosion Results

The erosion of the unlined spillway model at relatively gentle slopes of 0.72% and 1.55% occurred at critical flows of $0.0058\,m^3/s$ and $0.0032\,m^3/s$ respectively. The upstream side of the spillway model near the Perspex ramp was the first to be affected by the erosion process. This is due to the presence of high flow disturbance in this particular area which is a transition region between the erodible (sediment layers) and non erodible (Perspex ramp) regions. Erosion continued both upstream and downstream until the equilibrium was reached. The equilibrium was reached after approximately $600\,s$ for both slopes. In the case of the 0.72%-slope, the first layer of the six-layer sediment was widely and uniformly eroded along the erodible zone of the model. At the same time, isolated cubes in the second layer were also moved due to stream power. This can be seen in Figure 3.14 which shows the resultant erosion for this particular test.

Figure 3.14: Erosion extent in the unlined spillway model for the 0.72%-slope and $0.0058\,m^3/s$ (viewed from upstream)

For the 1.55%-slope the first layer was severely eroded only at the upstream and downstream part of the erodible zone. The middle part was lightly affected by the erosion. Nevertheless, the second layer was locally eroded in some places. The extent of erosion for this test is shown in Figure 3.15.

Figure 3.15: Erosion extent in the unlined spillway model for the 1.55%-slope and $0.0032\,m^3/s$ (viewed from downstream)

In short, the erosion was more severe in the case of the 0.72%-slope than for the 1.55%-slope. This could be because of high flow rate ($0.0058\,m^3/s$) that was needed to initiate erosion for the 0.72%-slope compared to $0.0032\,m^3/s$ in the case of the 1.55%-slope. In both cases, the majority of the eroded particles was carried as a bed load while a few were transported as suspended loads for a brief period before being deposited downstream.

3.3.2 Test Results for Steep Slopes (2.59% and 3.52%)

3.3.2.1 Hydraulic Results

The same measurement procedure for water depth was followed as described in section 3.2.4 and flow velocity was computed using Equation 3.7. Tables 3.2 summarises the recorded water depth during the test for the 2.59%-slope and the 3.52%-slope.

Table 3.2: Flow results of physical model test for 2.59% and 3.52% slopes

Slope = 2.59%				Slope = 3.52%			
Position	**Water depth (m)**	**Discharge (m^3/s)**	**Velocity (m/s)**	**Position**	**Water depth (m)**	**Discharge (m^3/s)**	**Velocity (m/s)**
1	0.081	0.0019	0.16	1	0.069	0.0017	0.17
2	0.016	0.0019	0.81	2	0.014	0.0017	0.83
3	0.026	0.0019	0.51	3	0.018	0.0017	0.64
4	0.014	0.0019	0.92	4	0.014	0.0017	0.83
5	0.010	0.0019	1.36	5	0.007	0.0017	1.66
V-notch	0.072	0.0019		V-notch	0.069	0.0017	

The average velocities at the spillway model (positions 2, 3 and 4) are $0.75\,m/s$ and $0.77\,m/s$ for the 2.59%-slope and the 3.52%-slope respectively. The corresponding average water depths for the same control points are $0.019\,m$ and $0.015\,m$ for the 2.59%-slope and the 3.52%-slope respectively.

3.3.2.2 Erosion Results

The erosion of the unlined spillway model at relatively steep slopes of 2.59% and 3.52% occurred at critical flows of $0.0019\,m^3/s$ and $0.0017\,m^3/s$ respectively. Erosion began at the upstream side of sediment layers near the Perspex ramp because of high flow turbulence in this region. Erosion continued both upstream and downstream until the equilibrium was reached. Equilibrium was reached after approximately $670\,s$ for the 2.59%-slope and $1080\,s$ for the 3.52%-slope. In the case of the 2.59%-slope, the erosion was specifically aggressive near the transition region located between the end of the perspex ramp and the beginning of the sediment layers. In this region, the erosion reached the fifth layer of sediment. Erosion was generally limited to the third and fourth layers over the remaining area. This can be seen in Figure 3.16 depicting the resultant erosion.

Figure 3.16: Erosion extent in the unlined spillway model for the 2.59%-slope and $0.0019\,m^3/s$ (viewed from upstream)

For the 3.52%-slope, erosion is more severe and reached the last layer of sediment in the transition region. The extent of erosion was limited to the third and fourth layers over the rest of the area. This can be seen in the figure below.

Figure 3.17: Erosion extent in the unlined spillway model for the 3.52%-slope and $0.0017\,m^3/s$ (viewed from upstream)

Although flow rates used in both cases did not varied significantly ($0.0019\,m^3/s$ and $0.0017\,m^3/s$), erosion was more intensive in the case of the steepest slope (3.52%) . This is due to the greater energy gradient present on the steep slope flume setup. In both cases, the majority of eroded particles was carried as a bed load while a few were transported as suspended loads for a brief period before being deposited downstream.

3.3.3 Summary of Results

To survey the extent and the depth of scour, three cross sections (upstream, midstream and downstream) were chosen across the width of the flume and at $375\,mm$ intervals along the erodible region. In order to reduce the effect of the turbulence on the erosion results, cross sections were chosen not be very close to the Perspex ramp where the flow was unstable. A cross section along the centreline of the sediment layers was also chosen to portray the longitudinal change caused by the erosion on the sediment layers.

3.3.3.1 Cross Section Results for 0.72% and 1.55% Slope Tests

After testing the unlined spillway model for the 0.72%-slope, cross sections describing the change of elevation at upstream, midstream, downstream of the model were considered. These cross sections are given by graphs in Figures 3.18 (a)-(c). In addition, the longitudinal profile after the passage of flow is also shown in Figure 3.18 (d).

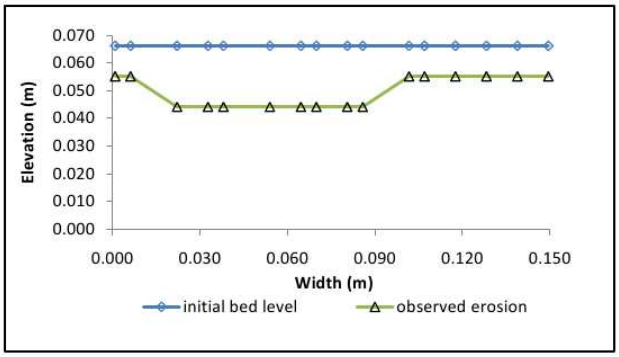

(a) Upstream cross section

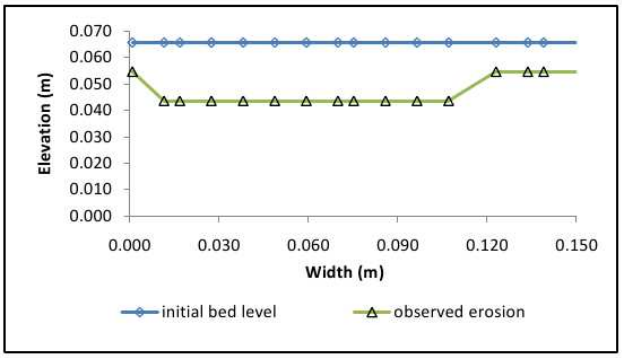

(b) Midstream cross section

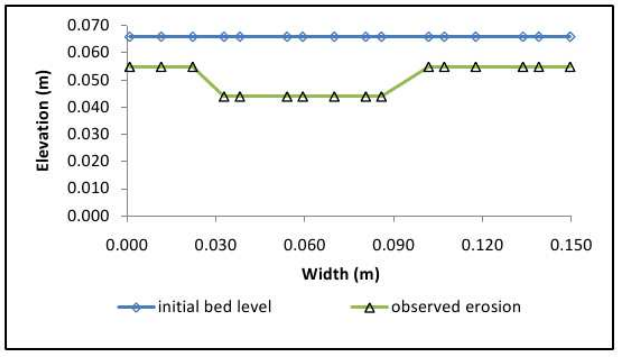

(c) Downstream cross section

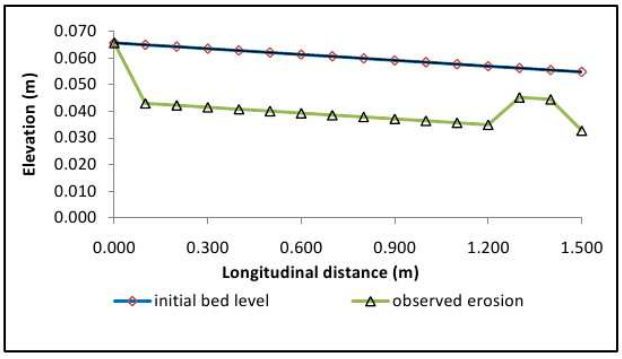

(d) Longitudinal profile

Figure 3.18: Cross sections for slope $= 0.72\%$, Q $= 0.0058\,m^3/s$

For the 1.55%-slope test, the resulting cross sections and longitudinal profile are given by the subsequent graphs (Figures 3.19 (a)-(d)).

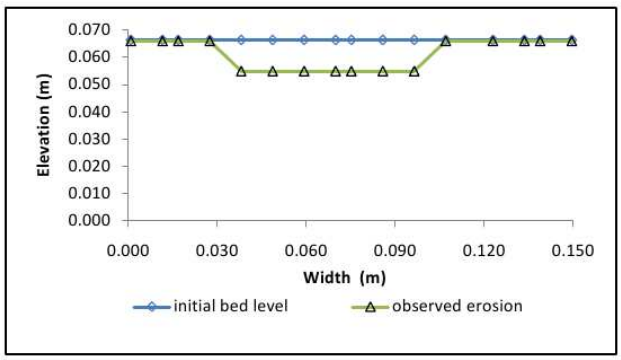

(a) Upstream cross section

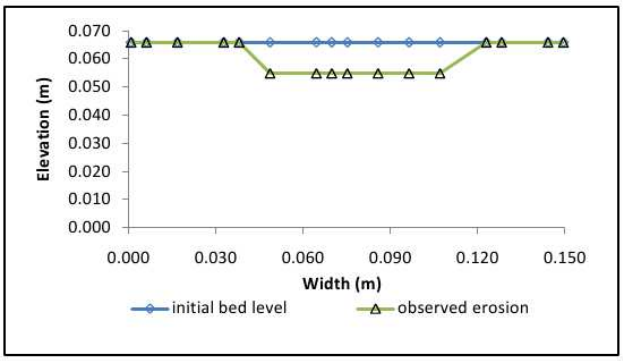

(b) Midstream cross section

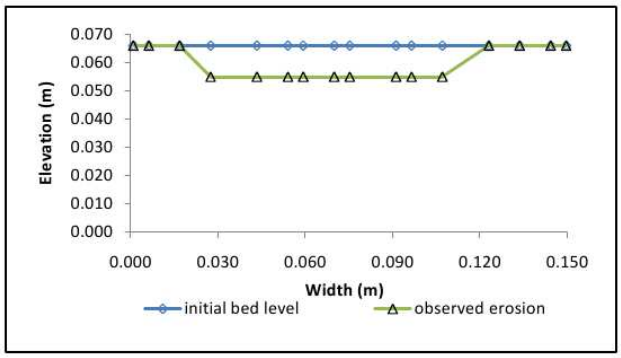

(c) Downstream cross section

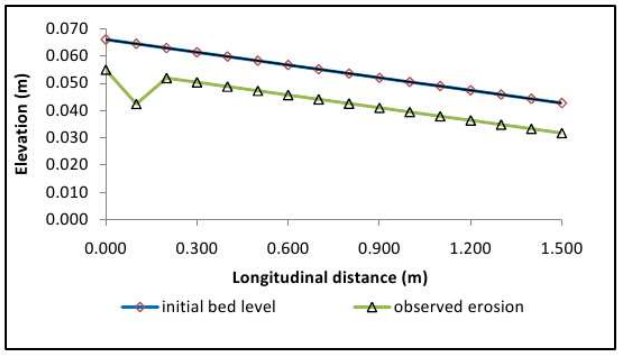

(d) Longitudinal profile

Figure 3.19: Cross sections for slope $= 1.55\%$, Q $=0.0032\, m^3/s$

3.3.3.2 Cross Section Results for 2.59% and 3.52% Slope Tests

Cross sections describing the change in elevation at upstream, midstream, downstream of the model were chosen in order to emphasize the spatial distribution of the erosion. Cross sections for the 2.59%-slope are given by graphs in Figures 3.20 (a)-(c) and the longitudinal profile of the model after the passage of flow is also shown in Figure 3.20 (d).

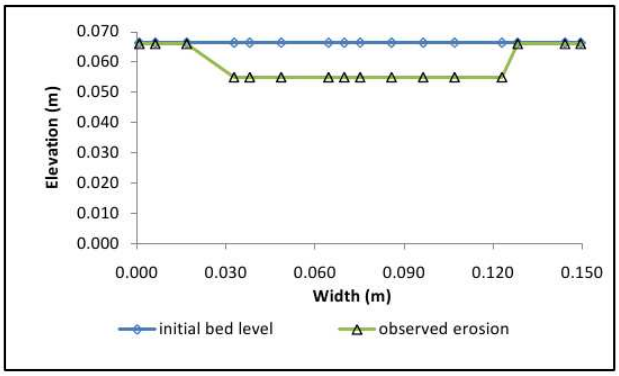

(a) Upstream cross section

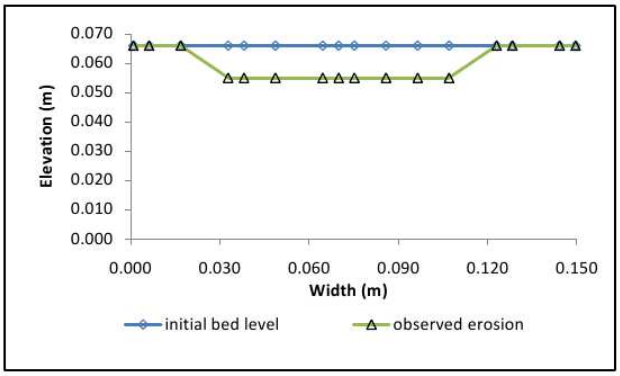

(b) Midstream cross section

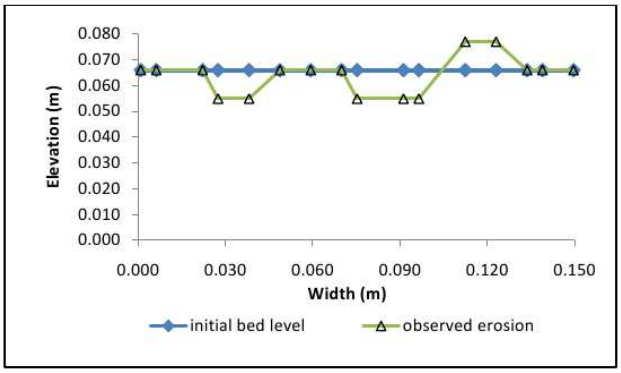

(c) Downstream cross section

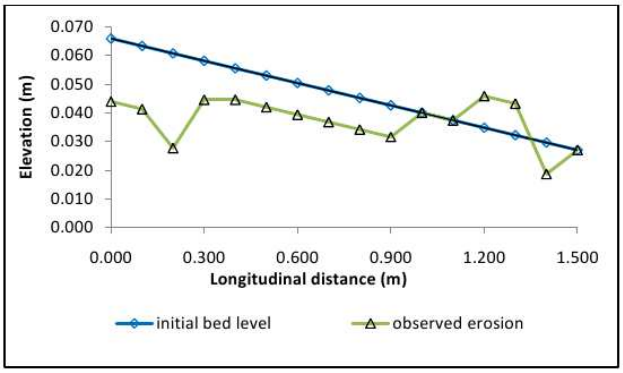

(d) Longitudinal profile

Figure 3.20: Cross sections for slope = 2.59%, Q =$0.0019\ m^3/s$

For the 3.52%-slope test the resulting cross sections and longitudinal profile are given by the subsequent graphs (Figures 3.21 (a)-(d)).

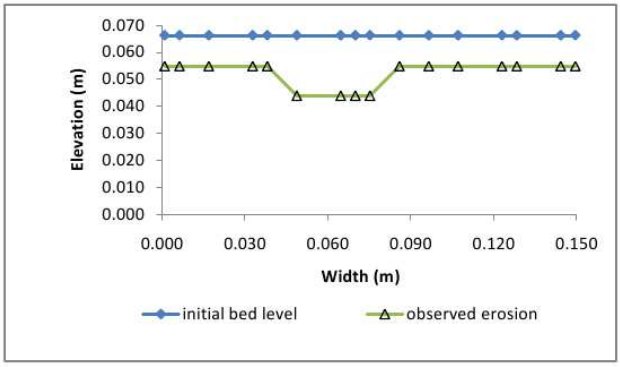

(a) Upstream cross section

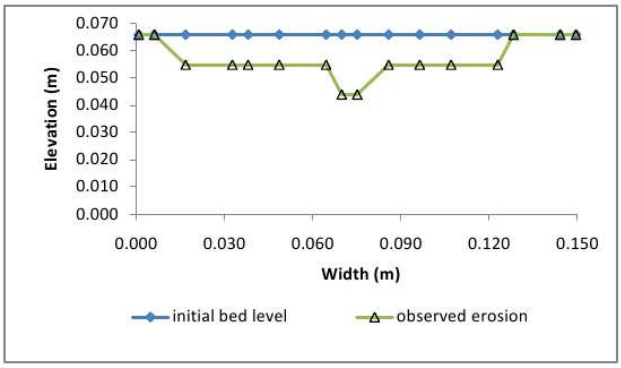

(b) Midstream cross section

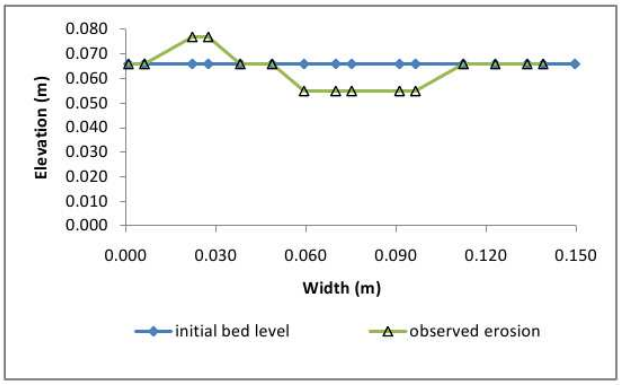

(c) Downstream cross section

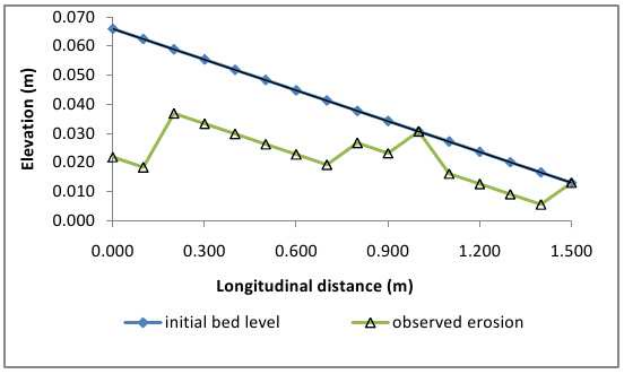

(d) Longitudinal profile

Figure 3.21: Cross sections for slope $= 3.52\%$, Q $= 0.0017\, m^3/s$

3.3.3.3 Gentle Slope and Steep slope Erosive Power Comparisons

Erosion on the model unlined spillway was obtained more easily on the steep slope setup. This is attributed to the greater energy gradient present on the steep slope flume setup. The energy gradient is directly proportional to the erosive power of water. A greater energy gradient thus increases the erosive power of water, which in turn leads to greater erosion.

4. CCHE2D Numerical Modelling of Laboratory Tests

4.1 Background on CCHE2D Model

The CCHE2D Model was used in this research. The model is a two-dimensional hydrodynamic model for unsteady turbulent open channel flow and sediment transport simulations. It was developed by the National Centre for Computational Hydroscience and Engineering (NCCHE), hosted at the University of Mississippi School of Engineering. This version of the model is able to simulate unsteady open channel flows and also the steady state solution as a special case. The model is capable of predicting river bed and bank erosion for both uniform and non-uniform sediment (Wu, 2001). In addition, the effect of hydraulic structures on river morphology can be investigated by using the CCHE2D Model, and therefore it can be used in the preliminary design of new structures for cost-effectivity and sustainability, as pointed out by Zhang (2006).

The CCHE2D Model comprises a CCHE2D Mesh Generator that generates meshes for the CCHE2D-GUI and the CCHE2D numerical model. The CCHE2D-GUI provides a graphical interface for the data input, file management, and visualisation of results. The process of the CCHE2D Model is depicted in Figure 4.1 and more details on its different components are given in subsequent sections.

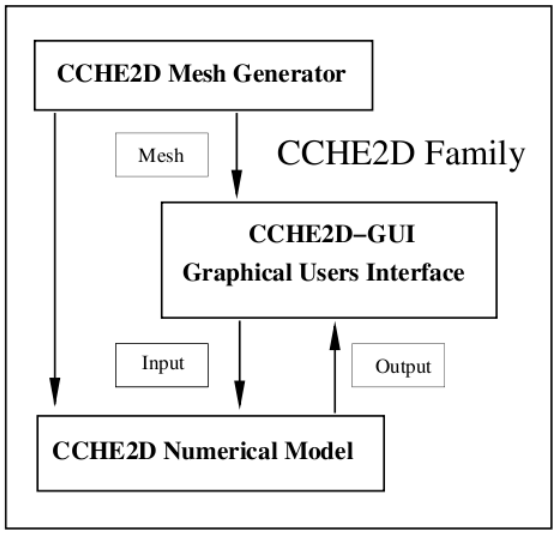

Figure 4.1: CCHE2D model process (Zhang, 2005)

4.1.1 General Procedure of the CCHE2D Model

The numerical modelling based on solving the Navier-Stokes equations is an initial-boundary value problem. Therefore, boundary conditions and initial conditions are required to perform CCHE2D simulations. The following procedures are carried out for CCHE2D numerical simulation:

- Mesh generation:

  The CCHE2D Mesh Generator is used to generate a mesh which represents a computational domain. Like any numerical model system, the mesh is a key element in the CCHE2D model because the reliability of simulation results could largely depend on the quality of the mesh used.

- Boundary conditions:

  In the CCHE2D Model, the behaviour of the flow in the simulated area is controlled by boundary conditions and therefore the chosen values for boundary conditions should be as close to the natural conditions as possible.

- Parameter setting:

  Many physical parameters and numerical parameters are required to perform numerical simulation. Consequently Flow parameters and sediment parameters that control the simulation processes must be provided.

- Simulation:

  The simulation starts after boundary conditions and parameters have been specified. The CCHE2D Model offers two different simulations. The flow simulation is carried out first and its results are used to perform sediment transport simulation.

- Results interpretation:

  Once the simulation is completed, results can be visualised and analysed through the Graphical User Interface provided by CCHE2D Model.

4.2 Governing Equations in the CCHE2D Model

4.2.1 Governing Equations

In the CCHE2D Model, it is assumed that the effect of vertical motion is usually of insignificant magnitude in the case of many open channel flows (Zhang, 2006). Therefore, the depth integrated two-dimensional equations are generally used in this model to deal with the open channel hydraulics. The momentum equation and the continuity equation are the main governing equations used in the CCHE2D Model.

The momentum equations for depth-integrated two-dimensional turbulent flows in a Cartesian coordinate system are:

$$\frac{\partial u}{\partial t} + u\frac{\partial u}{\partial x} + v\frac{\partial u}{\partial y} = -g\frac{\partial Z}{\partial x} + \frac{1}{h}\left(\frac{\partial(h\tau_{xx})}{\partial x} + \frac{\partial(h\tau_{xy})}{\partial y}\right) - \frac{\tau_{bx}}{\rho h} + f_{Cor}v \tag{4.1a}$$

$$\frac{\partial v}{\partial t} + u\frac{\partial v}{\partial x} + v\frac{\partial v}{\partial y} = -g\frac{\partial Z}{\partial y} + \frac{1}{h}\left(\frac{\partial(h\tau_{yx})}{\partial x} + \frac{\partial(h\tau_{yy})}{\partial y}\right) - \frac{\tau_{by}}{\rho h} + f_{Cor}u \tag{4.1b}$$

In this model, free surface elevation for flow is computed by the depth-integrated continuity equation :

$$\frac{\partial Z}{\partial t} + \frac{\partial(hu)}{\partial x} + \frac{\partial(hv)}{\partial y} = 0 \tag{4.2}$$

where u and v are the depth-integrated velocity (m/s) components in the x and y directions respectively; g is the gravitational acceleration (m/s^2); Z is the water surface elevation (m); ρ is water density (kg/m^3); h is the local water depth (m); f_{Cor} is the Coriolis parameter; τ_{xx}, τ_{xy}, τ_{yx} and τ_{yy} are the depth integrated Reynolds stresses (N/m^2); and τ_{bx} and τ_{by} are shear stresses (N/m^2) on the bed surface and flow interface.

4.2.2 Turbulence Models

The turbulence Reynolds stresses in Equations 4.1 are solved by making use of Boussinesq's assumption:

$$\tau_{xx} = 2v_t\frac{\partial u}{\partial x} \tag{4.3a}$$

$$\tau_{xy} = \tau_{yx} = v_t\left(\frac{\partial u}{\partial y} + \frac{\partial v}{\partial x}\right) \tag{4.3b}$$

$$\tau_{yy} = 2v_t\frac{\partial v}{\partial y} \tag{4.3c}$$

Two turbence models are available in the CCHE2D Model namely, Eddy Viscosity Model and Two-dimensional $k-\varepsilon$ Model. These models are presented in the following sections.

4.2.2.1 The Eddy Viscosity Model

In this model, two methods are available for the computation of eddy viscosity . First the eddy viscosity coefficient v_t is calculated using the depth integrated parabolic eddy viscosity formula:

$$v_t = \frac{A_{xy}}{6} k u^* h \tag{4.4}$$

where u^* is shear velocity (m/s), k is the von Karman's constant (0.41) and A_{xy} is a coefficient to adjust the value of eddy viscosity. Its value by default is set to 1.

The second approach is the depth integrated mixing length model where the eddy viscosity v_t is expressed as follows:

$$v_t = \bar{l}^2 \sqrt{2\left(\frac{\partial u}{\partial x}\right)^2 + 2\left(\frac{\partial v}{\partial y}\right)^2 + \left(\frac{\partial u}{\partial x} + \frac{\partial v}{\partial y}\right)^2 + \left(\frac{\overline{\partial U}}{\partial z}\right)^2} \tag{4.5}$$

where

$$\bar{l} = \frac{1}{h}\int kz\sqrt{\left(1-\frac{z}{h}\right)}dz = kh\int_0^1 \lambda\sqrt{1-\lambda}d\lambda \approx 0.267kh \tag{4.6a}$$

$$\frac{\partial \overline{U}}{\partial z} = C_m \frac{u^*}{hk} \tag{4.6b}$$

with, $\lambda = \frac{z}{h}$. Where U is total velocity (m/s), u^* is the total shear velocity (m/s) and C_m is a coefficient. A value of 2.34375 is assigned to this coefficient in such a way that Equation 4.5 be similar to Equation 4.4 in the case of uniform flow in which all the horizontal velocity gradients are non existent.

4.2.2.2 The Two-Dimensional $k-\varepsilon$ Model

The turbulence kinetic k and the rate of dissipation of turbulent energy ε are given in the CCHE2D Model by; $k = \frac{1}{2}\overline{u_i' u_i'}$ and $\varepsilon = \mu_t \overline{\frac{\partial u_i'}{\partial x_j}\frac{\partial u_i'}{\partial x_j}}$.

The depth-integrated governing equations for k and ε are given as follows:

$$\frac{\partial k}{\partial t} + u\frac{\partial k}{\partial x} + v\frac{\partial k}{\partial y} - \frac{\partial}{\partial x}\left(\frac{v_t}{\sigma_k}\frac{\partial k}{\partial x}\right) - \frac{\partial}{\partial y}\left(\frac{v_t}{\sigma_k}\frac{\partial k}{\partial y}\right) = P - \varepsilon + P_{kv} \tag{4.7a}$$

$$\frac{\partial \varepsilon}{\partial t} + u\frac{\partial \varepsilon}{\partial x} + v\frac{\partial \varepsilon}{\partial y} - \frac{\partial}{\partial x}\left(\frac{v_t}{\sigma_\varepsilon}\frac{\partial \varepsilon}{\partial x}\right) - \frac{\partial}{\partial y}\left(\frac{v_t}{\sigma_\varepsilon}\frac{\partial \varepsilon}{\partial y}\right) = C_{1\varepsilon}\frac{\varepsilon}{k}P - C_{2\varepsilon}\frac{\varepsilon^2}{k} + P_{\varepsilon v} \tag{4.7b}$$

where,

$$P = -\overline{u_i' u_j'} u_{i,j} = v_t \left[2\left(\frac{\partial u}{\partial x}\right)^2 + 2\left(\frac{\partial v}{\partial y}\right)^2 + \left(\frac{\partial u}{\partial x} + \frac{\partial v}{\partial y}\right)^2 \right] \tag{4.8}$$

$$P_{kv} = C_k \frac{U_*^3}{h}, \qquad P_{\varepsilon v} = C_\varepsilon \frac{U_*^4}{h^2} \tag{4.9}$$

$$U_* = \sqrt{C_f (u^2 + v^2)} \tag{4.10}$$

$$C_k = \frac{1}{\sqrt{C_f}}, \qquad C_\varepsilon = 3.6 \frac{C_{2\varepsilon}}{C_f^{3/4}} \sqrt{C_\mu} \tag{4.11}$$

and C_f is the friction coefficient.

A local eddy viscosity, therefore, can be estimated from k and ε as:

$$v_t = \frac{C_\mu k^2}{\varepsilon} \tag{4.12}$$

The following values are used in the CCHE2D Model as empirical constants in the above equations:
$C_\mu = 0.09, \quad C_{1\varepsilon} = 1.45, \quad C_{2\varepsilon} = 1.90, \quad \sigma_k = 1.3$.

4.2.3 Shear Stress on the Bed

In the CCHE2D Model two alternative ways are adopted to estimate the shear velocity. The first is using the depth-integrated logarithmic law:

$$\frac{U}{u^*} = \frac{1}{z}\left[\frac{z_0}{h} - 1 + ln\left(\frac{h}{z_0}\right)\right] \tag{4.13}$$

where,

$$U = \sqrt{u^2 + v^2} \tag{4.14a}$$

u and v are the previous numerical results of the velocity components in the time-stepping scheme. For different flow conditions (smooth, rough and transition) different formulas are used to compute the variable z_0:

$$z_0 = 0.11 \frac{\nu}{u_*}; \qquad u_* k_s/\nu \leq 5 \tag{4.15a}$$

$$z_0 = 0.0333 k_s; \qquad u_* k_s/\nu \geq 70 \tag{4.15b}$$

$$z_0 = 0.11 \frac{\nu}{u_*} + 0.0333 k_s; \qquad 5 < u_* k_s/\nu < 70 \tag{4.15c}$$

where k_s is the roughness height (m) of the bed surface and ν is the kinematic viscosity (m^2/s) of the fluid. Since u^* is implicit, Equation 4.13 is solved iteratively. Therefore the Darcy-Weisbach coefficient f_c can be obtained after the calculation of u^* as follows:

$$\left(\frac{f_c}{8}\right)^{-0.5} = 3 + 2.5ln\left(\frac{u^*h}{\nu}\right); \qquad \frac{u^*k_s}{\nu} \leqslant 5 \tag{4.16a}$$

$$\left(\frac{f_c}{8}\right)^{-0.5} = 6 + 2.5ln\left(\frac{h}{k_s}\right); \qquad \frac{u^*k_s}{\nu} \geqslant 70 \tag{4.16b}$$

$$\left(\frac{f_c}{8}\right)^{-0.5} = 6 + 2.5ln\left(\frac{h}{k_s + 3.3\frac{\nu}{u^*}}\right); \qquad 5 < \frac{u^*k_s}{\nu} < 70 \tag{4.16c}$$

Finally the shear stress components are obtained from the following formulas:

$$\tau_{bx} = \frac{1}{8}\rho f_c u U \tag{4.17a}$$

$$\tau_{by} = \frac{1}{8}\rho f_c v U \tag{4.17b}$$

The second method consists of the use of the Manning's coefficient for the computation of the shear velocity and stress components on the bed surface:

$$\tau_{bx} = \frac{1}{h^{\frac{1}{3}}}\rho g n^2 u U \tag{4.18a}$$

$$\tau_{by} = \frac{1}{h^{\frac{1}{3}}}\rho g n^2 v U \tag{4.18b}$$

and the shear velocity is computed as follows:

$$(u^*)^2 = \frac{\tau}{\rho} = \frac{1}{\rho}\sqrt{\tau_{bx}^2 + \tau_{by}^2} \tag{4.19}$$

Although the second approach is more efficient for practical application, the first approach is recommended especially for detailed near field simulation with experimental data under condition of the availability of the roughness parameter (Zhang, 2005).

4.3 Sediment Transport Capacity in CCHE2D Model

4.3.1 Sediment Transport Mode

The movement of sediment is conventionally divided into suspended load and bed load along the vertical as showed in Figure 4.2. The bed load is defined as the part of the sediment moving on or near the

bed by rolling, saltation or sliding , whereas the suspended load moves in suspension and occupies the flow depth above the bed load layer. According to the availability in stream bed, the moving sediment is also broken into bed-material load and wash load as depicted in Figure 4.2. The former generally consists of particles found in the bed whereas the latter refers to fine sediments namely, silt and clay. In the CCHE2D Model, the total load sediment transport which involves both bed load and suspended load is simulated although the difference in characteristics of bed load and suspended load is taken into account in this model.

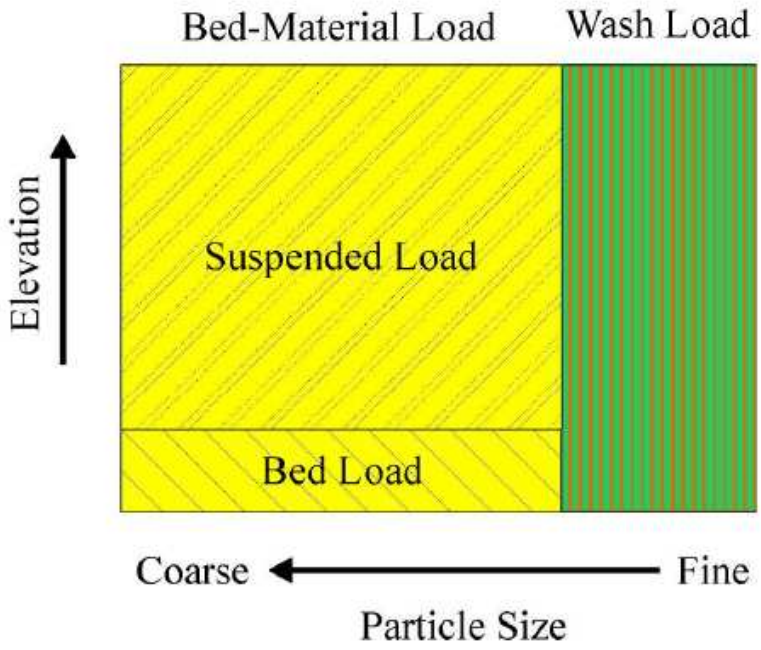

Figure 4.2: Sediment transport modes (Wu, 2001)

4.3.2 CCHE2D Model Approaches of Total-Load Transport Modelling

In the CCHE2D Model, three approaches are adopted for the nonuniform sediment transport modelling namely;

- bed-load type model; only bed load or bed-material load without taking into account the diffusion of suspended load is simulated
- suspended-load type model that simulates only suspended load or bed-material load treated as suspended load

- bed load and suspended load are separately computed.

In this thesis, only the first approach is adopted for the numerical simulations. Therefore, more details on bed load type are given in the next sections.

4.3.3 Configuration of Sediment Transport in the CCHE2D Model

In the CCHE2D Model the full water depth (h) is divided into bed-load zone and suspended-load zone. In this model the thickness of the bed-load zone (δ) is assumed to be twice the sediment size (Wu, 2001). Figure 4.3 shows the configuration of sediment transport in the CCHE2D Model.

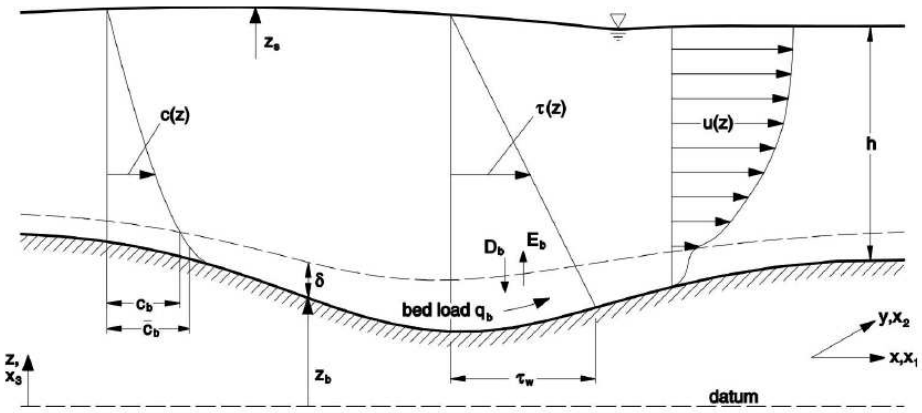

Figure 4.3: Configuration of sediment transport (Wu, 2001)

4.3.4 CCHE2D Governing Equations for Sediment Transport

In the CCHE2D Model, governing equations for both suspended-load transport and bed-load transport are provided. However, the main focus of this thesis is on bed-load transport and therefore, only governing equations pertaining to bed-load transport are presented in this study. In the case of non-uniform sediment transport, the depth-integrated convection-diffusion equation of bed-load transport is given in the CCHE2D Model as follows:

$$\frac{\partial(hC_k)}{\partial t} + \frac{\partial(UhC_k)}{\partial x} + \frac{\partial(VhC_k)}{\partial y} = \frac{\partial}{\partial x}\left(\varepsilon_s h \frac{\partial C_k}{\partial x}\right) + \frac{\partial}{\partial y}\left(\varepsilon_s h \frac{\partial C_k}{\partial y}\right) + E_{bk} - D_{bk} \qquad (4.20)$$

where,

h = flow depth (m)

C_k = concentration of the k^{th} size class of sediment (kg/m^3)

U, V = depth-averaged flow velocities in x and y directions respectively (m/s)

E_{bk}, D_{bk} = entrainment (upward) and deposition (downward) fluxes of the k^{th} size class of sediment at the interface between suspended-load zone and bed-load zone $(kg/s/m^2)$

ε_s = eddy diffusivity of sediment (m^2/s)

The continuity equation of bed load transport in the CCHE2D Model is given by:

$$(1-p')\frac{\partial z_{bk}}{\partial t}+\frac{\partial(\delta\overline{c}_{bk})}{\partial t}+\frac{\partial q_{bkx}}{\partial x}+\frac{\partial q_{bky}}{\partial y}=-E_{bk}+D_{bk} \tag{4.21}$$

where,

P' = porosity of bed material

$\overline{c}_{bk}$ = average concentration of bed load at the bed load zone (kg/m^3)

q_{bkx}, q_{bky} = components of bed load transport rate in x and y directions (m^2/s)

z_{bk} = elevation of the k^{th} size class of sediment in z direction (m).

4.3.5 Non-equilibrium Transport in the CCHE2D Model

Unlike other sediment transport models that adopt the assumption of local equilibrium for bed load transport simulation, the CCHE2D Model is able to implement a full non-equilibrium transport model for both bed load and suspended load (Wu, 2001).

4.3.6 Boundary Conditions and Initial Conditions for Sediment Transport

To simulate the sediment transport in the CCHE2D Model, the inflow sediment discharge is required at each inlet boundary. In addition, the time series of inflow sediment discharge is needed in case of unsteady conditions simulation. For nonuniform sediment transport, the size distribution and the fractional sediment discharge of the inflow sediment are also required.

4.3.7 Empirical Formulas of Non-cohesive Sediment Transport in the CCHE2D Model

Although several formulas are available for sediment transport capacity, the CCHE2D Model provides four formulas or modules capable of analysing the sediment transport capacity. The formulas that are used in the CCHE2D Model are:

- modified Engelund and Hansen's formula
- modified Ackers and White's formula
- SEDTRA module
- Wu, Wang and Jia's Formula

Further details are given on these different formulas for sediment transport capacity in the following sections.

4.3.7.1 Modified Engelund and Hansen's Formula

The Engelund and Hansen formula was modified to calculate the fractional transport capacity for non uniform bed-material load (Wu, 2001). The modified formula is given by

$$f'\phi_k = 0.1(\varepsilon_k \tau_{*k})^{5/2} \tag{4.22}$$

with

$$f' = \frac{2gRS}{U^2}$$

$$\phi_k = \frac{q_{t*k}}{p_{bk}\sqrt{(\gamma_s/\gamma - 1)g d_k^3}}$$

$$\varepsilon_k = \left(\frac{p_{ek}}{p_{hk}}\right)^m, \quad \tau_{*k} = \frac{\tau_o}{(\gamma_s - \gamma)d_k}$$

where,

f' = friction factor

ϕ_k = dimensionless sediment transport rate

τ_{*k} = dimensionless bed shear stress

ε_k = correction factor accounting for the hiding and exposure effect of nonuniform sediment transport

q_{t*k} = bed-material load transport rate (m^2/s)

d_k = diameter of the k^{th} size class of bed material (m)

γ_s, γ = unit weight of sediment and unit weight of water respectively (N/m^3)

U = average flow velocity (m/s)

R = hydraulic radius of channel (m)

S = energy slope

m = power index and its default value in CCHE2D Model is 0.45

p_{bk} = bed material gradation

p_{hk}, p_{ek} = hiding and exposure possibilities for the k^{th} size class of bed material.

According to Wu et al.(Wu, 2001), the modified Engelund and Hansen's formula is recommended for uniform or quasi-uniform sediment, but it is not as good as Wu, Wang and Jia's Formula and the SEDTRA module in the prediction of fractional transport rate of nonuniform sediment mixtures.

4.3.7.2 Modified Ackers and White's Formula

Proffit and Sutherland (Wu, 2001) proposed a bed-material load transport formula based on a previous formula developed by Ackers and White. The modified Akers and White formula for the k^{th} size class of sediment is

$$G_{gr,k} = C\left(\frac{F_{gr,k}}{A}\right)^m \tag{4.23}$$

with

$$F_{gr,k} = \varepsilon_k \frac{U_*^n}{[(\gamma_s/\gamma - 1)gd_k]^{1/2}} \left[\frac{V}{\sqrt{32}\log(\alpha h/d_k)}\right]^{1-n}$$

$$G_{gr,k} = \frac{C_{*k}h}{d_k\gamma_s/\gamma}\left(\frac{U_*}{V}\right)^n$$

where ε_k is given as follows:

$$\varepsilon_k = \begin{cases} 1.30, & d_k/d_u > 3.7 \\ 0.53\log(d_k/d_u) + 1.0, & 0.075 < d_k/d_u \leq 3.7 \\ 0.40, & d_k/d_u \leq 0.075 \end{cases} \tag{4.24}$$

and,

U_* = shear velocity (m/s)

V = flow velocity (m/s)

γ_s/γ = specific gravity which is a ratio of the density of sediment relative to the density of water and 2.65 is the default value in the CCHE2D Model

d_k, d_u = mean diameter of the k^{th} size fraction and the reference diameter used by Proffit and Sutherland (Wu, 2001) (m)

h = flow depth (m)

α = ratio between the near-bed concentration and the depth-averaged concentration

C_{*k} = depth-averaged concentration (kg/m^3).

n, A, m and C are coefficients of Ackers and White Formula (Wu, 2001). According to Proffit and Sutherland (Wu, 2001), this method can provide good prediction for experimental cases, but it is not recommended for field study. In Further studies conducted by Wu and Wang (Wu, 2001) it was found that the modified Ackers-White formula is not applicable to very fine sediment. However, the method can provide reliable results for single-size sediment transport.

4.3.7.3 SEDTRA Module

The main characteristic of the SEDTRA module is the use of three different established transport relations to compute the transport rate for different size classe. These transport relations are (Wu, 2001):

- Laursen's formula for size classes from $0.010\,mm$ to $0.25\,mm$
- Yang's formula for size classes from $0.25\,mm$ to $2.0\,mm$
- Meyer-Peter and Mueller's formula for size classes from $2.0\,mm$ to $50.0\,mm$.

In this module, total discharge of sediment C_{*t} is calculated as:

$$C_{*t} = \sum_k p_k C_{*k} \tag{4.25}$$

where,

C_{*k} = sediment transport capacity for the k^{th} size class (g/m^3)

p_k = percentage of k^{th} size class of sediment.

The hiding and exposure effects of nonuniform sediment mixtures are taken into account in this method by adjusting d_{ek}, which is the sediment size used in the critical flow strength calculation. The sediment size is then recalculated using the following equation (Wu, 2001):

$$d_{ek} = d_k \left(\frac{d_k}{d_m} \right)^{-x} \tag{4.26}$$

where, d_k, d_m are the mean size of k^{th} size class and the mean diameter of bed material respectively and x is given by $x = 1.7/B$. B is a parameter defined as:

$$B = \left(\frac{d_c}{d_c}\right)^{1/2} \sum p_m \tag{4.27}$$

where, d_c and d_f are the diameters of the coarse and fine modes respectively and p_m is the portion of the sediment mixture contained in the coarse and fine modes.

In the CCHE2D model, the parameter x is specified as an input value when the SEDTRA module is activated to calculate sediment transport capacity. Its value varies between 0 and 1.

The SEDTRA module can be used for the calculation of single-size sediment transport because of the above-mentioned transport relations that are utilised by this module.

4.3.7.4 Wu, Wang and Jia's Formula

The bed load transport capacity proposed by Wu, Wang and Jia (Wu, 2001) is given by:

$$\phi_{bk} = 0.0053 \left[\left(\frac{n'}{n}\right)^{3/2} \frac{\tau_b}{\tau_{ck}} - 1\right]^{2.2} \tag{4.28}$$

with

$$\phi_{bk} = \frac{q_{b*k}}{p_{bk}\sqrt{(\gamma_s/\gamma - 1)g d_k^3}}$$

$$\tau_{ck} = 0.03(\gamma_s - \gamma) d_k (p_{hk}/p_{ek})^{0.6}, \quad n' = d_{50}^{1/6}/20$$

where,

ϕ_{bk} = dimensionless bed load transport capacity

q_{b*k} = equilibrium transport rate of the k^{th} size class of bed load per unit width (m^2/s)

p_{bk} = bed material gradation in the mixing layer

n, n' = Manning's roughness coefficient for channel bed and the Manning's coefficient corresponding to the grain roughness respectively

τ_b, τ_{ck} = bed shear stress and the critical shear stress (N/m^2)

p_{hk}, p_{ek} = hiding and exposure probabilities for the k^{th} size class of bed material

d_k = diameter of the k^{th} size class of bed material (m)

γ_s, γ = unit weight of sediment and the unit weight of water respectively (N/m^3).

The Equation 4.28 was calibrated by using several sets of laboratory data for nonuniform bed load as well as the field data from natural rivers (Wu, 2001). In the CCHE2D Model , Wu, Wang and Jia's formula is set as the default formula for sediment transport capacity calculation.

4.4 Numerical Model Setup and Calibration

4.4.1 Bathymetry Development

The bathymetry data is obtained from laboratory flume geometry. The data consists of points with known heights above the flume floor along transverse sections at regular intervals along the flume. This data file is then imported onto the CCHE2D Mesh Generator to generate mesh. The rest of the bathymetry is created by interpolation between the sections along the gridlines.

For this mathematical model, a $5\,mm$ by $5\,mm$ size curvilinear mesh was generated with a total of around 32500 grids. A fine grid size was chosen in order to increase the accuracy of the flow and sediment transport simulations. The mesh representing the complete bathymetry of the laboratory flume is depicted in Figures 4.4 and 4.5.

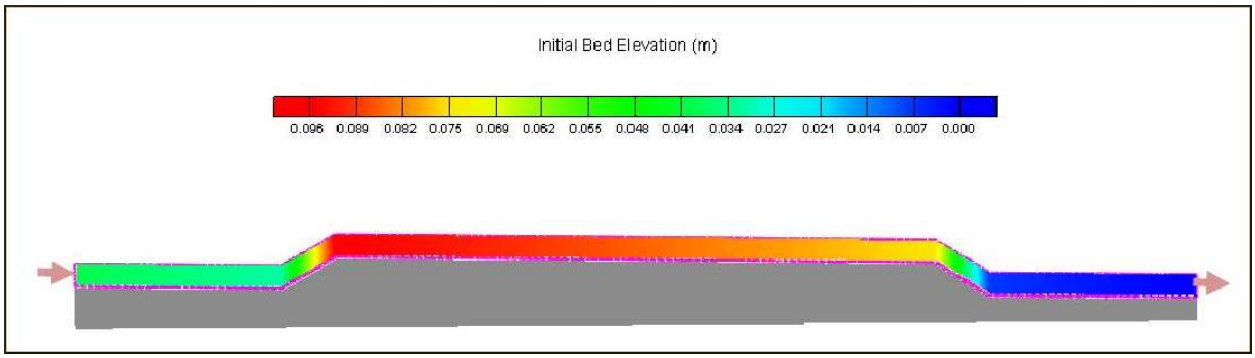

Figure 4.4: Laboratory flume bathymetry as modeled in the CCHE2D Model

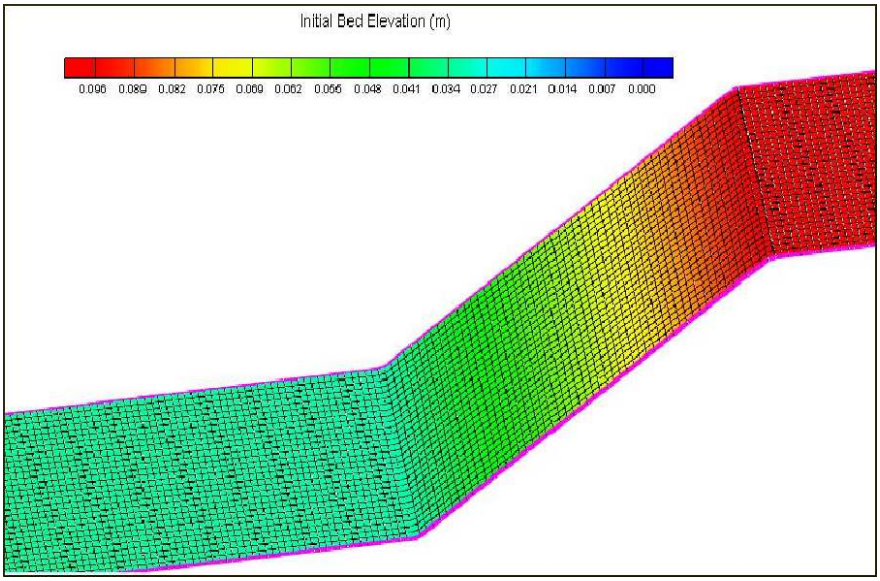

Figure 4.5: A close up of the laboratory flume bathymetry showing the 5 mm by 5 mm grid curvilinear mesh

4.4.2 Initial Flow Conditions Setup

In addition to the geometry information, the information of the initial flow conditions including initial water surface level, initial bed elevation, bed roughness, bed erodibility, maximum deposition thickness and maximum erosion thickness are also required in the mesh file.

The initial bed elevation is imported from the generated mesh and an initial water surface level is defined and linearly interpolated along the flume bathymetry.

The bed roughness (Manning's roughness n value) of the erodible zone was computed as 0.016 (see Subsection 3.1.6) whereas a bed roughness of 0.011 (corresponding to the glass material roughness) was assigned to the rest of the simulation area (Figure 4.6).

Erodible bed was restricted to the part of the flume where cubes were packed (see Figure 4.7). Note that 1 corresponds to erodible bed zone and 0 corresponds to non erodible bed zone in Figure 4.7. Default values were finally used for maximum deposition and erosion thickness.

These initial flow conditions were calibrated in accordance with observed conditions of the physical model for different test slopes.

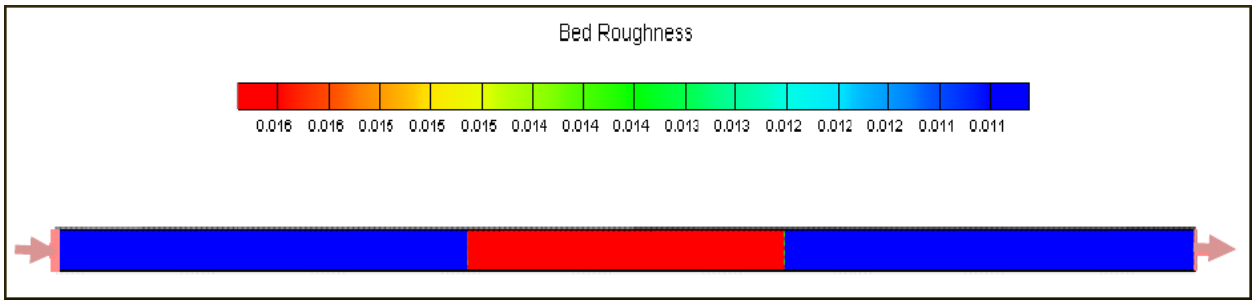

Figure 4.6: Bed roughness of the laboratory flume as modeled in the CCHE2D Model

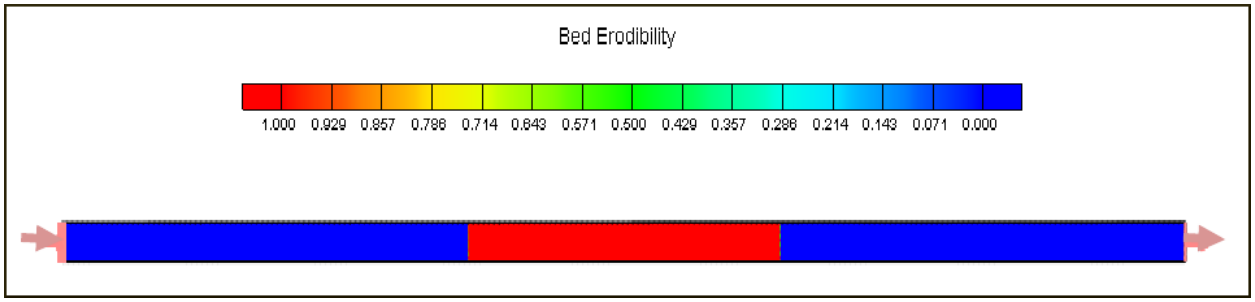

Figure 4.7: Erodibility of the laboratory flume bathymetry as modeled in the CCHE2D model

4.4.3 Inlet and Outlet Boundary Conditions Setup

In the inlet boundary condition, the total discharge option was used and a flow rate was entered for each simulation. Water surface level was defined for the output boundary condition as observed in the physical model test.

4.4.4 Sediment Transport Setup

The sediment transport model was set up by using two separate sediment transport capacity formulas namely, Wu, Wang and Jia's formula and the modified Ackers and White's formula provided by the CCHE2D Model. Since the main focus of this study is on bed load transport, total load as bed load model is chosen as the transport mode in the simulation.

4.5 Flow and Sediment Parameters

Flow and sediment parameters that were used in the CCHE2D Model are shown in Table 4.1 with their different values. In this Table, the different size classes correspond to d_{33}, d_{66} and d_{99} and were determined by using the particle size distribution graph in Figure 3.2.

Table 4.1: Flow and sediment parameters used in the mathematical model

	Parameter		Value
Flow	Turbulence model		Parabolic Eddy Viscosity (default)
	Turbulence viscosity coefficient		1 (default)
	Depth to consider dry		$0.001\,m$
	Wall slipness coefficient		1 (total slip condition)
	Coriolis force coefficient		0 (default)
	Gravitational acceleration		$9.81\,m/s^2$
	Von Karman Constant		0.41 (default)
	Fluid kinematic viscosity		$10^{-6}\,m^2/s$
Sediment	Size class diameter	class 1	$4.43\,mm\,(33\%)$
		class 2	$4.82\,mm\,(33\%)$
		class 3	$5.64\,mm\,(34\%)$
	Number of layers		1
	Sediment specific gravity		1.424 (computed)
	Porosity		0.130 (computed)
	Bed load rate		$0\,kg/m.s$

4.6 CCHE2D Simulation Procedures

Before the numerical simulation was carried out, special care was taken in order to establish the initial flow conditions and the initial bed conditions for the simulation of the conditions experienced during the laboratory flume tests.

After all the initial conditions and the boundary conditions were set, the simulation was performed. Basically the simulation of sediment transport is divided into two steps. Firstly, flow simulation was carried out with steady flow condition. After the flow simulation, sediment transport simulation was executed. The sediment transport simulation was run for approximately the same period of time that it took the respective physical model tests to reach their state of equilibrium. In the subsequent sections simulation results are presented.

4.7 Simulation Results for Gentle Slopes (0.72% and 1.55%)

The laboratory flume test for the 0.72%-slope and the 1.55%-slope were numerically simulated and results of the flow simulation and sediment transport simulation are detailed in the next subsections.

4.7.1 Flow Simulation Results

The simulated average water depth, flow velocity and shear stress for the 0.72%-slope at the erodible section of the simulation zone are $0.061\,m$, $0.63\,m/s$ and $1.80\,N/m^2$ respectively. Numerical flow simulation results of the laboratory flume test for the 0.72%-slope are shown in Figures 4.8 (a)-(d).

For the 1.55%-slope, values of $0.031\,m$, $0.71\,m/s$ and $2.87\,N/m^2$ were found as simulated average water depth, flow velocity and shear stress respectively at the location of the erodible zone. Numerical flow simulation results of the laboratory flume test for the 1.55%-slope are shown in Figures 4.9 (a)-(d).

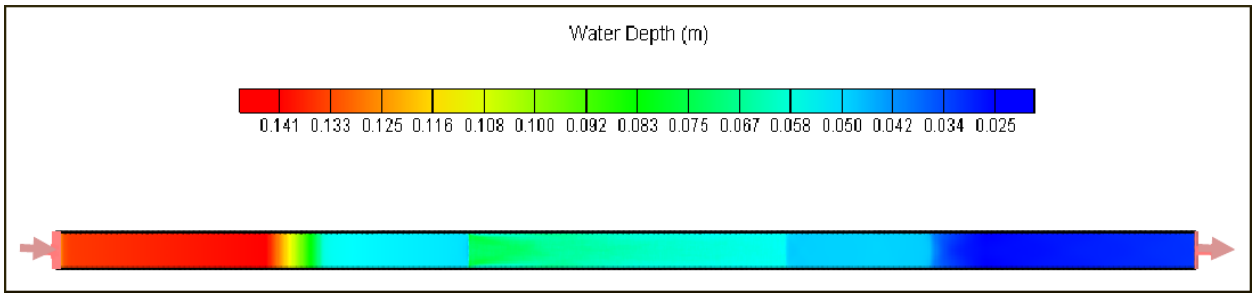

(a) Simulated water depth

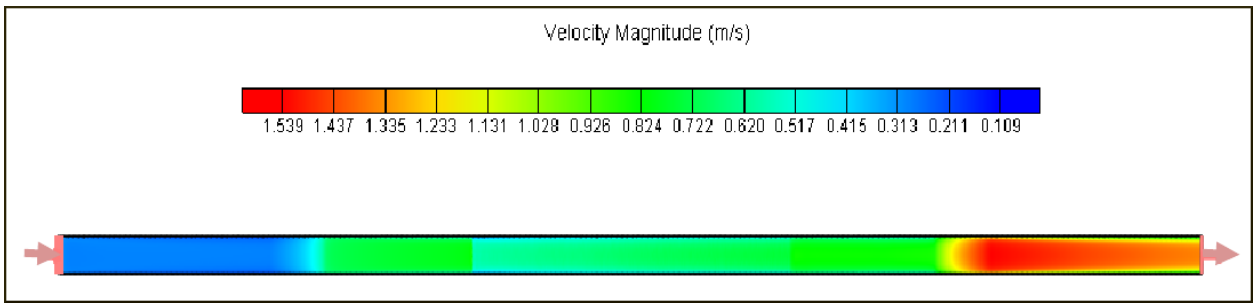

(b) Simulated velocity

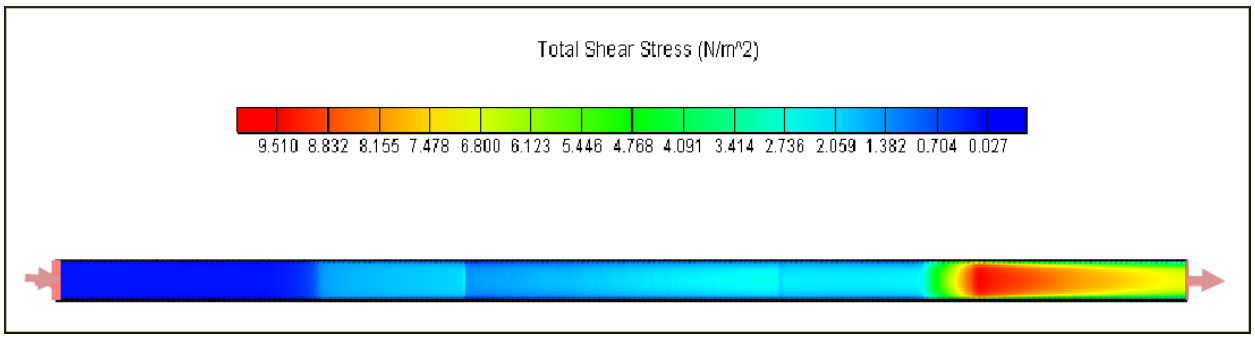

(c) Simulated shear stress

Figure 4.8: Simulated flow results for slope $=0.72\%$, Q $= 0.0058\, m^3/s$

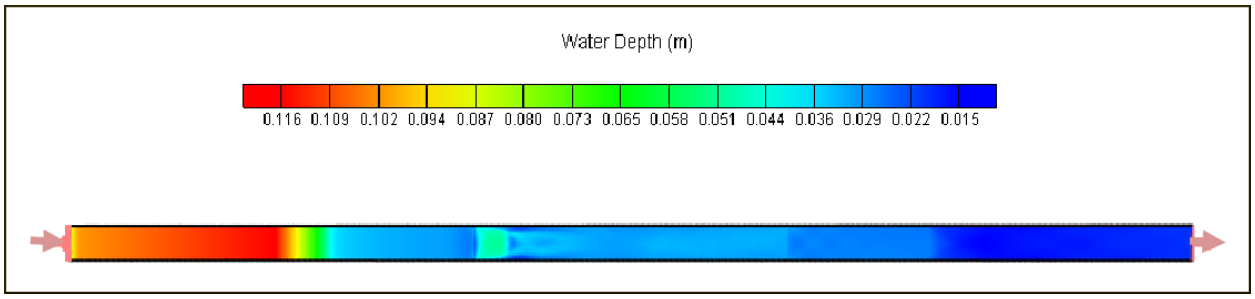

(a) Simulated water depth

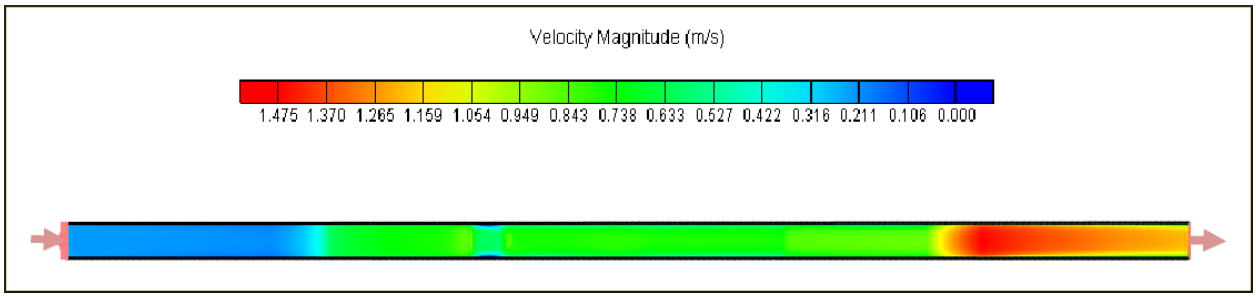

(b) Simulated velocity

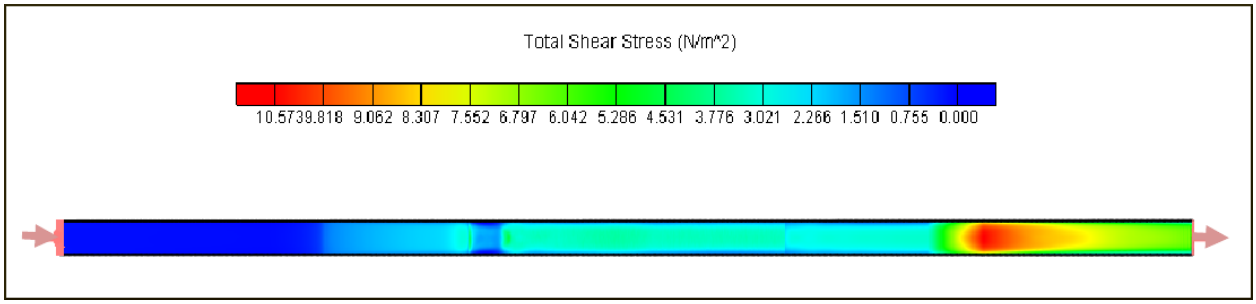

(c) Simulated shear stress

Figure 4.9: Simulated flow results for slope $= 1.55\%$, Q $= 0.0032\, m^3/s$

4.7.2 Sediment Transport Simulation Results

After flow simulation, sediment transport was simulated in order to test the capability of the numerical model to predict the erosion process. The results of erosion simulation for the 0.72%-slope and the 1.55%-slope are given in Figures 4.10 and 4.11.

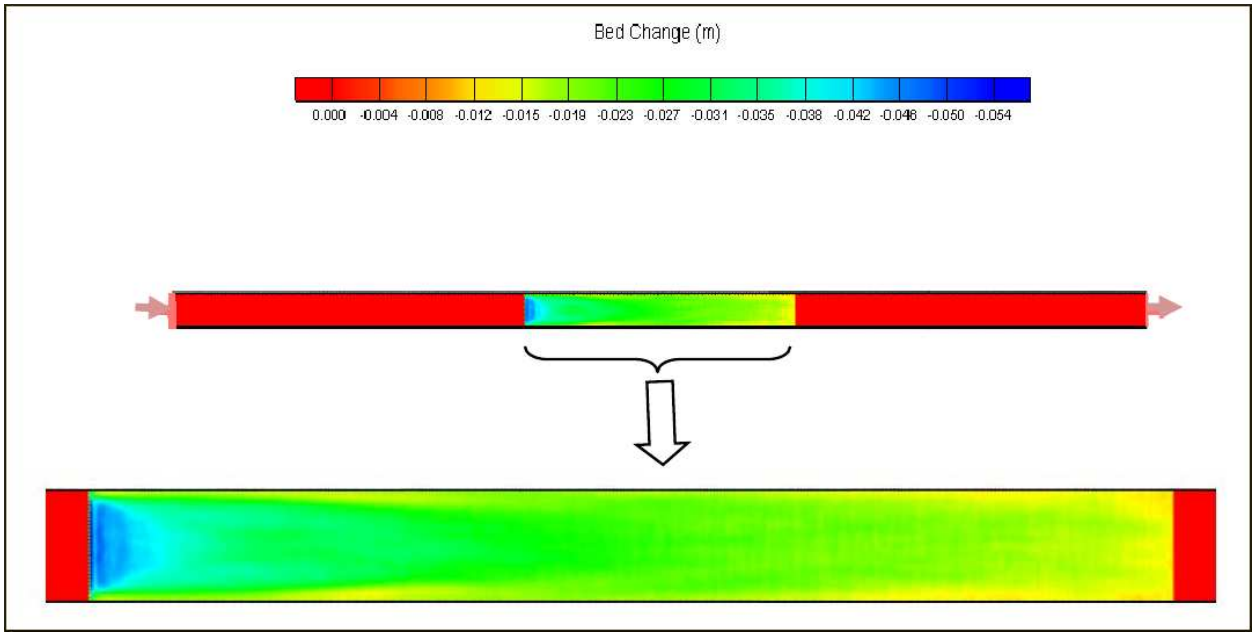

Figure 4.10: Simulated bed erosion for a 0.72%-slope

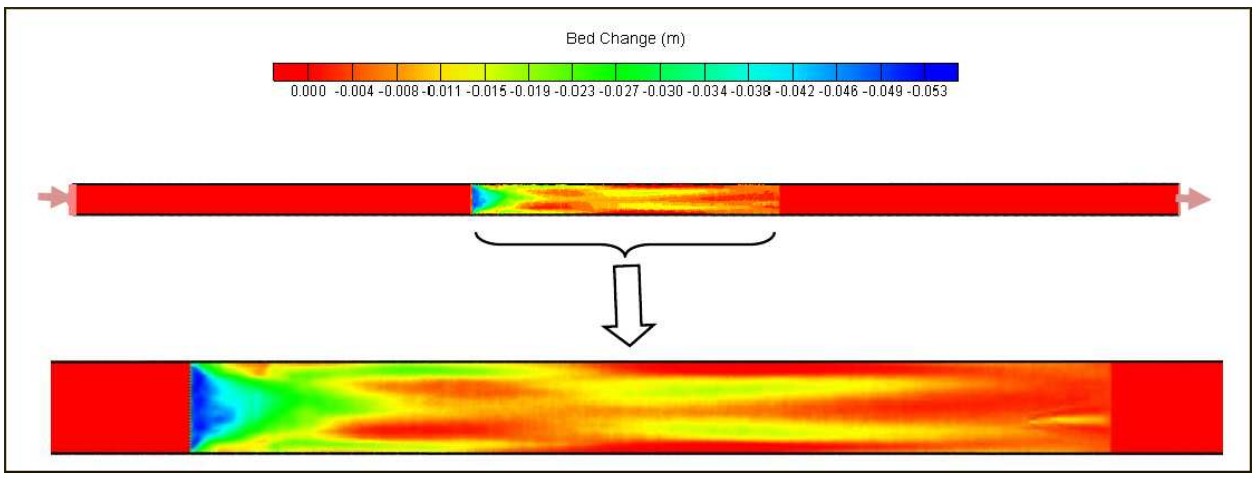

Figure 4.11: Simulated bed erosion for a 1.55%-slope

4.8 Simulation Results for Steep Slopes (2.59% and 3.52%)

The laboratory flume test for the 2.59%-slope and the 3.52%-slope were numerically simulated and the results of flow simulation and sediment transport simulation are detailed in the next subsections.

4.8.1 Flow Simulation Results

The simulated average water depth, flow velocity and shear stress for the 2.59%-slope at the erodible part of the simulation area are $0.021\,m$, $0.59\,m/s$ and $3.16\,N/m^2$ respectively. Numerical flow simulation results of the laboratory flume test for the 2.59%-slope are shown in Figures 4.12 (a)-(d).

For the 3.52%-slope, values of $0.015\,m$, $0.77\,m/s$ and $4.32\,N/m^2$ were found as simulated average water depth, flow velocity and shear stress respectively at the location of the erodible zone. Numerical flow simulation results of the laboratory flume test for the 3.52%-slope are shown in Figures 4.13 (a)-(d).

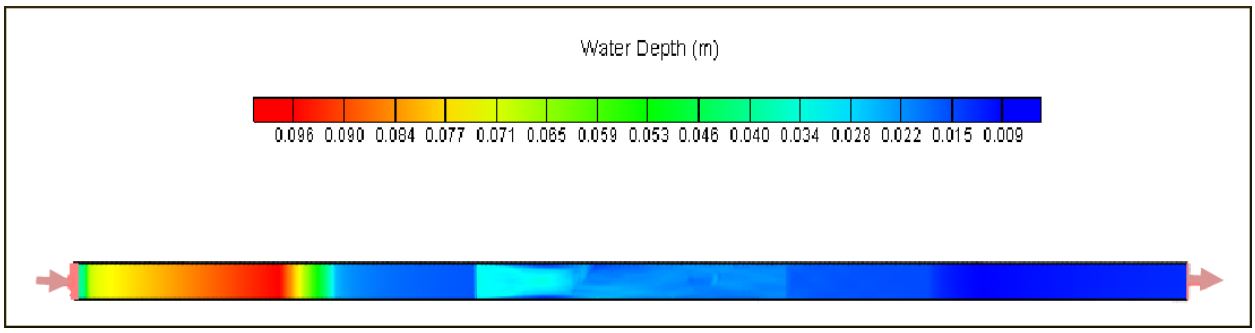

(a) Simulated water depth

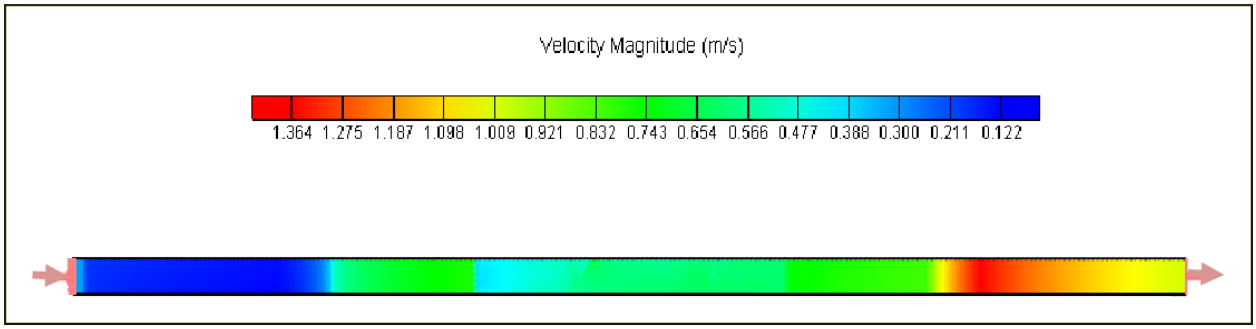

(b) Simulated velocity

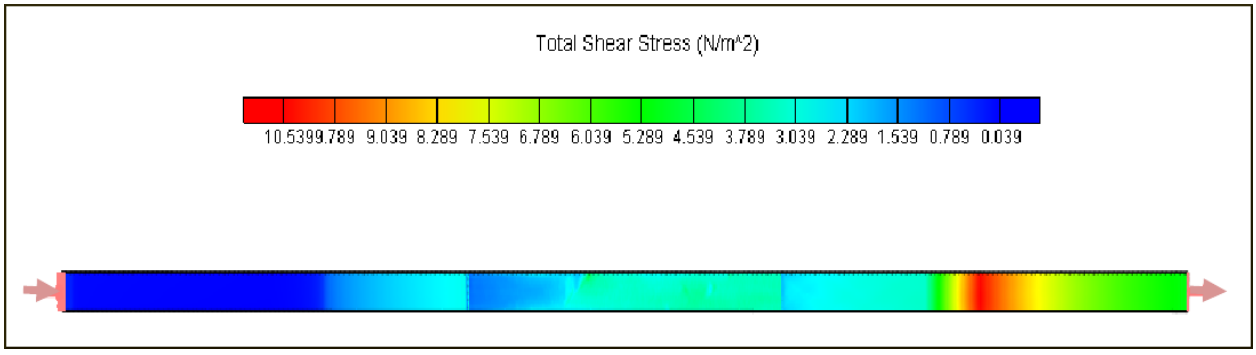

(c) Simulated shear stress

Figure 4.12: Simulated flow results for slope $= 2.59\%$, Q $= 0.0019\, m^3/s$

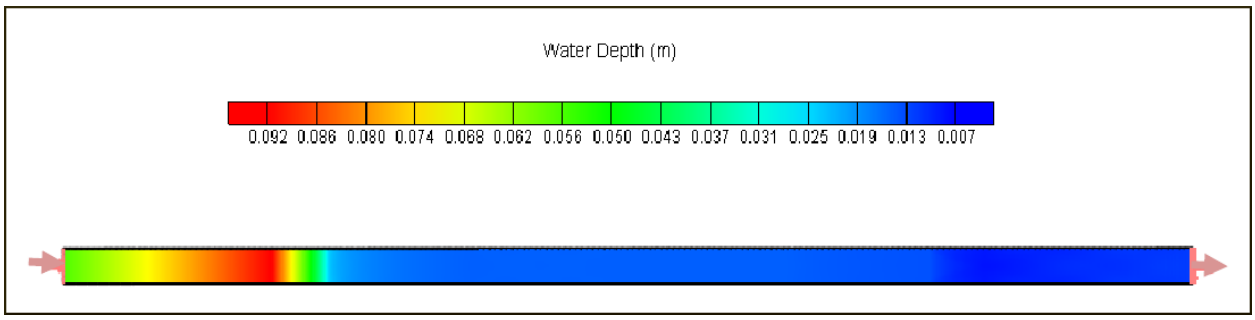

(a) Simulated water depth

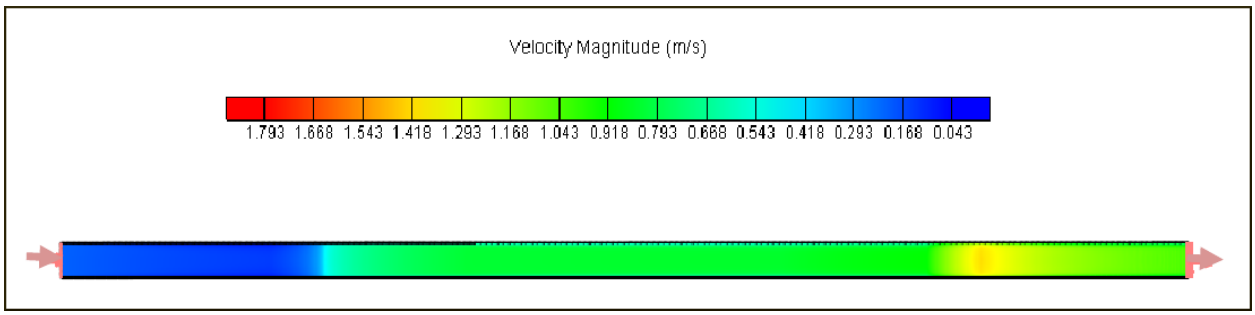

(b) Simulated velocity

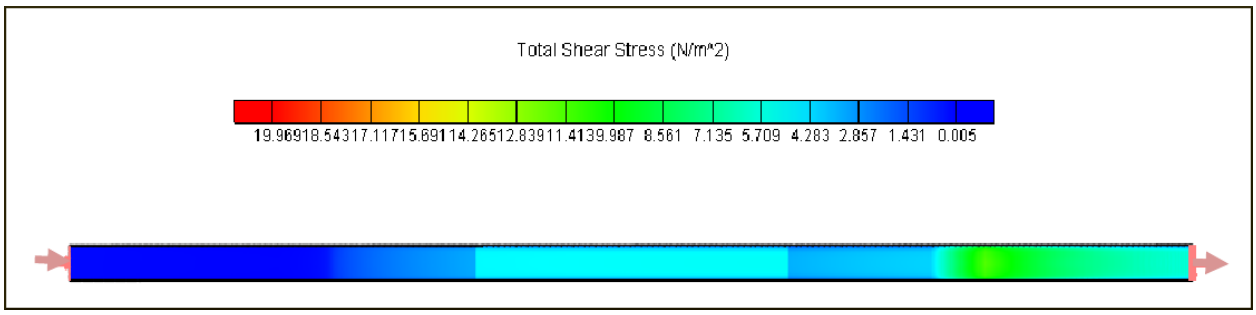

(c) Simulated shear stress

Figure 4.13: Simulated flow results for slope $= 3.52\%$, Q $= 0.0017\, m^3/s$

4.8.2 Sediment Transport Simulation Results

After flow simulation, sediment transport was simulated in order to assess the erosion process. The results of erosion simulation for 2.59%-slope and 3.52%-slope are given in Figures 4.14 and 4.15.

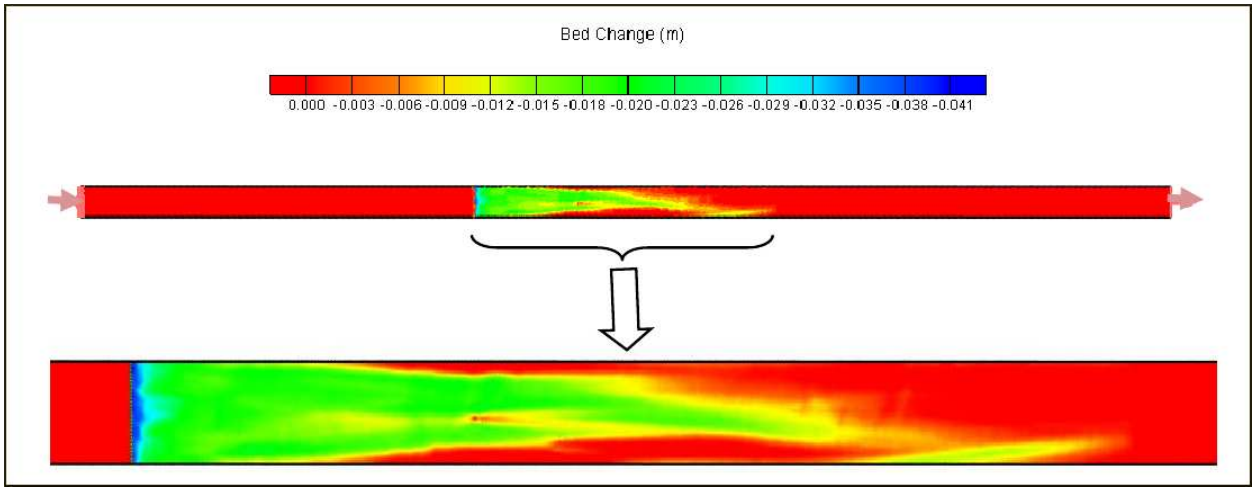

Figure 4.14: Simulated bed erosion for a 2.59%-slope

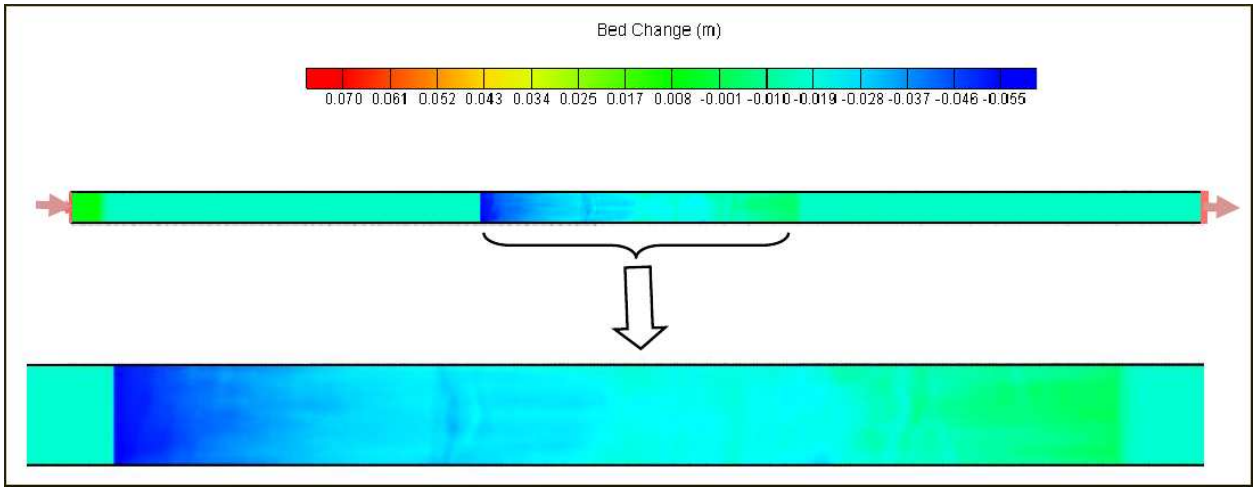

Figure 4.15: Simulated bed erosion for a 3.52%-slope

4.9 Results of Numerical Modelling against Laboratory Tests

4.9.1 Flow Results Comparison

The flow velocity, the water depth and the shear stress at the erodible part of both models (physical and numerical) were compared. These parameters correspond to the mean values. The shear stress at the bed for the physical model is calculated by using the Chézy formula (Chadwick et al., 2004).

$$\tau_0 = \rho g R S_0 \tag{4.29}$$

where,

τ_0 = bed shear stress (N/m^2)

ρ = water density (kg/m^3)

g = gravitational acceleration (m/s^2)

R = hydraulic radius (m)

S_0 = bed slope

Comparison of the flow results for different slope tests are given in the following Tables.

Table 4.2: Comparison of the flow results for 0.72% and 1.55% slopes

	Slope = 0.72%			Slope = 1.55%		
	Water depth (m)	Velocity (m/s)	Shear stress (N/m^2)	Water depth (m)	Velocity (m/s)	Shear stress (N/m^2)
Observed	0.057	0.70	2.29	0.029	0.73	3.18
Simulated	0.061	0.63	1.80	0.031	0.71	2.87

Table 4.3: Comparison of the flow results for 2.59% and 3.52% slopes

	Slope = 2.59%			Slope = 3.52%		
	Water depth (m)	Velocity (m/s)	Shear stress (N/m^2)	Water depth (m)	Velocity (m/s)	Shear stress (N/m^2)
Observed	0.019	0.75	3.85	0.015	0.77	4.32
Simulated	0.021	0.59	3.16	0.016	0.75	3.98

The simulated water depth is slightly higher than the observed water depth for gentle slopes (0.72% and 1.55%). However, the water depth is accurately simulated as observed during the physical test.

Although the observed shear stress is relatively higher than the simulated shear stress, the observed shear stress and the simulated shear stress show the same magnitude of value. The observed velocity and the simulated velocity are also in good agreement as indicated in Tables 4.2 and 4.3.

4.9.2 Sediment Transport Results Comparison

4.9.2.1 Comparison of Bed Erosion Results for 0.72% and 1.55% Slopes

The erosion observed during the laboratory flume test was compared with the erosion predicted by the mathematical model. Therefore, the bed change from the actual erosion observed during the physical model was plotted using CCHE2D Model. Both observed bed erosion and simulated bed erosion are shown in Figures 4.16 (a) and (b).

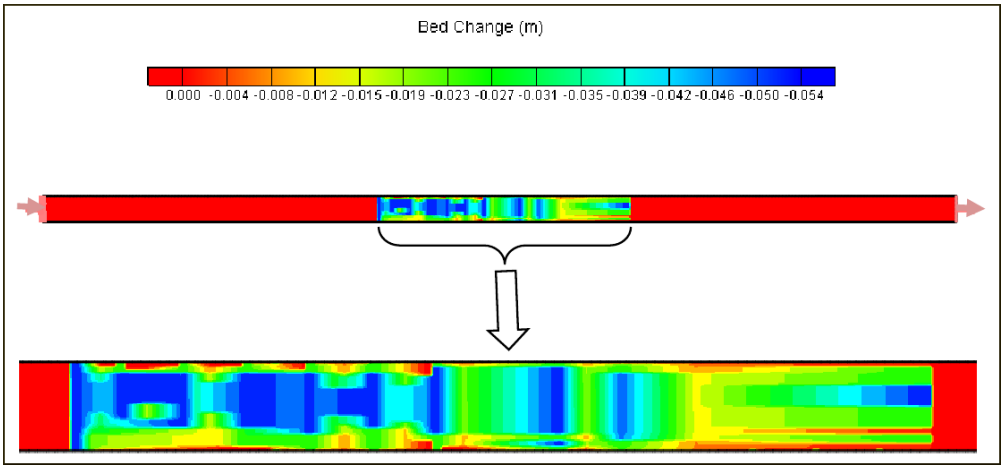

(a) Observed bed erosion

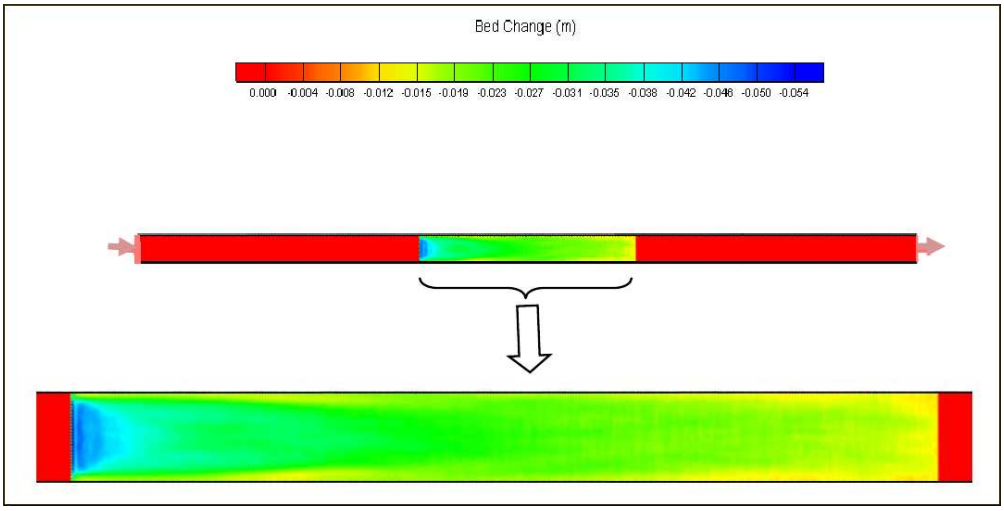

(b) Simulated bed erosion

Figure 4.16: Bed erosion for slope $= 0.72\%$, Q $= 0.0058\, m^3/s$

For the 1.55%-slope the observed bed erosion and the simulated bed erosion are shown in Figures 4.17 (a) and (b).

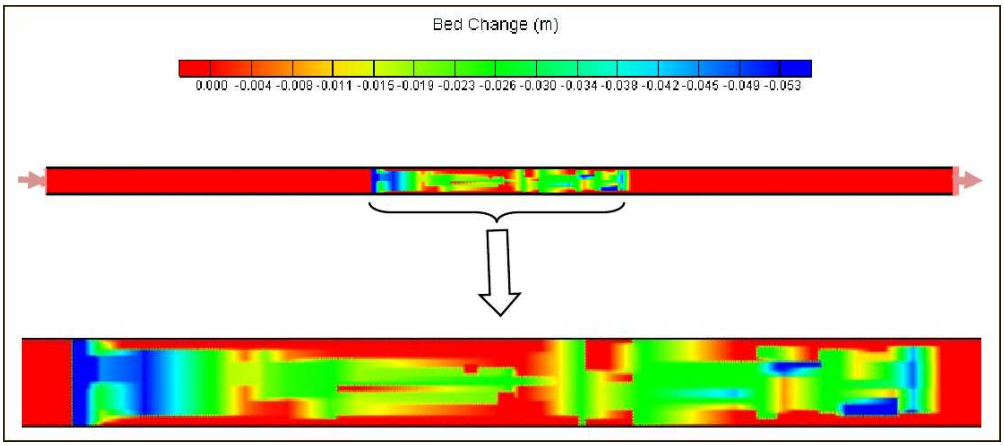

(a) Observed bed erosion

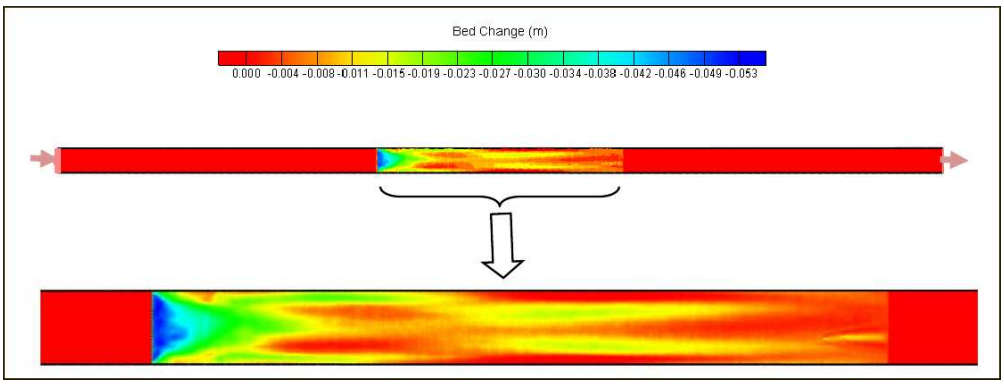

(b) Simulated bed erosion

Figure 4.17: Bed erosion for slope $= 1.55\%$, Q $= 0.0032\, m^3/s$

4.9.2.2 Comparison of Cross Section Results for 0.72% and 1.55% Slopes

The erosion predicted by the numerical model was compared with the actual erosion observed during the laboratory flume test. Therefore, typical cross-sections of observed and simulated changes in elevation at upstream, midstream and downstream of the model were plotted against each other. In addition, the longitudinal profiles in both models were compared. Cross sections and longitudinal profile for 0.72%-slope are shown by graphs in Figures 4.18 (a)-(d).

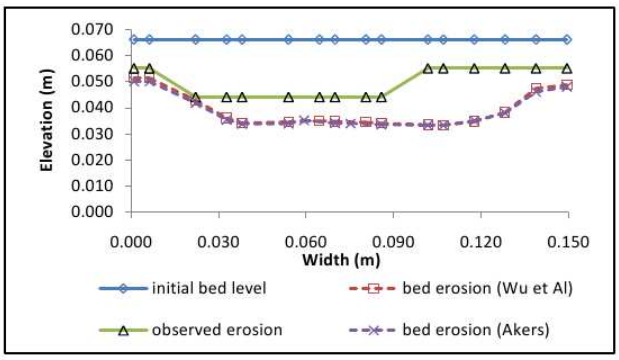

(a) Upstream cross section

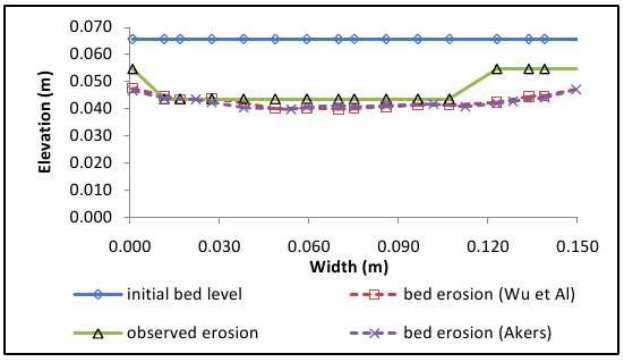

(b) Midstream cross section

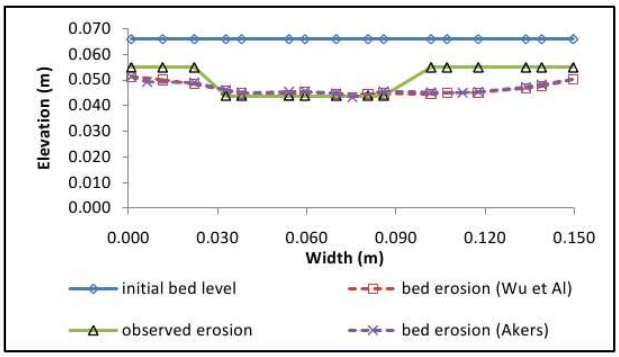

(c) Downstream cross section

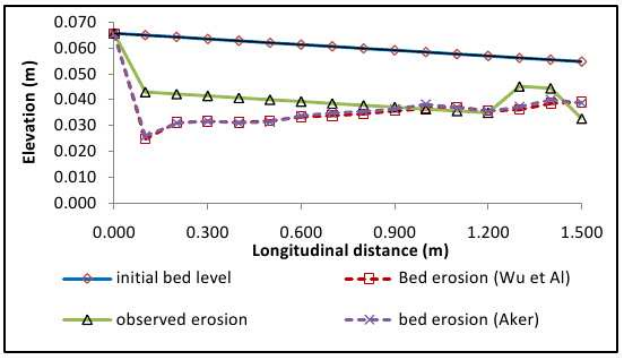

(d) Longitudinal profile

Figure 4.18: Cross sections for slope $= 0.72\%$, Q $= 0.0058\, m^3/s$

For the 1.55%-slope the cross sections and longitudinal profile are given by the subsequent graphs (Figures 4.19 (a)-(d)).

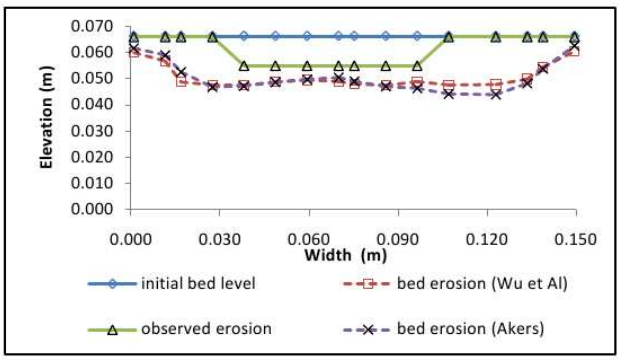

(a) Upstream cross section

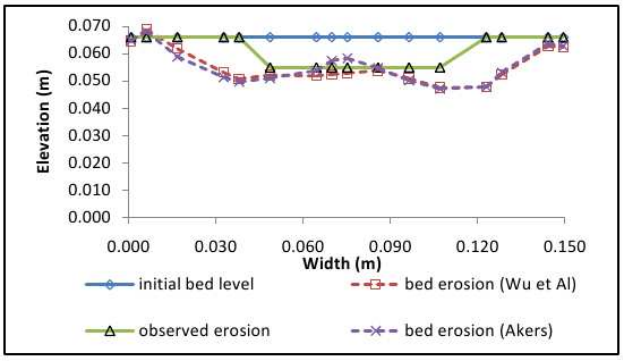

(b) Midstream cross section

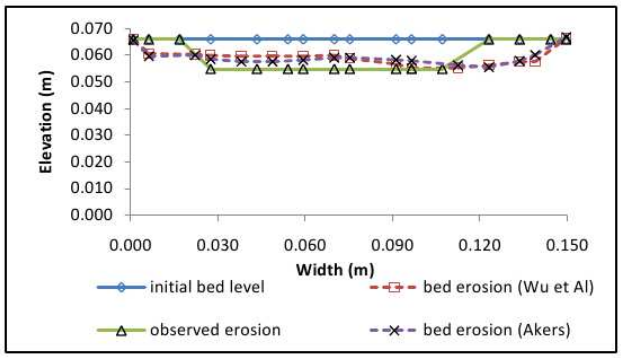

(c) Downstream cross section

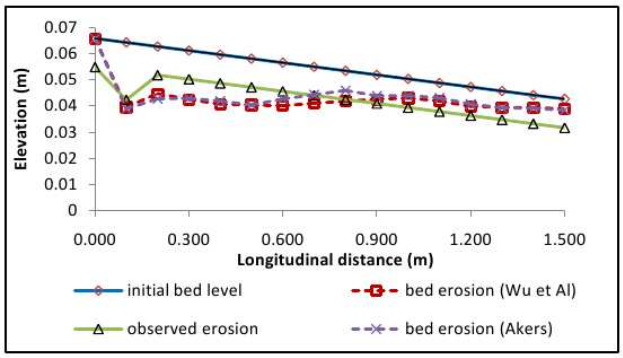

(d) Longitudinal profile

Figure 4.19: Cross sections for slope = 1.55%, Q = $0.0032\, m^3/s$

4.9.2.3 Comparison of Bed Erosion Results for 2.59% and 3.52% Slopes

For steep slopes (2.59% and 3.52%), the erosion predicted by the mathematical model was also compared with the erosion observed during the physical model test. In this regard, the bed change from the actual erosion observed during the physical model was plotted using CCHE2D Model. Both observed bed erosion and simulated bed erosion are shown in Figures 4.20 (a) and (b).

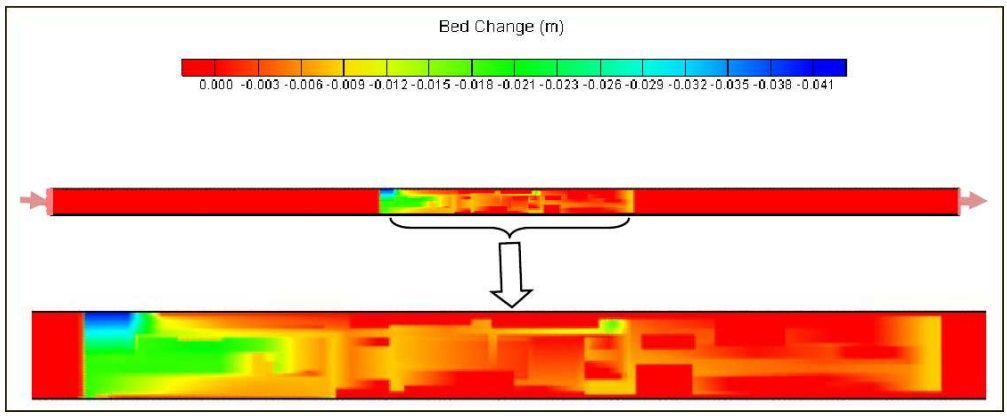

(a) Observed bed erosion

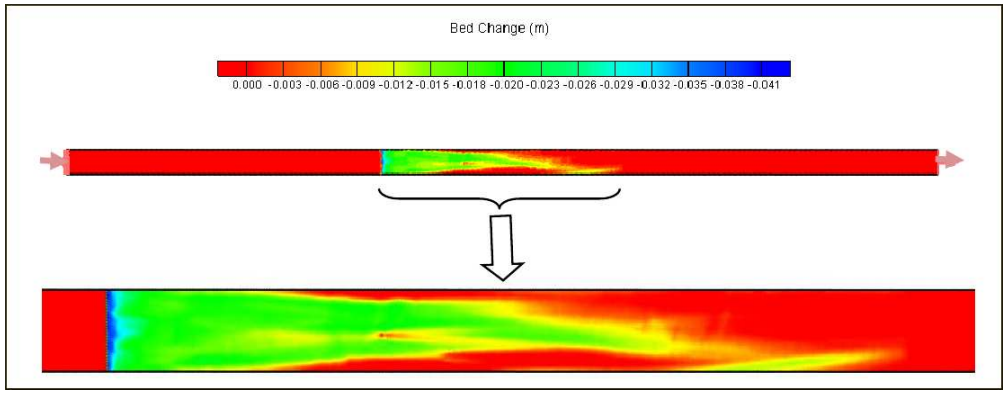

(b) Simulated bed erosion

Figure 4.20: Bed erosion for slope $= 2.59\%$, Q $= 0.0019\, m^3/s$

For the 3.52%-slope the observed bed erosion and the simulated bed erosion are shown in Figures 4.21 (a) and (b).

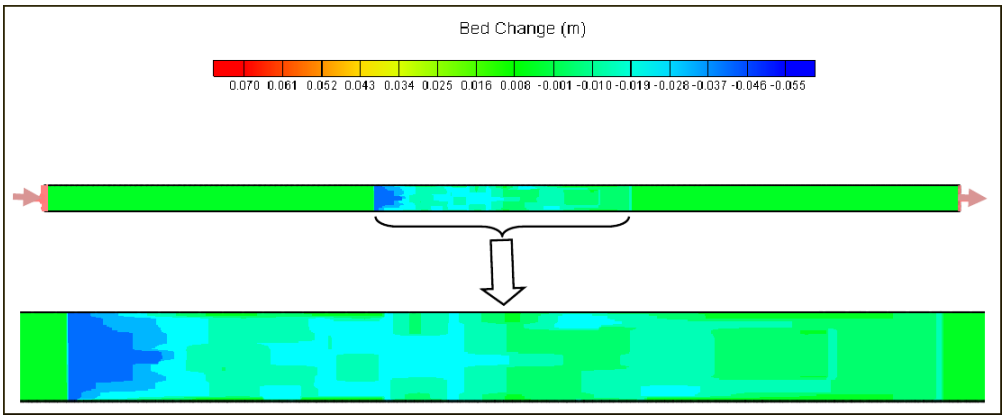

(a) Observed bed erosion

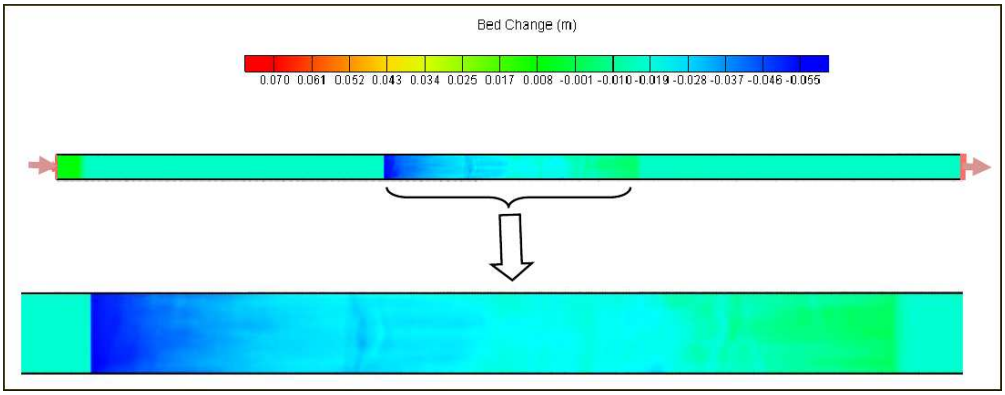

(b) Simulated bed erosion

Figure 4.21: Bed erosion for slope $= 3.52\%$, Q $= 0.0017\, m^3/s$

4.9.2.4 Comparison of Cross Section Results for 2.59% and 3.52% Slopes

For steep slopes (2.59% and 3.52%), the erosion predicted by the mathematical model was also compared with the erosion observed during the physical model test. In this regard, cross-sections of observed and simulated change of elevation at upstream, midstream and downstream of both models were plotted against each other. The longitudinal cross section for the numerical model and the laboratory flume test was also plotted. Cross-section plots for the 2.59% slope are illustrated by graphs in Figures 4.22 (a)-(d).

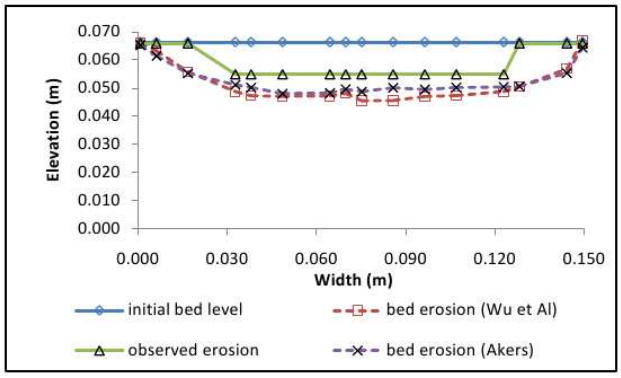

(a) Upstream cross section

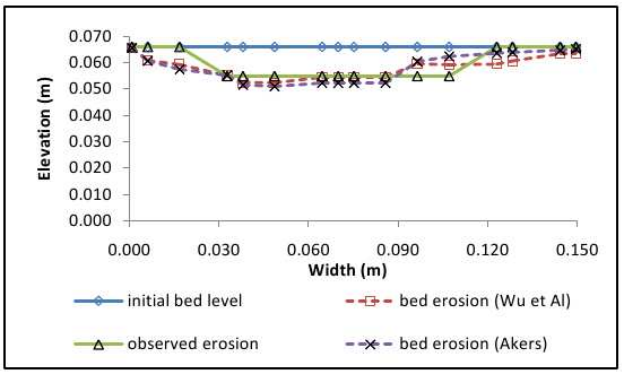

(b) Midstream cross section

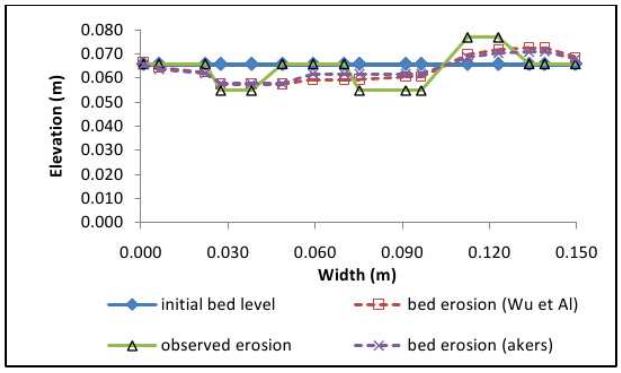

(c) Downstream cross section

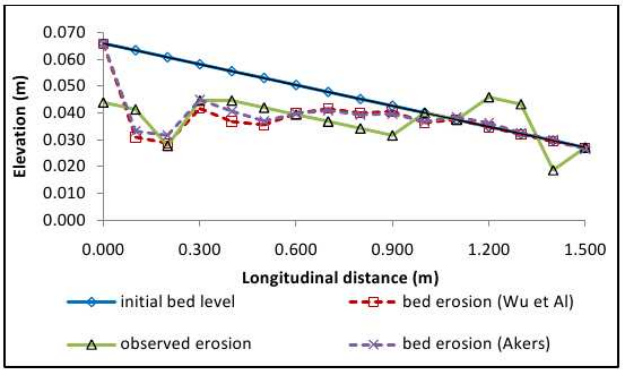

(d) Longitudinal profile

Figure 4.22: Cross sections for slope = 2.59%, Q = $0.0019\, m^3/s$

For the 3.52%-slope the compared cross sections and longitudinal profile are given by the subsequent graphs (Figures 4.23 (a)-(d)).

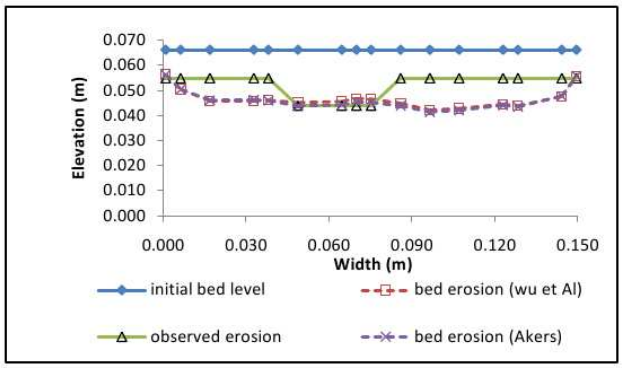

(a) Upstream cross section

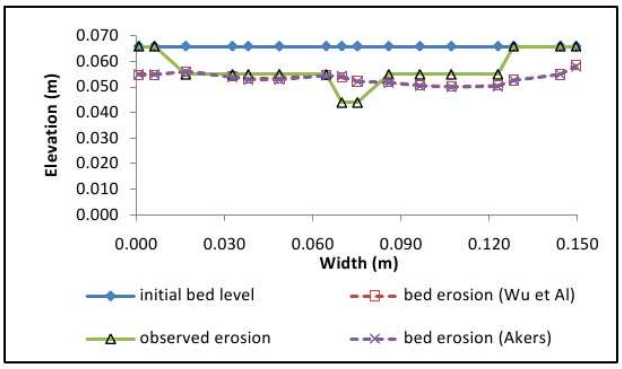

(b) Midstream cross section

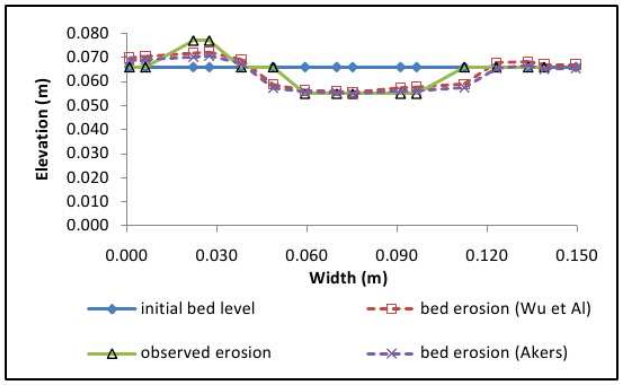

(c) Downstream cross section

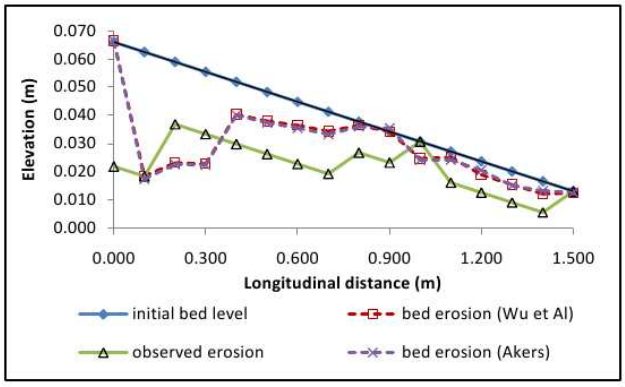

(d) Longitudinal profile

Figure 4.23: Cross sections for slope $= 3.52\%$, Q $= 0.0017\, m^3/s$

4.9.3 Validation of Numerical Model for Scour Prediction

The validation of the numerical model was made by comparing the prediction of erosion by the sediment transport simulation with the actual erosion observed during the laboratory flume test. Results of the comparison of cross sections presented in Figures 4.18 to 4.23 show that the two sediment transport capacity formulas, namely Wu, Wang and Jia's and the modified Ackers and White formula led to similar erosion depth results. Results also show that the simulated bed level and observed bed level reasonably led to the same magnitude of erosion with an average relative error of 10.4%. However, the simulated bed levels are smoother than the observed bed level cases (see Figures 4.16, 4.17, 4.20 and

4.21). These discrepancies between the simulated erosion and the observed erosion could be attributed to the use of the effective diameter which is defined as a sphere with the same settling velocity and the same relative density as an average cube would have. The effective diameter used as diameter size of the PVC cubes in the numerical model was smaller than the actual size of the cubes. A smaller particle diameter is generally expected to produce a deep erosion depth and a smooth bed level. In addition, the interlocking effect due to the packing of cubes during the laboratory tests could limit the erosion.

In view of the comparison between the simulated erosion and observed erosion during the laboratory flume test, it is evident that the mathematical modelling can provide a reasonable and detailed erosion prediction tool that can be considered reliable on condition that the model is correctly calibrated and set up to reflect the actual conditions of a particular case study.

5. Field Investigation: Case Study of Mokolo Dam

5.1 Background on Mokolo Dam

Mokolo Dam previously known as Hans Strijdom Dam, is located approximately $45\,km$ South of Lephalale on the Mokolo River, in the Limpopo Province. The dam is a rockfill embankment type dam and has a right flank concrete spillway with a maximum height of $57\,m$ above the lowest foundation. Classified as a large dam and completed in 1980, Mokolo Dam was primarily built for irrigation and industrial/mining usage for the surrounding areas.

5.1.1 Hydrological Investigation

According to the Department of Water Affairs (DWA, 2003), the largest historical flood peak ($2023\,m^3/s$) occurred in 1943. Since 1962, apart from the largest recorded flood peaks in $1975/76$ and 1996 (i.e. $1490\,m^3/s$ and $914\,m^3/s$) there are only seven years where the maximum flood peaks for those particular years were more than $400\,m^3/s$. The design flood for the dam ($1:100$ year) is $1615\,m^3/s$ and the Regional Maximum Flood (RMF) is estimated to be $6570\,m^3/s$ (DWA, 2003).

5.1.2 Historical Scour

Mokolo Dam is a rockfill embankment type dam with unlined spillway excavated in sandstone rock. Figures 5.1 and 5.2 show that the spillway chute is crossed by geological fault from the right bank to the left bank which undermines the quality of the rock in the field. During a large flood in 1996 ($914\,m^3/s$) the unlined spillway of Mokolo Dam scoured about $25\,m$ deep and a more than $300\,m$ long channel in the spillway discharge channel. General scour also occurred closer to the Crump weir forming the crest of the spillway as indicated in Figures 5.3 and 5.4.

Figure 5.1: Satellite image of Mokolo Dam spillway chute

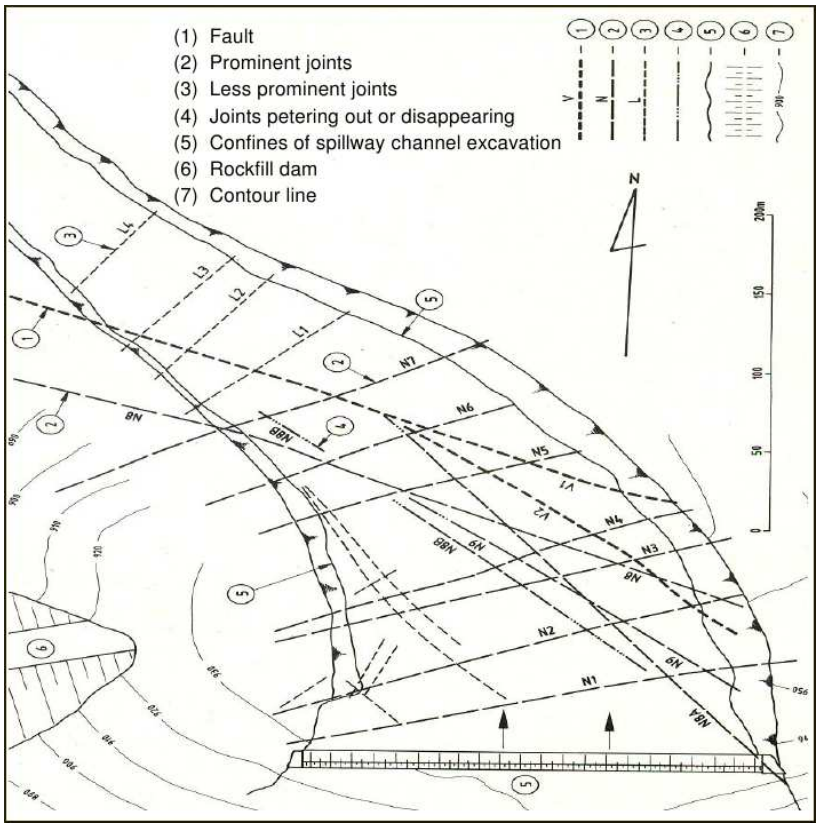

Figure 5.2: Joints and faults in Mokolo Dam spillway chute (Van Schalkwyk, 1994)

Figure 5.3: Deepest scour location viewed from upstream (2008)

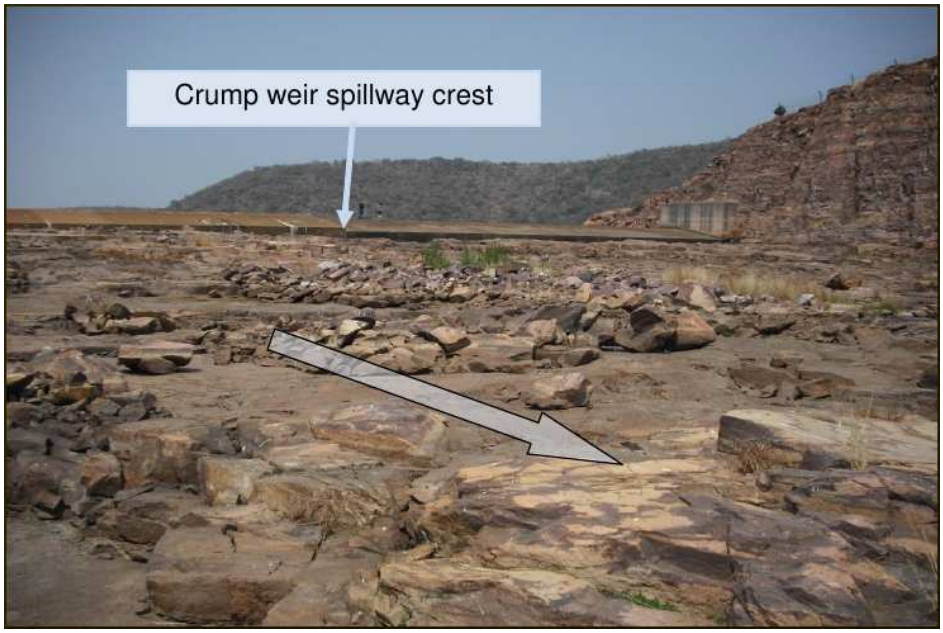

Figure 5.4: General scour downstream of Crump weir forming crest spillway (2008)

5.2 Test using Annandale Method on Mokolo Dam Spillway Chute

The Annandale method based on the stream power of the flow and the Erodibility Index of the rock was used to determine if it could predict the observed scour that occurred during a large flood in 1996.

5.2.1 Stream Power Determination

For the computation of stream power, it is assumed that the total energy (1996 flood) was dissipated in the observed scoured channel area with a particular discharge determined from flow simulation in section 5.3. From flow simulation, the discharge (Q) was found to be $800\,m^3/s$ and the total energy head (H) was $10\,m$, which was estimated by the difference between upstream water level and downstream water level. The area (A) on which the total energy was dissipated was assumed to correspond to the scoured channel area which is about $20\,m \times 300\,m$. The unit stream power was then computed using Equation 2.14 (see Section 2.6.2) and its value was $13\,kW/m^2$ for this particular case.

5.2.2 Erodibility Index Determination

The Erodibility Index was estimated by making use of tables and equations that were published by Annandale (1995) and Van Schalkwyk (1994) (see Appendix A). The mass strength number (M_s) for rock was determined by assuming a soft rock and making use of Tables A.1 and A.2 in Appendix A. A value of 8.39 as strength number for rock was used. Since the rock quality designation (RQD) ranges from 5 to 100 and assuming a soft rock, a value of 25 was estimated as RQD and considering multiple joint set a value of 5 was given as joint set number (J_n). The block size number (K_b) which is the ratio RQD$/J_n$ was computed to be 5. The joint roughness (k_d) for sandstone (rock type on Mokolo Dam spillway chute) is given by Table A.4 in appendix A as 1. The last geomechanical parameter required for Erodibility Index (K) computation is the joint structure number (J_s) which is essentially based on the orientation of the major joint sets with respect to water flow direction. An 80° dip angle in the direction of stream flow was assumed, which corresponds to a value of 0.67 for J_s (see Table A.5 in Appendix A). In summary the value of the erodibility index (K) for the unlined spillway of Mokolo Dam was estimated at 28 by making use of Equation 2.9 (see Section 2.6.1) . By plotting these computed values on Annandale's graph it was found that the corresponding plot is above the threshold line (Figure 5.5). That is, scour of the rock is possible, as observed during the flood of 1996.

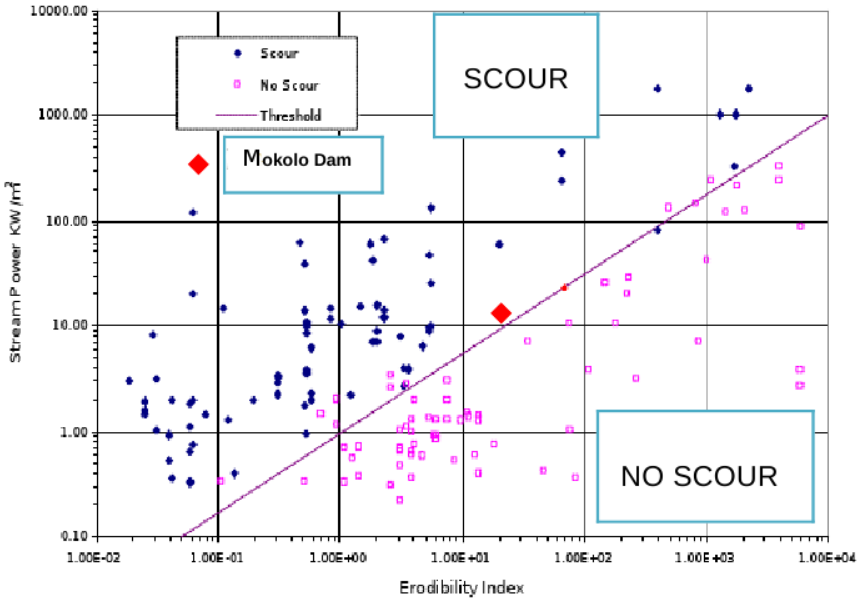

Figure 5.5: Erodibility Index Method on Mokolo Dam spillway chute

5.3 Mathematical Modelling of Rock Scour of Mokolo Dam Spillway

A large flood in 1996 left a scoured deep channel in the spillway and scour also occurred closer to the Crump weir. It is possible that future floods could erode the spillway further with the erosion channel cutting back upstream towards the Crump weir hydraulic control. This could result in the Crump weir failure and consequently a dam break condition could occur during a large flood. The possible future retrogressive erosion of the spillway was investigated after calibrating the model against the 1996 flood scour and then a recommended design discharge flood (RDD) with scour was simulated.

5.3.1 Model Setup and Calibration

The numerical model used is CCHE2D which is a two-dimensional, depth-averaged numerical model for simulating unsteady and turbulent, free-surface flow in open channels (Zhang, 2006). Model calibration was carried out against the observed 1996 flood (Figure 5.6) which peaked at just over $900\,m^3/s$. During 1996, following the flood, DWA (2003) carried out a survey of the spillway which indicated the deep scour (Figure 5.7). In this study the surveyed 1996 spillway was modified by removing the deep scour channel to create a pre-scour condition which was the condition at the beginning of the 1990's. The modification did not take into account the previous scour (which was a narrow channel) due to floods

occurred before 1996. A curvilinear mesh of $2\,m \times 10\,m$ grid size was generated and the bathymetry used in the model is shown in Figure 5.8.

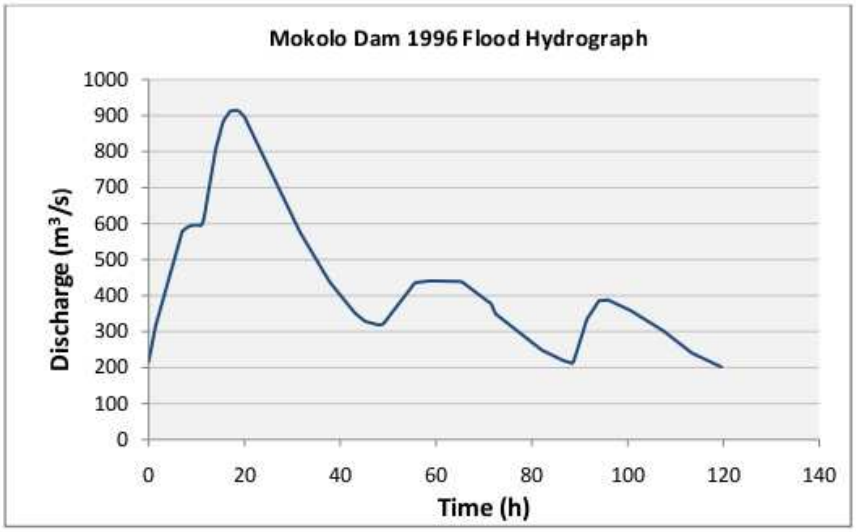

Figure 5.6: Observed 1996 flood with a duration of 5 days

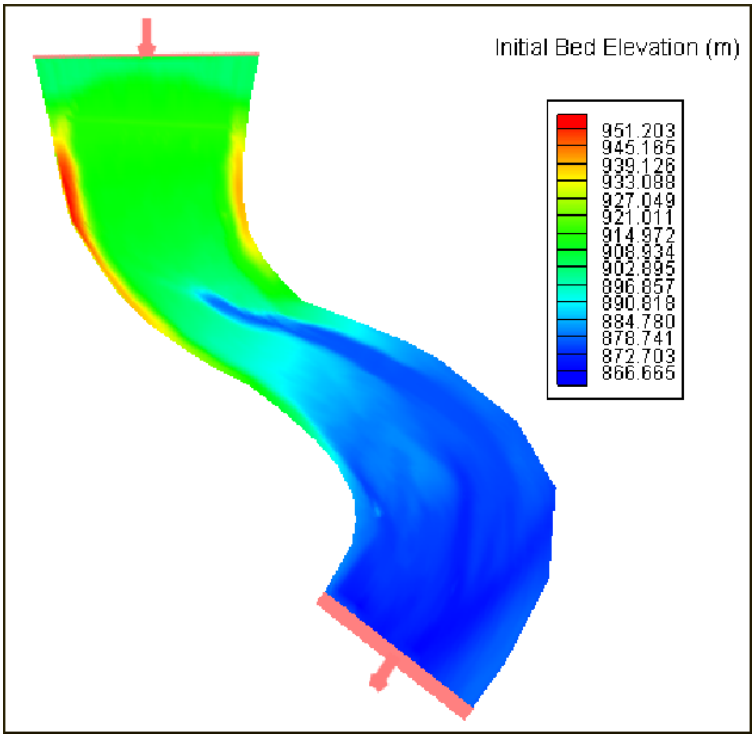

Figure 5.7: Mokolo Dam observed bathymetry surveyed following 1996 flood (bed levels indicated in masl)

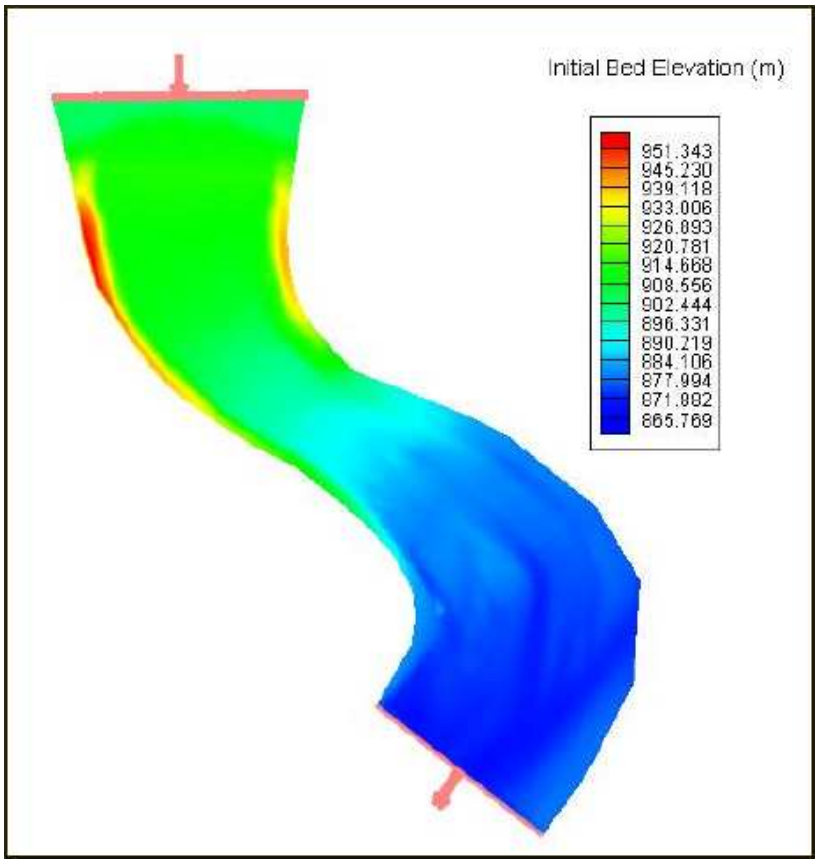

Figure 5.8: Mokolo Dam bathymetry modified from post flood survey (Pre-1996 flood)

5.3.2 Calibration Results

Several assumptions were made during the calibration of the spillway scour model. These are:

- The spillway scour could be described by non-cohesive sediment transport and critical conditions for erosion.
- Rocks of $0.1\,m$ in diameter were considered.
- A rock porosity of 0.1 was used.
- A spillway chute Manning's roughness of $n = 0.033$ was used.
- Uniform material characteristics on model area were considered.

The CCHE2D Model was set up using Total Load as Bed Load Model for the transport mode option and the Wu, Wang and Jia formula as bed load equation. The calibration results are shown in Figures 5.9 and 5.10. The upstream end of the eroded channel formed more or less where it was observed in the field, but further downstream the simulation tends to scour more to the right than observed. This could be because of the fault with poorer quality rock in the field. Nevertheless the extent of the scour and also scour upstream closer to the Crump weir seems realistic when compared with observed data. In the vicinity of the Crump weir the simulated depth of scour area varied from 1 to $7\,m$ whereas in the scour channel it is about $34\,m$ (Figure 5.10).

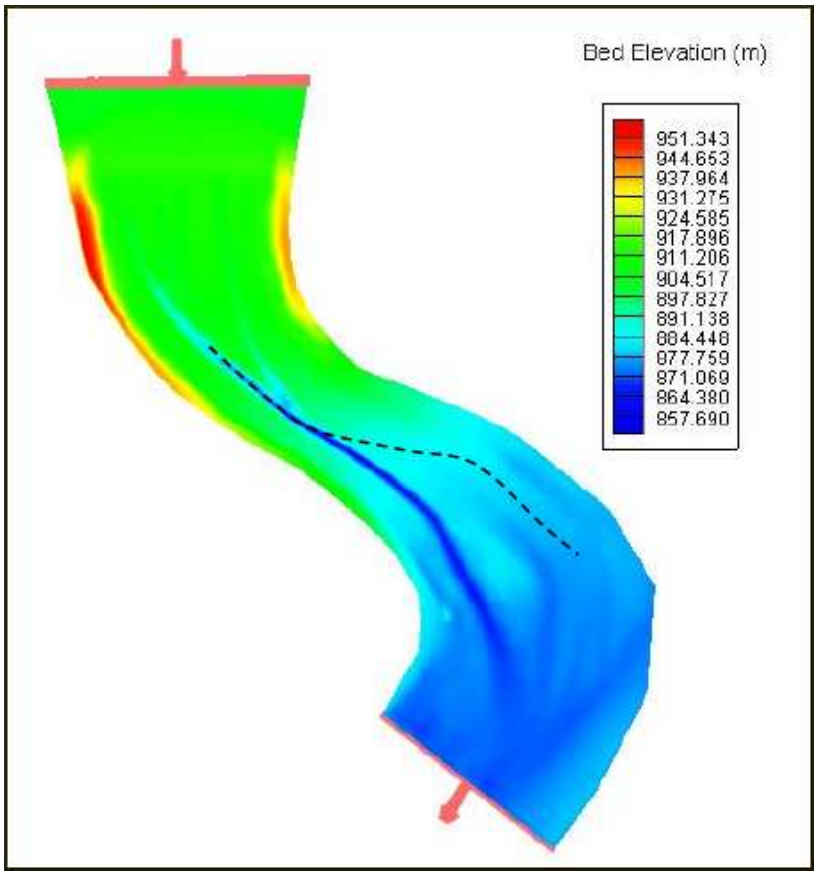

Figure 5.9: Calibrated bed level scour following the 1996 flood (dotted line is the observed centreline of scour channel)

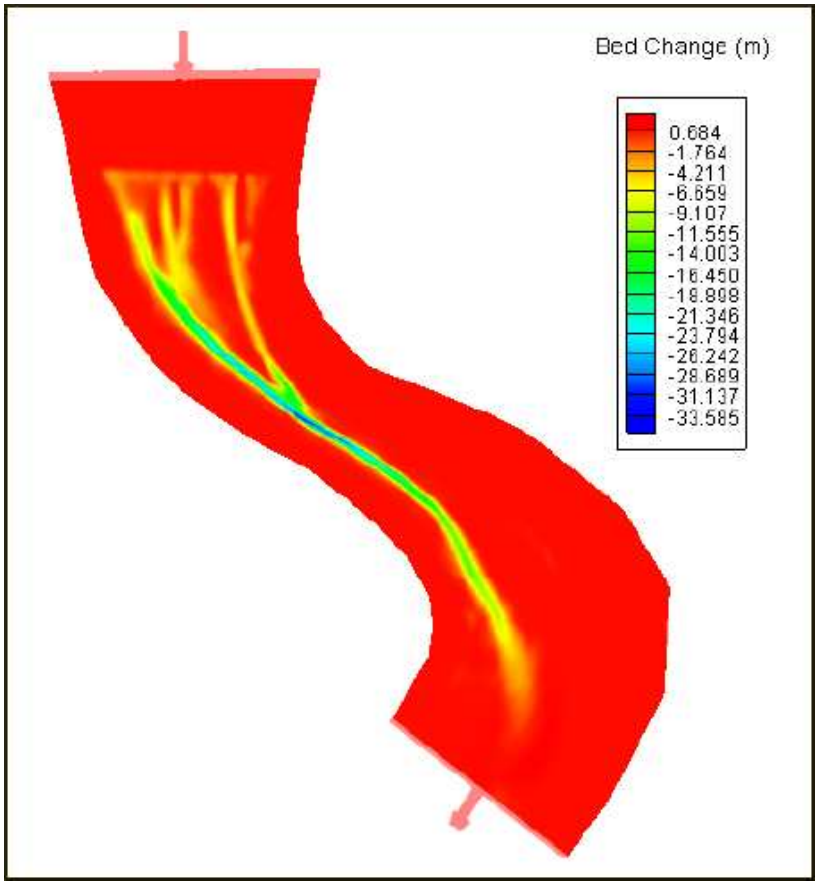

Figure 5.10: Calibrated bed level change following the 1996 flood

5.3.3 Model Setup and Calibration for the New Bathymetry

In order to investigate the sensitivity of the CCHE2D Model to certain parameters, a new bathymetry from 2007 survey of Mokolo Dam spillway was set up for the mathematical modelling. Unlike the first bathymetry, the new bathymetry was wider than the previous bathymetry in order to reduce the boundary effect on the simulation results of the simulated area of interest (spillway channel area). The new bathymetry is illustrated in Figure 5.11.

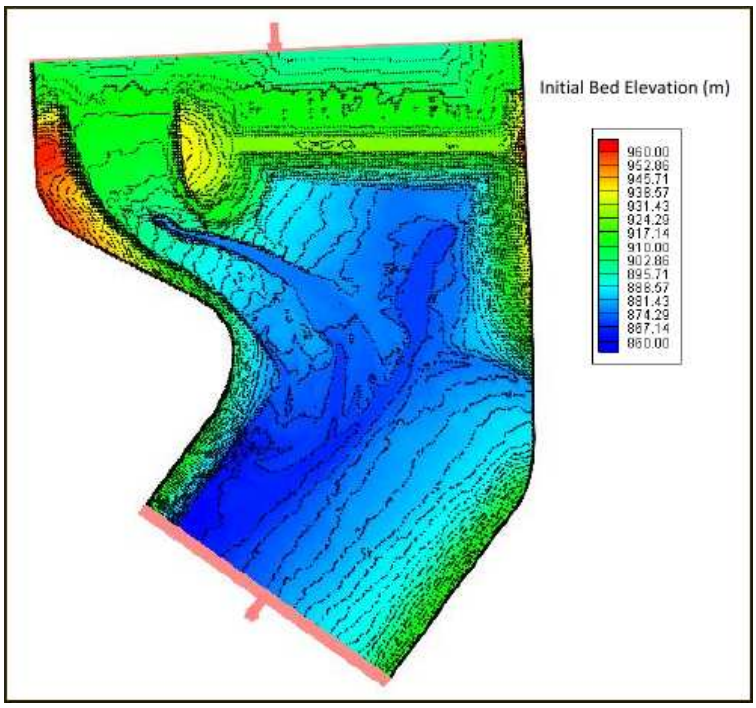

Figure 5.11: Mokolo Dam observed bathymetry with contour lines from 2007 survey (bed levels indicated in masl)

Similar to the previous spillway scour simulations, model calibration was carried out against the observed 1996 flood (Figure 5.6) in order to create a pre-scour condition which was the condition at the beginning of the 1990's. Therefore, the surveyed bathymetry (see Figure 5.11) was altered by removing the deep scour channel. A curvilinear mesh of $5\,m \times 7\,m$ grid size was generated and the new bathymetry that was used in the model is shown in Figure 5.12.

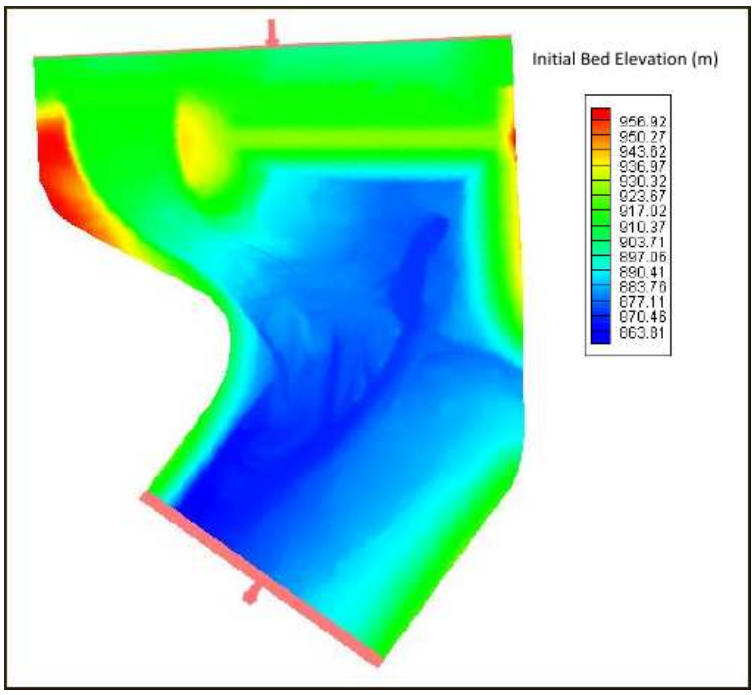

Figure 5.12: Mokolo Dam bathymetry modified from post flood survey (Pre-1996 flood)

5.3.4 Calibration Results

The numerical model was calibrated against the 1996 flood, which was the largest flood ($914\,m^3/s$) recorded from 1996 to 2007 according to DWA (2010). It is, therefore, assumed that the scoured deep channel in the spillway observed on the 2007 survey of Mokolo Dam bathymetry (see Figure 5.11) occurred during the 1996 flood event.

Unlike the first Mokolo Dam spillway scour simulation where it was assumed that there were uniform material characteristics on model area, in this scour simulation, the non-uniformity of material characteristics was assumed. The following assumptions were therefore made during the calibration of the spillway scour model:

- The spillway scour could be described by non-cohesive sediment transport and critical conditions for erosion.
- Rocks of $0.5\,m$ (calibrated) in diameter, which is similar to the joints in the field.
- A rock porosity of 0.1.

- Manning's roughness of the spillway chute, the adjacent area to the spillway chute and the rest of the model area were assumed to be 0.030, 0.045 and 0.06 respectively.

- The non-uniform rock material quality on model area was ensured by fixing only the actual location of the fault in the field as erodible zone.

The model was set up using Total Load as Bed Load Model for the transport mode option and the Wu, Wang and Jia formula as bed load equation. The calibration results are shown in Figures 5.13 to 5.15.

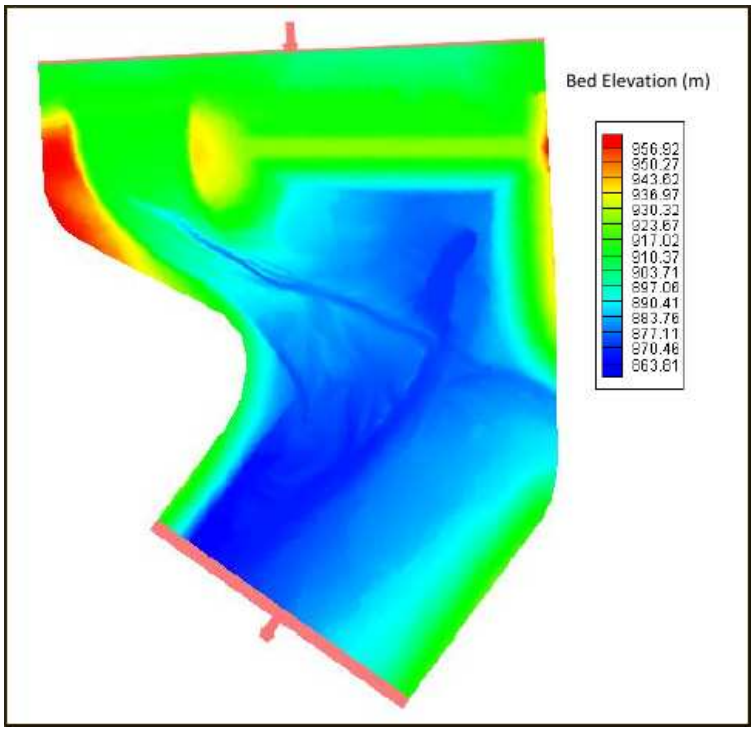

Figure 5.13: Calibrated bed level scour following the 1996 flood

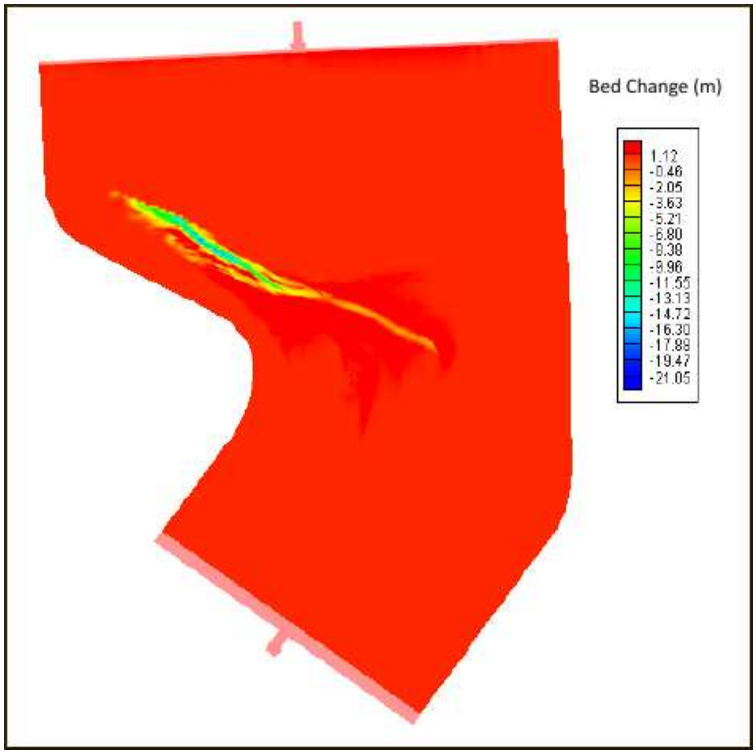

Figure 5.14: Calibrated bed level change following the 1996 flood

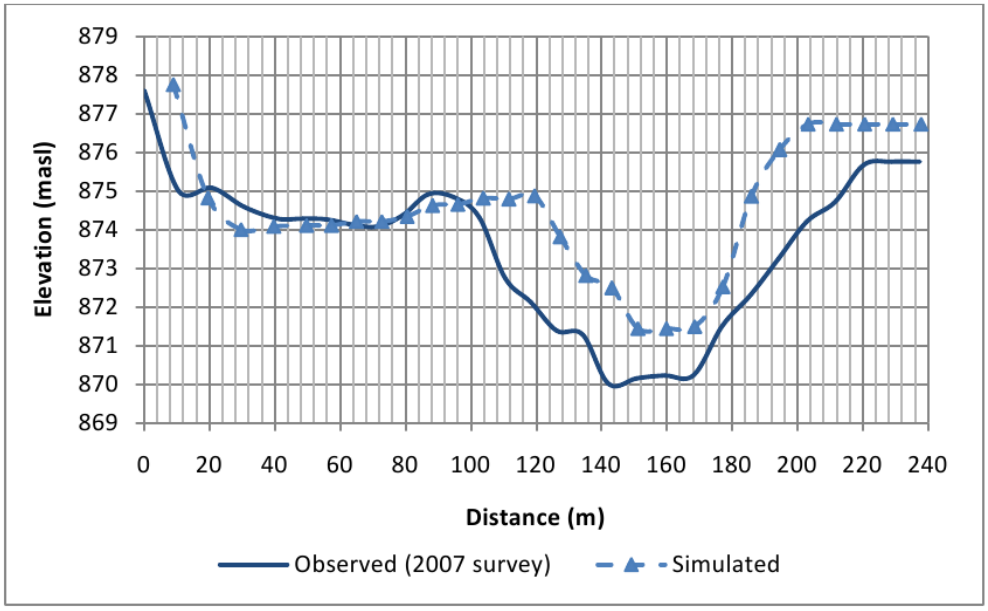

Figure 5.15: Typical cross section through scour trench following the 1996 flood

Although the simulated scour depth was $4\,m$ less than the scour depth in the field, the eroded channel accurately formed where it was observed in the field (Figure 5.13). The extent of the simulated scour depicted in Figure 5.14 shows that the scoured channel could cut back towards the crump weir . The deepest simulated scour depth is about $21\,m$ in the scoured channel while the eroded materials are deposited further downstream of spillway channel.

5.3.5 Simulation of the Recommended Design Flood Spillway Scour for the New Bathymetry

5.3.6.1 Model Setup

The Recommended Design Discharge (RDD) flood peak ($2085\,m^3/s$) was used with the hydrograph shape determined by DWA (2003) as shown in Figure 5.16. It was assumed that the reservoir is full at the start of the flood. The starting bathymetry of this simulation was the 2007 bed profile survey (see Figure 5.11), thus already scoured conditions.

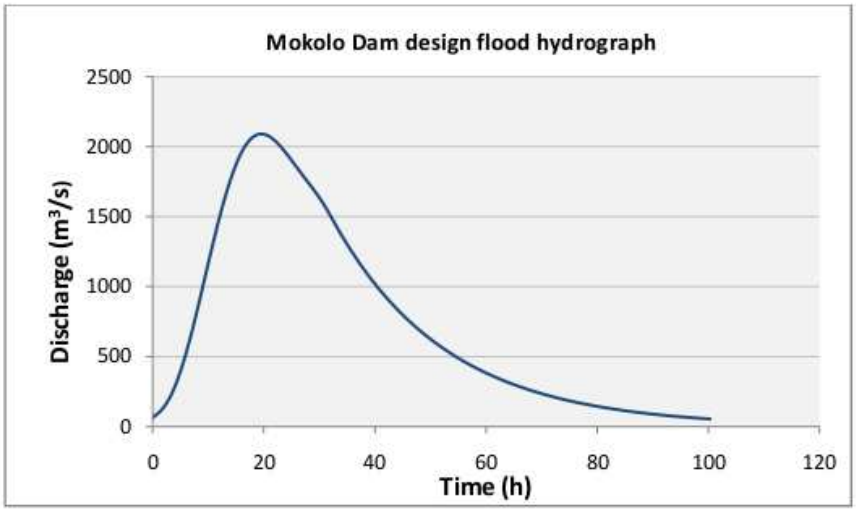

Figure 5.16: Design flood hydrograph of Mokolo Dam (DWA, 2003)

5.3.6.2 Results and Discussion

The simulated bed level changes during the RDD flood are shown in Figure 5.17. As observed in the first simulation, the spillway scour simulation shows that the deep trench caused by the 1996 flood could be scoured up to $17\,m$ deeper which could result in a total depth of $42\,m$ (considering $25\,m$ scour depth from the 1996 post-flood surveyed scour pattern). The flow velocities inside the scoured channel ranged from $4\,m/s$ up to $9\,m/s$ (see Figure 5.18).

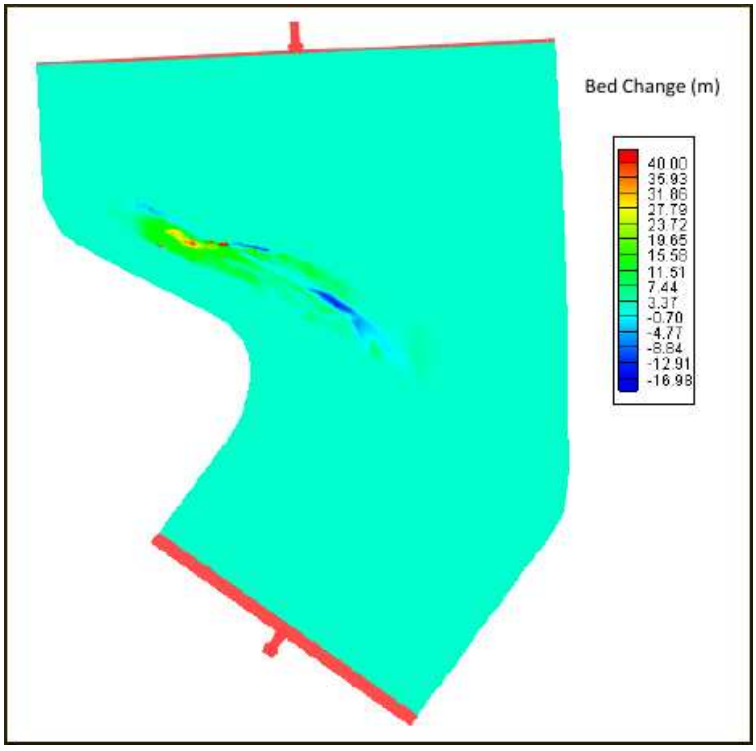

Figure 5.17: Mokolo Dam design flood simulated bed level change

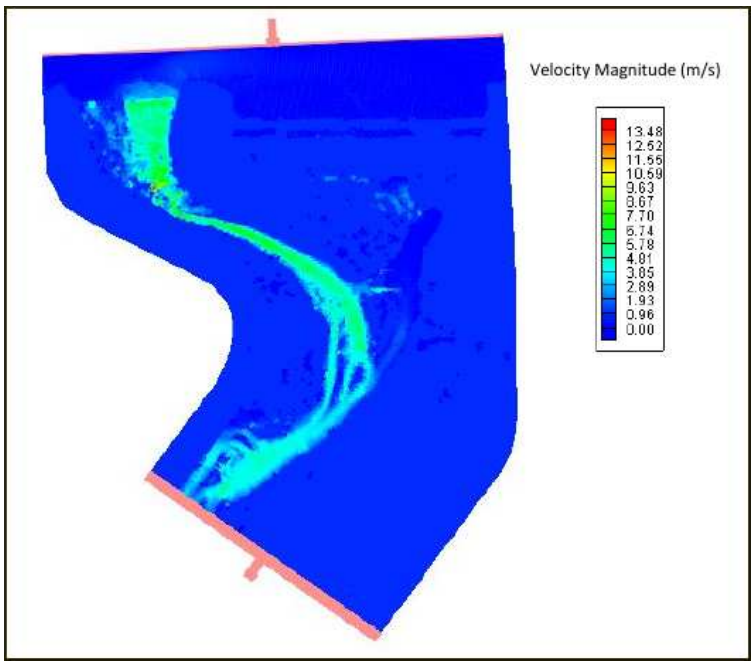

Figure 5.18: Mokolo Dam design flood simulated flood peak velocity

5.3.6 Summary of model simulations

A two-dimensional hydrodynamic model was calibrated against the observed 1996 flood scour of the unlined Mokolo Dam spillway chute. Two simulated models were set up with different bathymetries. Results of comparison of both simulated models with the observed scour in the field, in terms of average velocity in the scoured channel, the length of scour and the maximum depth of scour are presented in Table 5.1.

Table 5.1: Comparison summary of simulated models

	Observed	**1996 bathymetry**	**2007 bathymetry**	**Predicted (Q = RDD)**
v (m/s)		2.5	4	6.5
Length of scour (m)	300	520	400	480
Maximum depth of scour (m)	25	34	21	42

The orientation of the simulated deep scour was not correct in the first simulated model and this could be explained by the assumption of uniform material characteristics on the model area regardless of the

presence of a fault with poorer rock quality in the field. Nevertheless, the upstream end of the scour channel was simulated in the correct location and the extent (especially upstream near the Crump weir) and depth of scour were similar to the post-1996 flood survey as shown in Table 5.1.

For the second simulation model, the non-uniformity of material characteristics on the model area was assumed and the simulated scour depth was accurately orientated . Furthermore, the magnitude of the erosive power in this case was in good agreement with the observed scour in the field compared to the first simulated model. The scour length and the maximum scour depth were reasonably simulated compared to the first simulated model (see Table 5.1). This is due to the use of a relatively big sediment size ($0.5\,m$) as a calibrated parameter in the model. This seems realistic because the bed material in the field is largely composed of blocks of rock of similar size.

Simulation of the RDD of $2085\,m^3/s$ using a hydrograph (routed) over $70\,h$ (shape specified by DWA (2003)), with a starting bathymetry that was the 2007 survey, indicated further scour upstream of the current deep trench for the simulated model. This could cause the failure of the Crump weir hydraulic control in several places. Consequently the scour could cause an increase in the flood peak downstream and after the flood the reservoir would drain to the scoured bed level at the Crump weir location.

Additional simulations using the new bathymetry were undertaken in order to investigate the potential sensitivity of the numerical model to the effective diameter. Therefore, different rock diameters were simulated and the simulation results are given in Table 5.2

Table 5.2: Model sensitivity results to effective diameter

Diameter (m)	0.1	0.3	0.5	0.7
Maximum depth of scour (m)	32	28	21	12

Upon comparison of the scour results of the simulated rock diameters, it is was seen that the CCHE2D Model is sensitive to certain parameters especially to sediment size as depicted in Table 5.2

6. Methodology for Determination of Critical Flow Parameters at Incipient Motion

6.1 Erosion Threshold in terms of Particle Reynolds Number and Stream Power

The erosion threshold relationship between particle Reynolds number (Re_*) and the stream power (P) was established as follows:

The Shield diagram relating the particle Reynolds number, the particle size, the shear velocity and the Shields parameter was used (Figure C.1 in Appendix C). From this graph, for a given value of the particle Reynolds number, the corresponding values of particle size and shear velocity at incipient motion condition were determined.

The depth of water and the velocity for rough turbulence flow conditions were computed as follows (Basson and Rooseboom, 1997):

$$D = \frac{u_*^2}{gS} \tag{6.1}$$

and

$$V = 18\log(12D/k_s)\sqrt{DS} \tag{6.2}$$

where,

D = flow depth or hydraulic mean depth (m)

V = flow velocity (m/s)

k_s = roughness height ($= 2d_{50}$) (m)

u_* = shear velocity (m/s)

d_{50} = particle size (m)

S = longitudinal bed slope

g = gravitational acceleration (m/s^2).

The only unknown in Equations 6.1 and 6.2 was the longitudinal slope (S). To illustrate the methodology, three slopes were assumed namely; 1:100, 1:500 and 1:10000.

Finally, the unit stream power for each slope was calculated by:

$$P = \rho g V D S \tag{6.3}$$

where,

P = unit stream power (W/m^2)

ρ = density of water (kg/m^3)

d_{50} = particle size (m)

S = longitudinal bed slope

g = gravitational acceleration (m/s^2).

The erosion threshold that relates the particle Reynolds number and the unit stream power is shown in Figure 6.1 and calculation details are given in Appendix C.

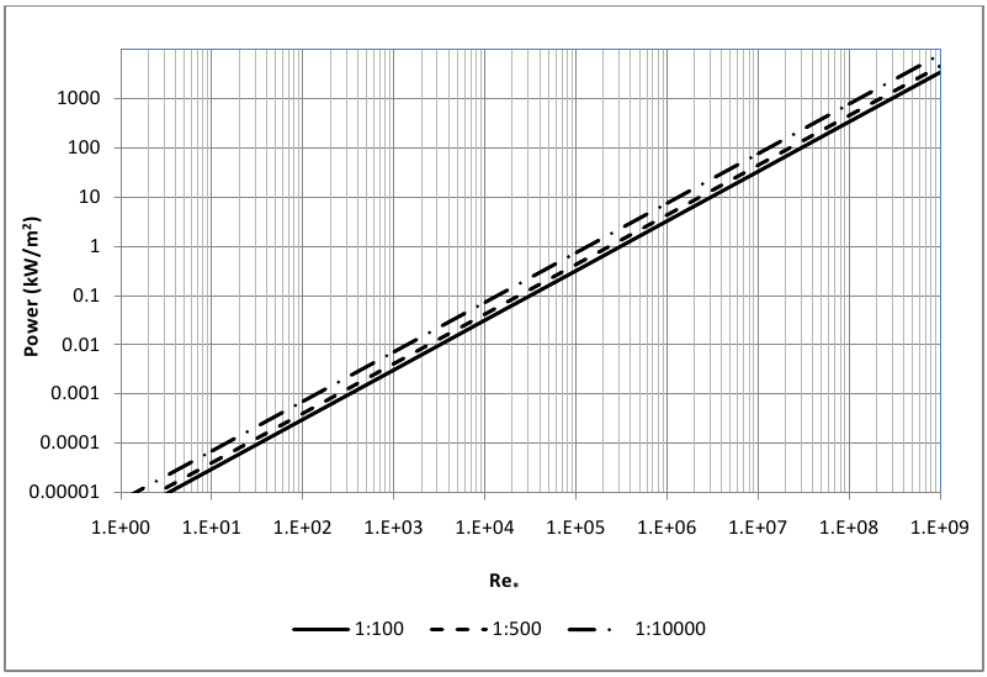

Figure 6.1: Relationship between unit stream power and particle Reynolds number

6.2 Procedure for Estimation of Flow Velocity and Shield's Parameter at Incipient Motion Condition

To find the critical flow velocity and/or the Shield's parameter under condition of incipient motion the procedure is described as follows:

1. Determine of Erodibility Index of the bed material.

2. Use Annandale's (1995) threshold relationship (see Figure 2.5 in section 2.6.1) to determine the corresponding unit stream power.

3. Use the erosion threshold portrayed in Figure 6.1 to find the particle Reynolds number for a given slope.

4. When the particle Reynolds number is known, determine the dimensionless critical velocity by using Yang's diagram (Figure 2.9) and determine the Shield's parameter by the use of Shield's diagram (Figure 2.8).

5. When the dimensionless critical velocity (V_{cr}/w) is known and since the settling velocity (w) is a function of geometrical properties of the particle (size and density) (see Equation 3.2), the critical flow velocity (V_{cr}) can be determined.

6.3 Case Study Example of Application of the Methodology

The case study consists of investigating the condition of incipient motion of bed rock of the proposed Metolong Dam. The dam is a Roller Compacted Concrete (RCC) type dam and has a stepped concrete spillway with concrete apron and end sill. Metolong Dam has approximately a maximum height of $80\,m$ and its Regional Maximum Flood (RMF) is estimated to be $1559\,m^3/s$.

The procedure as described in the previous section was followed in order to determine the condition of incipient motion of bed rock of the proposed Metolong Dam.

6.3.1 Erodibility Index Calculation

By making use of tables of rock mass design parameter-foundation provided by the geotechnical report of Metolong Dam (see Tables C.3 and C.4 in Appendix C), formulas and Tables published by Annandale (1995) (see Section 2.6.1), the Erodibility Index of the rock of Metolong Dam was calculated.

Erodibility Index parameters of Metolong Dam are summarised in Table 6.1 and details on parameter calculations are given in Appendix C.

Table 6.1: Erodibility Index parameter of Metolong Dam

UCS (Mpa)	M_s	RQD	J_n	K_b	K_d	J_s	Erodibility Index (K)
69	52.9	100	1	100	1	5	5290

6.3.2 Stream Power Determination

After the Erodibility Index had been determined the stream power was determined by using the erodibility threshold graph proposed by Annandale (1995) (Figure 2.5 in Section 2.6.1). A value of $440\,KW/m^2$ was found as the corresponding stream power to initiate the scour.

6.3.3 Particle Reynolds Number Determination

By entering the stream power found and reading on the slope 1:10000 (assumed), the graph in Figure 6.1 gave a value of 10^7 for the particle Reynolds number.

6.3.4 Critical Flow Velocity and Shield Parameter Determination

Since the particle Reynolds number found is relatively high (10^7), the dimensionless critical velocity (V_{cr}/w) was given by Yang's graph and its value is 2.05 (Figure 2.9) whereas the Shield's parameter of 0.056 was given by Shield's diagram (Figure 2.8).

Finally the critical velocity that initiates the scour was then expressed as a function of particle size (d):

$$\omega = \left(\frac{4g(\rho_s-\rho)d}{3\rho C_D}\right)^{1/2} = \left(\frac{4\times 9.81\times(2110-1000)\times d}{3\times 1000\times 0.40}\right)^{1/2} \tag{6.4a}$$

$$\omega = 6.025\,d^{1/2} \tag{6.4b}$$

$$V_{cr} = 2.05\,\omega \tag{6.4c}$$

$$V_{cr} = 12.35\,d^{1/2} \tag{6.4d}$$

One of advantages of this method is that the related-flow parameter such as critical flow velocity which enables the initiation of particle movement can be determined and utilised for engineering design purpose and on the other hand, the Shield's parameter which is used as a parameter in mathematical modelling such as the CCHE2D Model can be estimated by using this method. This method can also contribute to limit field calibration by knowing critical conditions for erosion.

7. Conclusions and Recommendations

The investigation of the potential effects of scour has become an important and valuable research topic in engineering practice. Scour mainly caused by the natural processes of intense precipitation such as floods, is an international issue of potentially huge proportions, adversely affecting public safety, property, infrastructure and the environment.

An extensive review of the technical literature pertaining to the erodibility of rock and the potential for scour under hydraulic conditions has shown that despite the availability of sophisticated computers, most designs are still based on empirical formulas or physical model studies. This is because scour is a process of complex interaction of many physical factors which are not easily modelled numerically. The empirical formulas, however, have numerous limitations. The empirical formulas which principally focus on the prediction of scour in non-cohesive granular earth materials that are affected by flowing water, should only be applied to the kind of problem for which they were developed. In addition, they usually predict only one parameter which is the maximum scour depth. The predicted value of this parameter is largely variable depending on the formula that is used.

One of the reliable ways to investigate the scour process is the use of physical models. Although physical models are time consuming to construct and test and consequently cost-prohibitive, they can be efficient provided that they are constructed on a sufficiently large scale.

The key objective of this study was to assess the applicability of mathematical modelling to examine the scour process of unlined spillways. In this regard, a physical model was set up in the laboratory flume in order to investigate the erosion process in a controlled environment. The numerical modelling that was calibrated against data from physical model tests was carried out and the simulation results were satisfactory. From this, the mathematical modelling was validated and, therefore, used as scour prediction tool in a case study.

7.1 Physical Modelling

The physical model test consisted of the erosion of a movable bed made of special cable PVC sediment in a laboratory flume. Four different slopes ranging from 0.72% to 3.52% were tested and the erosion on the unlined spillway model was obtained more easily on the steep slope setup. This is attributed

to the greater energy gradient present on the steep slope flume setup. The energy gradient is directly proportional to the erosive force of water.

One of the limitations of the laboratory model used was its inability to accommodate a steeper slope than 3.52%. A typical slope of unlined spillway is generally steeper than this value. However, the physical model results were useful for comparison with mathematical modelling.

7.2 Mathematical Modelling

The mathematical model that was used in this study is the CCHE2D which is a two-dimensional hydrodynamic model for unsteady turbulent open channel flow and sediment transport simulations. The numerical model was calibrated in order to reflect the conditions of the laboratory flume test. The results of the simulations showed that the simulated bed level and observed bed level reasonably led to the same magnitude of erosion. Therefore the mathematical model was validated because of its ability to provide an accurate and detailed erosion prediction. The CCHE2D Model can be considered reliable provided that the model is correctly calibrated and set up to reflect the conditions of a particular case study.

In this regard, a prototype case study was simulated in order to test the ability of the CCHE2D model to predict erosion in natural conditions. A two-dimensional hydrodynamic model (CCHE2D Model) was calibrated against the observed 1996 flood scour at the Mokolo Dam unlined spillway. Two simulated models were carried out under different bathymetries. Simulations of the Recommended Design Discharge (RDD) of $2085\,m^3/s$ with a starting bathymetry of the post-flood 1996 survey indicated further scour upstream of the current deep trench. This could cause the failure of the Crump weir hydraulic control in several places. Consequently the scour will cause an increase in the flood peak downstream and after the flood, the reservoir would drain to the scoured bed level at the Crump weir location.

From the results of the mathematical modelling of Mokolo Dam unlined spillway, it appears that the standard 2D mathematical model using bedload sediment transport equations is capable of simulating the scour process and predicting the size and the location of a possible scour channel. Unlike most of the empirical methods that were used to investigate the scour process of rock, the time change is taken into account in the mathematical model. Nevertheless to get realistic results the model has to be calibrated against field conditions and suitable geotechnical information. The sensitivity to certain simulation parameters such as sediment size and bed roughness should be considered in the mathematical modelling.

The mathematical model can predict the temporal scour development, while empirical methods can only predict incipient conditions or equilibrium scour depth.

7.3 Recommendations for Further Research

In order to conduct an in-depth investigation into erosion process it is recommended to improve the physical model as follows:

- The physical model needs to be altered to a sufficiently large scale.
- Set up a physical model with the same slope as on the prototype spillway.
- Investigate the use of a geological material as sediment in order to reflect the natural conditions.

Further research work is required to quantify the incipient motion of the rock correctly in order to limit field calibration.

For the analysis of the unlined spillway prediction it is highly recommended that all three methods namely; analytical, physical and mathematical methods be utilised to obtain a reliable and conclusive result in erosion prediction. In this regard special consideration should be given to the limitations and sensitivities to each method.

9. References

Akhmedov, T. K. 1988. Calculation of the Depth of Scour in Rock Downstream of a Spillway. Water Power and Dam Construction, pages 25–27.

Annandale, G. 1995. Erodibility. Journal of Hydraulic Research, pages 471–494.

Annandale, G. W. 2006. Scour Technology: Mechanics and Engineering Practice. McGraw-Hill.

Annandale, G. W., Wittler, R. J., and Scott, G. 2000. Scour Downstream of Dams. Symposium on Scour of Foundations, International Society of Soil Mechanics and Geotechnical Engineering.

Armitage, N. and McGahey, C. 2003. A Unit Stream Power Model for the Prediction of Local Scour in Rivers. Technical Report No 1098/1/03, Cape Town.

Armitage, N. P. 2002. A Unit Stream Power Model for the Prediction of Local Scour. PhD thesis, University of Stellenebosch.

Baret, C. M. E. 2009. Unlined Spillway Erosion Prediction Modelling. Bachelor's degree thesis, University of Stellenbosch.

Basson, G. R. and Rooseboom, A. 1997. Dealing with Reservoir Sedimentation. Technical Report TT 91/97, Water Research Commission.

Breusers, H. N. C. and Raudkivi, A. J. 1991. Scouring. IAHR Hydraulic Structures Design Manual, Rotterdam: A. Balkema.

Cameron, C. P., Patrick, D. M., Bartholomew, C. O., Hatheway, A. W., and May, J. H. 1988. Geotechnical Aspects of Rock Erosion in Emergency Spillway Channels. Technical Report REMR-GT-3, Department of the army: US army corps of engineers.

Chadwick, A., Morfett, J., and Borthwick, M. 2004. Hydraulics in Civil and Environmental Engineering. Spon Press: London, 4^{th} edition.

Craig, R. F. 2004. Craig's Soil Mechanics. Spon Press: London, 7^{th} edition.

CUR 1995. Manual on the Use of Rock in Hydraulic Engineering. Centre for Civil Engineering Research and Codes (CUR), Netherlands.

DWA 2003. Mokolo Dam Frequency Analysis: Estimated Flood Peaks for Required Probability. Technical report, Department of Water Affairs. Hydrological Report.

DWA 2010. Department of Water Affairs: Hydrological Services - Surface Water (Data, Dams, Floods and Flows). http://www.dwaf.gov.za/hydrology/.

Henderson, F. M. 1966. Open Channel Flow. Macmillan.

Hoffmans, G. J. and Verheij, H. J. 1997. Scour Manual. A.A. Balkema.

Kirsten, H. A. D. 1982. Classification System for Excavation in Natural Materials. The Civil Engineering in South Africa, pages 293–308.

Raudkivi, A. J. 1998. Loose Boundary Hydraulics. A.A. Balkema.

Simons, D. B. and Sentũrk, F. 1992. Sediment Transport Technology: Water and Sediment Dynamics. Water Resources Publications: Littleton, Colorado.

Stephen, E. D. and Michael, W. B. 1999. Prediction Scour in Weak Rock of the Oregon Coast Range. Technical report, Oregon Department of Transport.

Van Schalkwyk, A. 1994. Erosion of Rock in Unlined Spillway. 18th ICOLD Congress on Large Dams, Durban, pages 555–571.

Wu, W. 2001. CCHE2D Sediment Transport Model. Technical Report NCCHE-TR-2001-3, National Center for Computational Hydroscience and Engineering (NCCHE).

Yang, C. T. 2003. Sediment Transport : Theory and Practice. Krieger Publishing Company, Malabar, Florida.

Zhang, Y. 2005. CCHE-GUI: Graphical User Interface for CCHE2D Model. Users Manual Version 2.2. Technical Report NCCHE-TR-2005-03, National Center for Computational Hydroscience and Engineering (NCCHE).

Zhang, Y. 2006. CCHE-GUI: Graphical User Interface for CCHE2D Model. Users Manual Version 3.0. Technical Report NCCHE-TR-2006-02, National Center for Computational Hydroscience and Engineering (NCCHE).

Appendix A. Geological Parameters

Table A.1: Table showing the mass strength number for rock (M_s) (Annandale, 1995)

Material description	Uniaxial strength	M_s
Very soft cohesive soil	0-80 kPa	0.02
Soft cohesive soil	80-140 kPa	0.04
Firm cohesive soil	140-210 kPa	0.09
Stiff cohesive soil	210-350 kPa	0.19
Very stiff cohesive soil	350-750 kPa	0.41
Very soft rock	1-3 Mpa	1-2
Soft rock	3-13 Mpa	2-8
Hard rock	13-26 Mpa	8-35
Very hard rock	26-106 Mpa	35-70
Extremely hard rock	106-212 Mpa	70-280

Table A.2: Joint count number (J_c) (Annandale, 1995)

Number of Joints Per Cubic Meter (J_c)	Ground Quality Designation (RQD)	Number of Joints Per Cubic Meter (J_c)	Ground Quality Designation (RQD)
33	5	18	55
32	10	17	60
30	15	15	65
29	20	14	70
27	25	12	75
26	30	11	80
24	35	9	85
23	40	8	90
21	45	6	95
20	50	5	100

Table A.3: Joint set number (J_n) (Annandale, 1995)

Description of joint sets	J_n
No joints	1.00
One joint set	1.22
One joint set plus random	1.50
Two joint sets	1.83
Two joint sets plus random	2.24
Three joint sets	2.73
Three joint sets plus random	3.34
Four joint sets	4.09
Multiple joint sets	5.00

Table A.4: Ratio of joint roughness to joint alteration (J_r/J_a) (Van Schalkwyk, 1994)

Rock type	Friction angle (degrees)	$J_r/J_a = \tan\phi$
Quartzite	65	2
Sandstone	40-55	1
Dolerite (sound)	40	0.8
Dolerite (decomposed)	25	0.5
Shale	20-22	0.4

Table A.5: Joint structure number (J_s) (Van Schalkwyk, 1994)

Dip direction	Dip angle	J_s for block aspect ratio of:			
		1:1	1:2	1:4	1:8
	90	1.0	1.0	1.0	1.0
Downstream	10	1.22	1.10	0.93	
	30	0.63	0.59	0.53	
	60	0.49	0.44	0.37	
Upstream	10	0.63	0.70	0.81	
	30	0.49	0.53	0.59	
	60	0.63	0.67	0.37	

Appendix B. Sediment Characteristic Calculations

Table B.1: Table showing cube data for a sample of 35 sediment particles

Cube	Mass (g)	Dimensions			Volume (mm^3)
		1	2	3	
1	1.96	11.3	11.2	10.5	1328.88
2	1.96	11.2	11.2	10	1254.4
3	1.87	11.5	11.3	10.3	1338.485
4	2.01	11.3	11.1	11	1379.73
5	2	11	11.1	11.4	1391.94
6	1.94	11.1	11.4	10.8	1366.632
7	1.82	11.2	11.4	10.1	1289.568
8	1.85	10.9	11.1	10.8	1306.692
9	1.86	11.3	11.1	10.2	1279.386
10	1.95	11.4	11.2	10.9	1391.712
11	1.87	11.4	11.1	10.5	1328.67
12	1.86	11.2	11	10.8	1330.56
13	2.02	11.3	11.2	11.3	1430.128
14	1.81	11.1	10.9	10.4	1258.296
15	1.94	11	11.2	11.2	1379.84
16	1.93	11	11	11.1	1343.1
17	1.9	11.2	11	10.9	1342.88
18	1.92	11.1	11.2	11	1367.52
19	1.87	11	11.2	10.8	1330.56
20	1.94	11.1	10.9	11.2	1355.088
21	1.77	11	10.8	10.8	1283.04
22	1.93	11	11.2	10.2	1256.64
23	1.89	11	11	10.9	1318.9
24	1.81	11	11	10.7	1294.7
25	1.9	11.1	11.2	10.8	1342.656
26	1.93	11	11.2	11.5	1416.8
27	1.85	11.2	11.2	10.5	1317.12
28	1.91	11.2	11.3	10.7	1354.192
29	1.91	11.2	11.2	10.8	1354.752
30	1.87	11	11.1	10.9	1330.89
31	2.05	11.4	11.3	11.1	1429.902
32	1.74	11.2	11.2	10	1254.4
33	1.83	11	11	10.6	1282.6
34	1.86	11.3	11	10.6	1317.58
35	1.87	11.2	11.3	10.2	1290.912
Average	1.897				1332.547
STDev	0.068				48.333

Table B.2: Table showing the sediment specific gravity calculations

Cube	Mass (g)	Dimensions (mm)			Volume (mm^3)	Density (kg/m^3)	Specific gravity
		1	2	3			
1	1.96	11.3	11.2	10.5	1328.88	1474.92	1.47
2	1.96	11.2	11.2	10	1254.4	1562.5	1.56
3	1.87	11.5	11.3	10.3	1338.48	1397.1	1.39
4	2.01	11.3	11.1	11	1379.73	1456.8	1.45
5	2	11	11.1	11.4	1391.94	1436.84	1.43
6	1.94	11.1	11.4	10.8	1366.63	1419.54	1.41
7	1.82	11.2	11.4	10.1	1289.56	1411.32	1.41
8	1.85	10.9	11.1	10.8	1306.69	1415.78	1.41
9	1.86	11.3	11.1	10.2	1279.38	1453.82	1.45
10	1.95	11.4	11.2	10.9	1391.71	1401.15	1.4
11	1.87	11.4	11.1	10.5	1328.67	1407.42	1.4
12	1.86	11.2	11	10.8	1330.56	1397.9	1.39
13	2.02	11.3	11.2	11.3	1430.12	1412.46	1.41
14	1.81	11.1	10.9	10.4	1258.29	1438.45	1.43
15	1.94	11	11.2	11.2	1379.84	1405.96	1.4
16	1.93	11	11	11.1	1343.1	1436.97	1.43
17	1.9	11.2	11	10.9	1342.88	1414.86	1.41
18	1.92	11.1	11.2	11	1367.52	1404	1.4
19	1.87	11	11.2	10.8	1330.56	1405.42	1.4
20	1.94	11.1	10.9	11.2	1355.08	1431.64	1.43
21	1.77	11	10.8	10.8	1283.04	1379.53	1.37
22	1.93	11	11.2	10.2	1256.6	1535.84	1.53
23	1.89	11	11	10.9	1318.9	1433.01	1.43
24	1.81	11	11	10.7	1294.7	1398	1.39
25	1.9	11.1	11.2	10.8	1342.65	1415.1	1.41
26	1.93	11	11.2	11.5	1416.8	1362.22	1.36
27	1.85	11.2	11.2	10.5	1317.12	1404.57	1.4
28	1.91	11.2	11.3	10.7	1354.19	1410.43	1.41
29	1.91	11.2	11.2	10.8	1354.75	1409.85	1.4
30	1.87	11	11.1	10.9	1330.89	1405.07	1.4
31	2.05	11.4	11.3	11.1	1429.9	1433.66	1.43
32	1.74	11.2	11.2	10	1254.4	1387.11	1.38
33	1.83	11	11	10.6	1282.6	1426.78	1.42
34	1.86	11.3	11	10.6	1317.58	1411.67	1.41
35	1.87	11.2	11.3	10.2	1290.912	1448.58	1.44
Average	1.897				1332.54	1424.18	1.42
STDev	0.068				48.33	38.55	0.04

Table B.3: Table showing falling velocity results

Cube	Distance fallen (m)	Time taken to fall (s)	Velocity (m/s)
1	0.5	1.88	0.265
2	0.5	2	0.25
3	0.5	1.81	0.276
4	0.5	1.93	0.259
5	0.5	1.96	0.255
6	0.5	1.93	0.259
7	0.5	1.97	0.253
8	0.5	1.87	0.267
9	0.5	2.09	0.239
10	0.5	1.75	0.285
11	0.5	1.94	0.257
12	0.5	1.96	0.255
13	0.5	1.93	0.259
14	0.5	1.81	0.276
15	0.5	1.87	0.267
16	0.5	1.97	0.253
17	0.5	1.81	0.276
18	0.5	1.94	0.257
19	0.5	1.9	0.263
20	0.5	2.12	0.235
21	0.5	1.94	0.257
22	0.5	1.88	0.265
23	0.5	1.87	0.267
24	0.5	1.97	0.253
25	0.5	1.85	0.27
26	0.5	1.97	0.253
27	0.5	1.94	0.257
28	0.5	1.84	0.271
29	0.5	1.84	0.271
30	0.5	1.96	0.255
31	0.5	1.78	0.28
32	0.5	1.91	0.261
33	0.5	1.85	0.27
34	0.5	1.97	0.253
35	0.5	2.09	0.239
Average		1.917	0.261
STDev		0.08	0.011

Table B.4: Table showing the sediments effective diameter for different coefficients of drag

Fall Velocity: $w = 0.261\,m/s$ Gravitational acceleration: $g = 9.81\,m/s^2$ Specific weight of Water: $\rho = 1000\,kN/m^3$ Specific weight of cube: $\rho_s = 1424.183\,kN/m^3$ Specific weight of submerged cube: $\rho_{s'} = 424.183\,kN/m^3$		
Drag coefficient C_d	**Effective diameter $D_s\,(m)$**	**Effective diameter (mm)**
0.1	0.00123	1.2305
0.15	0.00184	1.8457
0.2	0.00246	2.461
0.25	0.00307	3.0762
0.3	0.00369	3.6915
0.35	0.0043	4.3067
0.4	0.00492	4.92201
0.45	0.00553	5.5372
0.5	0.00615	6.1525
0.55	0.00676	6.76777
0.6	0.00738	7.383
0.65	0.00799	7.9982
0.7	0.00861	8.6135
0.75	0.00922	9.2287
0.8	0.00984	9.844

Table B.5: Table showing the sediments effective diameter for different falling velocities

Velocity	Effective diameter		Average	Percentage	cumulative
$w\,(m/s)$	$D_s\,(m)$	$D_s(mm)$	$D_s(mm)$	(%)	(%)
0.235	0.00401	4.01	4.192	11.428	11.428
0.239	0.00412	4.126			
0.239	0.00412	4.126			
0.25	0.0045	4.505			
0.253	0.00464	4.644	4.661	22.857	34.285
0.253	0.00464	4.644			
0.253	0.00464	4.644			
0.253	0.00464	4.644			
0.253	0.00464	4.644			
0.255	0.00469	4.691			
0.255	0.00469	4.691			
0.255	0.00469	4.691			
0.257	0.00478	4.788	4.844	25.714	60
0.257	0.00478	4.788			
0.257	0.00478	4.788			
0.257	0.00478	4.788			
0.259	0.00483	4.838			
0.259	0.00483	4.838			
0.259	0.00483	4.838			
0.261	0.00494	4.94			
0.263	0.00499	4.992			
0.265	0.00509	5.099	5.204	25.714	85.714
0.265	0.00509	5.099			
0.267	0.00515	5.154			
0.267	0.00515	5.1541			
0.267	0.0051	5.154			
0.27	0.0052	5.266			
0.27	0.0052	5.266			
0.271	0.0053	5.323			
0.271	0.0053	5.323			
0.276	0.0055	5.501	5.615	14.285	100
0.276	0.0055	5.501			
0.276	0.0055	5.501			
0.28	0.0056	5.688			
0.285	0.0058	5.885			
	Average	4.931			
	STDEV	0.421			

Table B.6: Table showing the sediments effective diameter for different fraction sizes

	fraction 1	**fraction 2**	**fraction 3**
	4.2	4.75	5.06
	4.425	4.8	5.25
	4.66	4.91	6.625
Average $D_s(mm)$	4.4283	4.82	5.645
$D_s(m)$	0.0044	0.00482	0.00564

Table B.7: Table showing the sediment porosity calculations

Method 1 - Calculated (Craig, 2004)			
	Test 1	**Test 2**	**Test 3**
M_s	0.001	0.0018	0.0018
V_s	1.332	1.332	1.3325
G_sP_w	1424.183	1424.183	1424.183
V_tP_w	0.00048	0.00048	0.00048
M_t	0.61053	0.61131	0.6099
P	1271.94	1273.5625	1270.625
e	0.1196	0.118	0.1208
n	0.1068	0.105	0.1078
Average = 0.1068 (10.65%) STDev = 0.0534			
Method 2 - Practical			
	Test 1	**Test 2**	**Test 3**
V_v	56	54	52.8
V_s	415	420	415
n	0.1349	0.128	0.127
Average = 0.13 (13.02%) STDev = 0.00411			

Table B.8: Table showing the bed roughness calculations for sediment particles

Vee Weir Discharge Calculation (m^3/s): $Q = \frac{8}{15}(2g)^{0.5}\tan(\alpha/2)h^{5/2}C_d$	
$h(m)$	0.0625
C_d	0.59
$Q(m^3/s)$	0.00136
$Q(l/s)$	1.36113
Slope Calculations:$S_0 = \triangle y/\triangle x$	
$\triangle y(mm)$	25.5
$\triangle x(mm)$	2467
Slope (S_0)	0.01033
Water Height Calculation (m)	
Upstream	0.0225
Midstream	0.0225
Downstream	0.021
Average	0.022
Mannings 'n' Value: $n = \frac{A^{5/3}}{QP^{2/3}}S_0^{1/2}$	
$A(m^2)$	0.0033
$P(m)$	0.194
S_o	0.01033
$Q(m^3/s)$	0.00136
$n(s/m^{1/3})$	0.0163

Appendix C. Incipient Motion Threshold Determinations

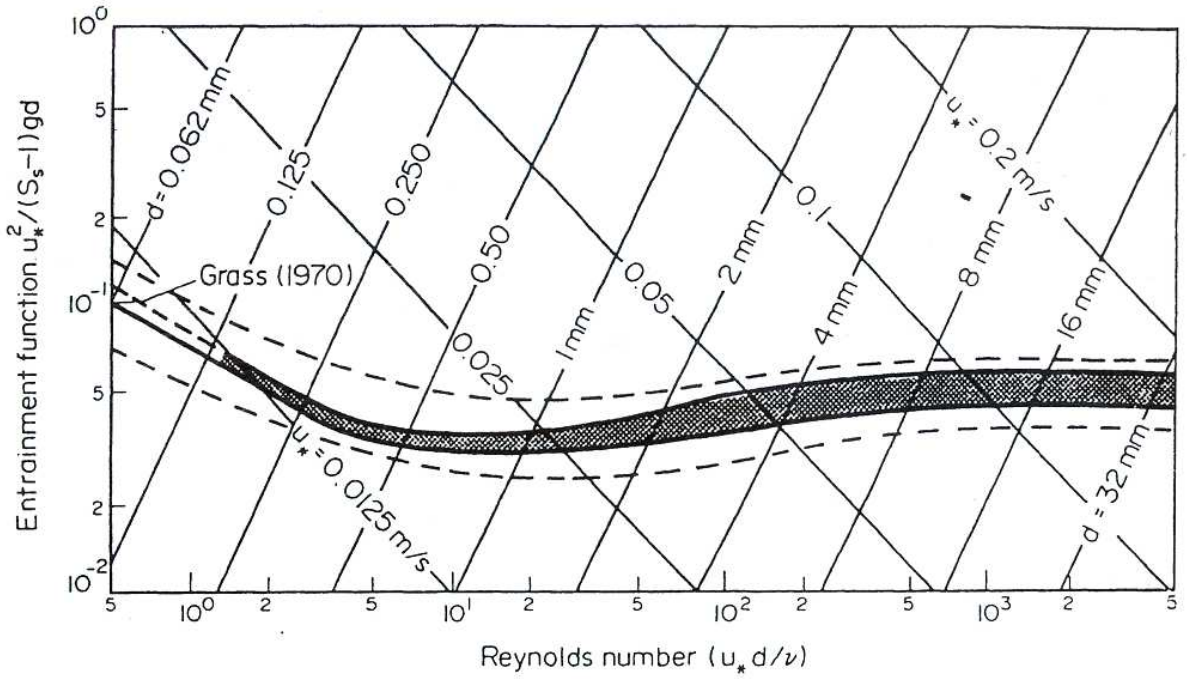

Figure C.1: Threshold of sediment entrainment as function of particle Reynolds number. The shaded band indicates the spread of data by Shields, the dashed lines the envelope to most of published data (Raudkivi, 1998)

Table C.1: Table showing data extracted from threshold's graph in Figure C.1 and different parameter calculations

Particle Reynold number	particle size (mm)	Shear velocity (m/s)	slope			water depth (m)			Velocity (m/s)			Stream power (W/m^2)		
Re_*			S_1	S_2	S_3	D_1	D_2	D_3	V_1	V_2	V_3	P_1	P_2	P_3
1	0.101	0.011	0.01	0.002	0.0001	0.001	0.006	0.127	0.052	0.072	0.108	0.006	0.009	0.013
2	0.179	0.012	0.01	0.002	0.0001	0.001	0.008	0.162	0.054	0.076	0.117	0.008	0.012	0.018
5	0.375	0.015	0.01	0.002	0.0001	0.002	0.011	0.231	0.059	0.085	0.134	0.013	0.019	0.03
10	0.604	0.018	0.01	0.002	0.0001	0.003	0.017	0.356	0.072	0.105	0.166	0.025	0.036	0.058
20	0.958	0.023	0.01	0.002	0.0001	0.005	0.028	0.567	0.091	0.132	0.209	0.05	0.073	0.116
50	1.8	0.031	0.01	0.002	0.0001	0.01	0.05	1.004	0.119	0.174	0.276	0.117	0.171	0.272
100	2.78	0.04	0.01	0.002	0.0001	0.016	0.084	1.684	0.158	0.229	0.361	0.261	0.379	0.597
200	4	0.056	0.01	0.002	0.0001	0.032	0.162	3.254	0.238	0.337	0.52	0.761	1.076	1.663
500	7.3	0.077	0.01	0.002	0.0001	0.061	0.305	6.106	0.329	0.464	0.716	1.971	2.781	4.289
1000	11.48	0.098	0.01	0.002	0.0001	0.098	0.493	9.876	0.421	0.593	0.913	4.083	5.75	8.851
2000	18.78	0.12	0.01	0.002	0.0001	0.147	0.738	14.762	0.503	0.713	1.105	7.291	10.336	16.005
5000	32	0.176	0.01	0.002	0.0001	0.317	1.588	31.778	0.783	1.092	1.666	24.426	34.043	51.946

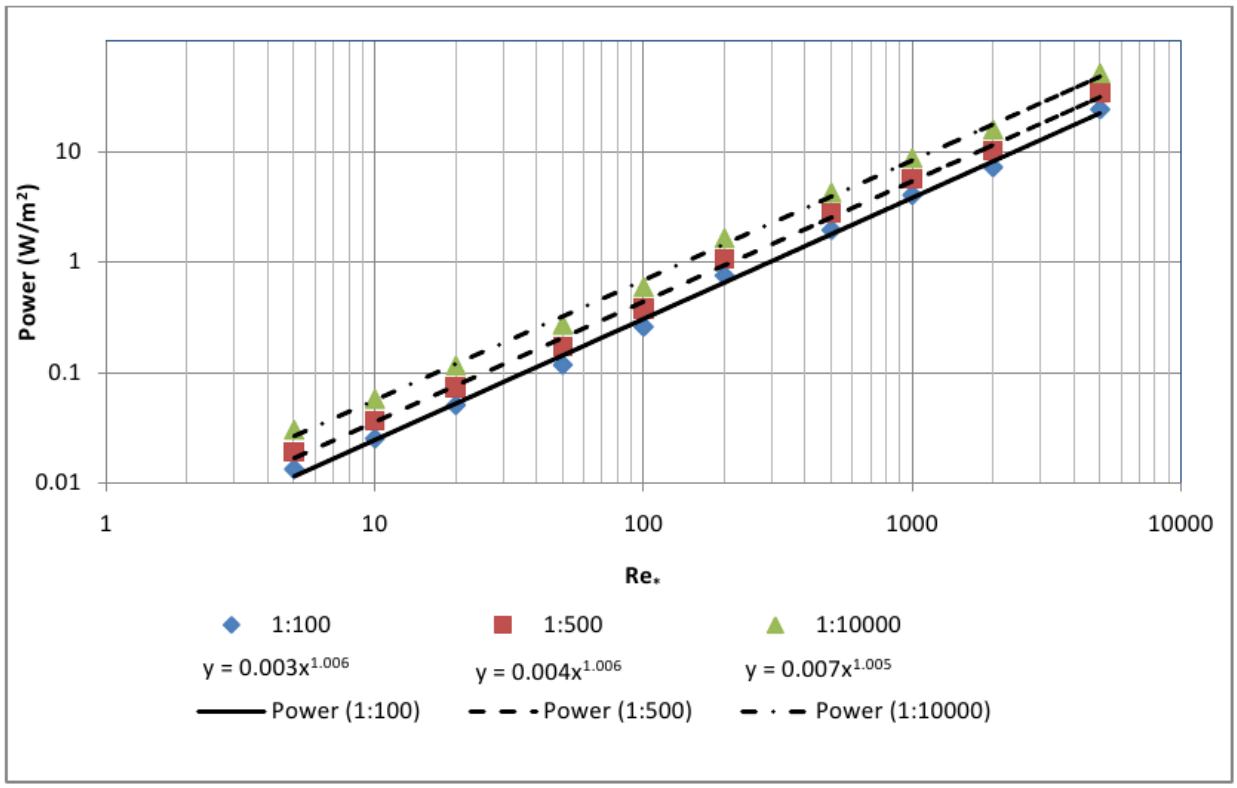

Figure C.2: Threshold of sediment incipient motion relationship between particle Reynolds number and stream power

Table C.2: Extended Values using trendlines' equations (see Figure C.2)

Re_*	$P(W/m^2)$			$P(KW/m^2)$		
	S_1	S_2	S_3	S_1	S_2	S_3
1	0.003	0.004	0.007	0.000003	0.000004	0.000007
10	0.030417	0.040556	0.07081	0.00003	0.00004	0.00007
100	0.308404	0.411206	0.716305	0.000308	0.000411	0.000716
1000	3.126952	4.169269	7.245995	0.003126	0.004169	0.007245
10000	31.704525	42.2727	73.298998	0.031704	0.042272	0.073298
100000	321.455791	428.607722	741.477607	0.321455	0.428607	0.741477
1000000	3259.27687	4345.702494	7500.635136	3.259276	4.345702	7.500635
10000000	33046.179286	44061.572381	75874.883981	33.046179	44.061572	75.874883
100000000	335058.974	446745.299	767.7373	335.058	446.745	767.534
1000000000	3397201.089	4529601.452	7764223.706	3397.201	4529.601	7764.223

C.1 Geological Parameters of Metolong Dam

Table C.3: Summary of laboratory test results-dam site

Location	Unit	Density (g/cm^3)	Durability class	Mineralogy	Saturated sample								Unsaturated sample (natural moisture content)			
					Water absorption (%)	P wave velocity (m/s)	UCS (MPa)	E_{tan} (GPa)	υ_{tan}	Tensile strength (MPa)	Triaxial shear strength (intact rock) c (MPa)	Triaxial shear strength (intact rock) ϕ (°)	UCS (MPa)	E_{tan} (GPa)	υ_{tan}	Tensile strength (MPa)
Abutments	Upper massive sandstone	2.20 (2.16-2.26)	NT	quartz (85%) feldspar (10%) opaques (1%) matrix (4%)	7.22 (6.42-8.19)	2418 (2078-2801)	45 (39-48)	12 (7-13)	0.55 (0.39-0.70)	NT	NT	NT	80 (60-99)	15 (14-16)	0.51 (0.42-0.60)	NT
	Sandstone	2.21 (2.09-2.31)	NT	NT	7.10 (5.15-9.28)	3034 (2700-3329)	57 (54-61)	16 (15-16)	0.51 (0.42-.61)	NT	NT	NT	79 (44-103)	16 (14-19)	0.28 (0.21-0.41)	NT
	Silty sandstone marker horizon	2.39	NT	NT	4.87	7084	11	11	0.46	NT	NT	NT	39	11	0.20	NT
	Lower massive sandstone	2.16 (2.13-2.18)	NT	quartz (86%) feldspar (8%) carbonate (<1%) opaques (<1%) matrix (6%)	7.80 (6.99-8.47)	2773 (2594-2997)	65 (51-81)	26 (21-29)	0.52 (0.42-0.59)	NT	NT	NT	82 (72-92)	19 (18-19)	0.43 (0.42-0.44)	NT
Foundation	Lower massive sandstone (SW)	2.18 (2.18-2.19)	NT	NT	7.84 (7.47-8.20)	2539 (2713-2366)	71 (66-77)	20 (20-21)	0.51 (0.49-0.53)	3.69 (3.13-4.50)	60	58	NT	NT	NT	NT
	Lower massive sandstone (UW)	2.11 (1.92-2.20)	Very high	quartz (86%) feldspar (8%) carbonate (<1%) opaques (<1%) matrix (6%)	6.90 (5.26-9.74)	3028 (2895-3413)	69 (65-74)	22 (18-28)	0.40 (0.23-0.64)	3.85 (3.50-4.58)	60	58	NT	NT	NT	6.91 (5.66-8.16)
	Sandstone / silty sandstone	2.39 (2.26-2.54)	Very high	quartz (43%) feldspar (5%) muscovite (4%) carbonate (3%) opaques (<1%) matrix (43%)	3.79 (1.72-6.41)	2838 (1637-3808)	84 (69-88)	23 (17-34)	0.26 (0.18-0.28)	5.96 (3.78-6.78)	85	59	NT	NT	NT	7.33 (6.71-7.95)
	Massive sandstone	2.38 (2.32-2.45)	Very high	NT	3.49 (3.00-3.98)	2077 (1460-2693)	42	11	0.55	2.07 (0.52-3.14)	NT	NT	NT	NT	NT	4.35
	Silty sandstone	2.50 (2.48-2.50)	NT	NT	5.85 (4.02-7.68)	2415 (1396-3433)	6 (2-10)	4 (4-5)	0.19 (0.04-0.35)	0.56 (0.32-1.04)	NT	NT	NT	NT	NT	3.25 (2.89-3.64)

Notes:
*Results reported as an average and a range
*Refer to Appendix K for the number of samples tested
*SW = slightly weathered
*UW = unweathered
*only intact failures have been considered for the strength results reported above

Table C.4: Rock mass design parameters-foundation

	Lower massive sandstone	Sandstone / silty sandstone	Massive sandstone	Silty sandstone
Foundation				
GSI	88	73	87	87
UCS (MPa)	69	84	42	6
mi	17.4*	16.8*	17	15
D	0	0	0	0
m_b	11.353	6.405	10.686	9.429
s	0.2636	0.0498	0.2359	0.2359
a	0.500	0.501	0.500	0.500
E (MPa)	20840	18601	10350	3764
c (MPa)	4.468	2.247	2.666	0.616
ϕ (°)	60.5	60.8	58.7	46.4

*m_i determined from triaxial test results

Where:

GSI = Geological Strength Index
UCS = uniaxial compressive strength of intact rock
m_i = Hoek-Brown intact rock parameter
D = disturbance factor
c = cohesion
E = Young's Modulus of the rock mass
m_b = Hoek & Brown criterion parameter
s = Hoek & Brown criterion parameter
a = Hoek & Brown criterion parameter

The values reported in the table above represents peak strength values.

C.2 Erodibility Index Calculation

The following formula was used to compute the Erodibility Index:

$$K = M_s K_b K_d J_s \tag{C.1}$$

where, M_s represents the mass strength number. This is a measure of the strength of an intact representative sample of material. It is the product of a material's uniaxial compressive strength and its coefficient of relative density. M_s is calculated as follows:

$$M_s = \lambda_b \lambda_s UCS \tag{C.2}$$

where,

λ_b = Material's unit weight ($9.81\,m/s^2 \times 2110\,kg/m^3 = 20.699\,KN/m^3$). Density of rock was $2110\,kg/m^3$ (see Table C.3).

λ_s = Unit weight of good quality rock was estimated at $27\,KN/m^3$ (Annandale, 1995).

UCS = Uniaxial compressive strength of intact rock ($= 69$ see Table C.4). Using Equation C.2, a value of 52.9 was found as mass strength number (Ms).

K_b = Particle/block size number = RQD/J_n, where RQD is the rock quality designation. The number of joint per cubic metre was assumed to be 5 which is the minimum value (Table A.2) and from (Table A.2), the value of RQD is 100. J_n is the joint set number. A value of 1 was given for J_n, which corresponds to intact rock with no or few joint/fissures (Table A.3). Therefore, K_b was computed to be 100.

K_d = Shear strength number. For sandstone rock the shear strength number is 1 (see Table A.4)

J_s = Relative ground structure number. A value of 1 was taken as relative ground structure number. This value corresponds to intact material (Table A.5).

After determining the value of all parameters, the Erodibility Index (K) was computed using Equation C.1:

$$K = 52.9 \times 100 \times 1 \times 1 = 5290$$